Doctoral Thesis

# Study on Improvement of Mechanical Properties in Structural Materials by Particle Size Control Process

September 2016

Doctoral Program in Advanced Mechanical Engineering and Robotics
Graduate School of Science and Engineering
Ritsumeikan University

Nur Zalikha Binti Khalil

Doctoral Thesis Reviewed

by Ritsumeikan University

# Study on Improvement of Mechanical Properties in Structural Materials by Particle Size Control Process

# (粒子径制御プロセスによる構造用材料の機械的特性改善に関する研究)

September 2016

2016年9月


Doctoral Program in Advanced Mechanical Engineering and Robotics

Graduate School of Science and Engineering

Ritsumeikan University

立命館大学大学院理工学研究科

機械システム専攻博士課程後期課程

Nur Zalikha Binti Khalil

ヌル　ザリカ　ビンティ　カリル

Supervisor: Professor AMEYAMA Kei

研究指導教員：飴山　惠教授

# Abstract

Study on Improvement of Mechanical Properties in Structural Materials by Particle Size Control Process

by

Nur Zalikha Binti Khalil

Doctoral Program in Advanced Mechanical Engineering and Robotics

Graduate School of Science and Engineering

Ritsumeikan University

Academic Advisor: Prof. Kei AMEYAMA

Owing to its many advantages like the ability to process high-melting point materials, synthesis alloy/composite materials, and ability to obtain a near net shape product for complex materials, powder metallurgy (P/M) has been utilized in many industrial fields. However, when compared to other route, (P/M) route suffers in terms of securing good toughness properties in the final product. There are various factors attributing to the lacking of toughness in structural material. For example in high-melting point materials, it can be attributed to the poor sinterability while for composite materials, the remaining pores due to the poor joining in the boundary of the involving elemental might be the contributing factor. Focusing on the particle size of the base material, this thesis has described the works conducted to improve the mechanical properties in structural materials by controlling various processing parameters.

Silicon Carbide (SiC) as a representative of structural ceramic has emerged as a very promising material due to its many exceptional properties like high thermal and high corrosion resistance. However, the poor sinterability of this material has limited its widespread applications. In present thesis, by utilizing the fundamental of powder metallurgy, an investigation has been carried out to clarify the relationship between SiC sinterability and dispersion in particle size distribution of initial powder. Several sets of powder having different particle size distribution and different variables (e.g: mean particle size and standard deviation) were prepared by mechanical milling followed by subsequent spark plasma sintering to make a compact. The sinterability of powder compacts were evaluated by relative density and flexural strength. Moreover, a statistical parameter namely, Coefficient of Variation, Cv has also been introduced to best describe the dispersion degree in particles size distributions having different variable, in such that the higher Cv value indicates higher relative dispersion in the initial powder. It is found that the sinterability and mechanical properties of sintered powder compact is improving with the increasing the Cv and it is envisaged that it is due to the enhanced packing structure in the initial powder.

Recently, the concept of “Harmonic Structure” concept introduced by Ameyama and co-worker has been proved to be effective in improving the mechanical properties of metallic material. Essentially, it is an exquisite heterogeneous microstructural design, consisting of bimodal grain size distribution, in which ductile coarse grained regions (termed as “core”) are enclosed in a continuously connected three-dimensional networks regions with high strength ultra-fine grained structure, known as “shell”. It has been reported that a variety of metals and alloys with such structure demonstrate excellent

combination of strength and ductility, when compared to its homogeneous counterpart. In harmonic structured material, the improvement of strength is contributed by the fine grain structure in the “shell” region, while the improvement/retention of ductility is associated by the existence of coarse grain structure at the “core” region. In conventional harmonic structured material, ultra-fine grained structure at the “shell” region is achieved through the severe plastic deformation (SPD) process of metallic powder, via controlled mechanical milling process and followed by subsequent consolidation process. However, with regard to Aluminum alloy, the conventional processing method of harmonic structured experienced some problems due to the difficulties of achieving fine grains via mechanical milling and/or retention of the same during subsequent sintering due to the low melting point of aluminum. Therefore it will be significant to fabricate a harmonic structured material with alternative strengthening mechanism than that of the conventional in harmonic structured material. In particular, an attempt has been made to fabricate a harmonic structure having a hard “shell” region which its strengthening mechanism is composed of solid solution and dispersion strengthening phase, while maintaining the “core” region as the softer pure aluminum phase. In this thesis, two elements of hard phase, namely SiC and Si has been adopted as the secondary elemental candidate to achieve the above mentioned purpose. The harmonic structure of Al-Si and Al-SiC demonstrate improvement in strength while retaining sufficient ductility when compared to its homogenous structure counterpart. Moreover, the deformation behavior of the proposed harmonic structure also demonstrates delayed plastic instability, leading to a higher uniform elongation.

In present thesis investigations has been conducted to improve the mechanical properties of two classes of structural materials via particle size control by using the

above mentioned approach and the following conclusions can be made specific to each material; 1) with regard to of SiC ceramic, the dispersion in the initial powder which is best expressed as Cv, plays important role in determining the sinterability and mechanical properties of powder compact in such that the increase of dispersion level in initial powder lead to improvement of sinterability and mechanical properties 2) for harmonic structured Al alloy, it is proved that the network structure of three dimensional interconnected network regions of hard phase, enclosing soft phase is effective in improving mechanical properties of Al based alloy in the similar manner as in the conventional harmonic structure material.

# Table of Contents

# Chapter 1

# Introduction

## 1.1 Introduction to Silicon Carbide

1.1.1 Silicon Carbide (SiC)

Silicon carbide is an important and attractive non-oxide class of ceramic which pose diverse industrial applications. It has emerged as an excellent candidate for high temperature applications, electronics, semiconductor devices, abrasion and cutting applications owing to its exceptional properties like high strength and hardness, chemical and thermal stability, high melting point, oxidation resistance and high erosion **[1]**. **Figure 1** illustrates the Si-C phase diagram. From this figure, it can be observed that the reaction between silicon and carbon generally takes place below the melting point of silicon and SiC is the only compound to be existed in the condensed state in addition to elemental silicon and carbon **[2]**.

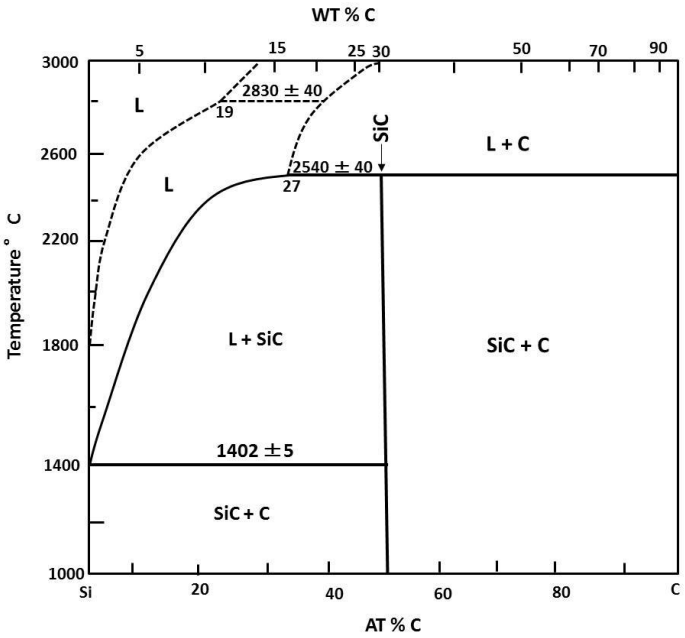


**Figure 1** The Si-C phase diagram **[2]**.

SiC in general exhibit one- dimensional polymorphism which is called polytypism in which all polytypes of SiC demonstrate identical planar arrangement of Si and C atoms, which are characterized by the stacking sequence of the identical planes. **Figure 2** illustrates the stacking sequence for five SiC polytypes. However, in spite of many polytypes existing, there are only three common crystalline structure exist namely; cubic, hexagonal and rhombohedral. To describe the these crystalline structure, crystal symmetry classification is usually used to describe different crystalline polytypes by assigning a number corresponding to the number of layers in the unit cell followed by a letter suffix designating the crystal symmetry; "C" for cubic, "H" for Hexagonal and "R" for rhombohedral. The most common SiC polytypes includes 3C, 4H, 6H, 15R and 9T. The cubic 3C is usually referred to as beta-silicon carbide β-SiC, having the zinc blend structure. On the other hand, any other polytypes are referred as alpha silicon carbide α-SiC which is 6H having a wurtzite structure **[2, 3]**. **Figure 3** illustrates the major structure exhibited by SiC phase.

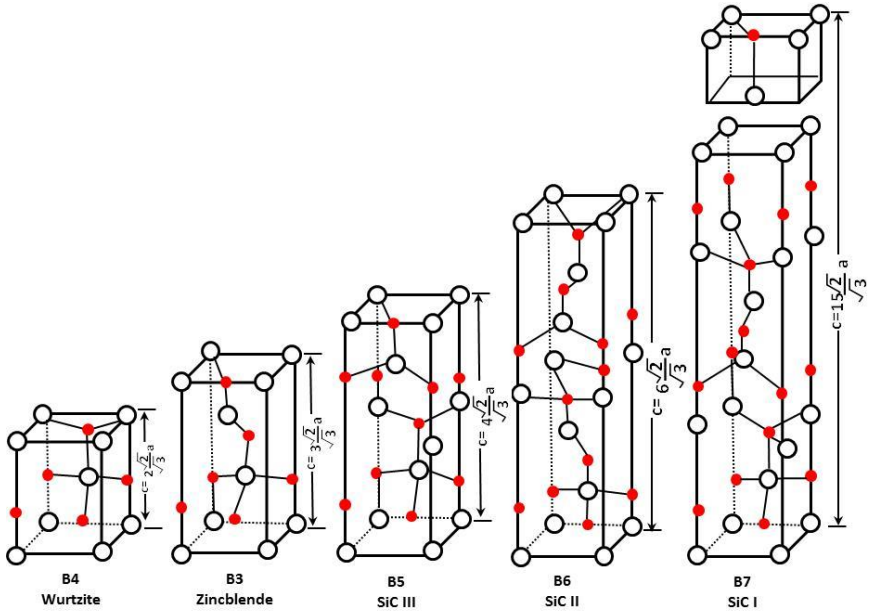


**Figure 2** Stacking sequence for five SiC polytypes **[1]**.

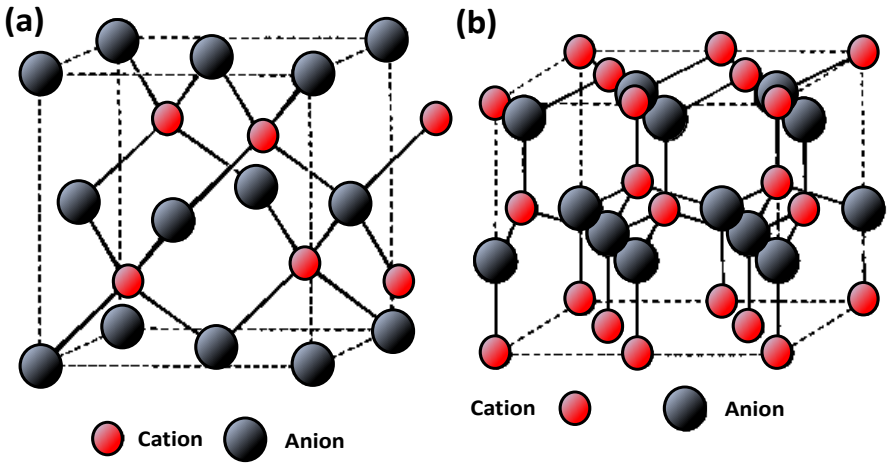


**Figure 3** SiC crystal structure (a) Zinc Blend Structure β-SiC and (b) Wurtzite Structure for 6H α-SiC **[4]**.

Silicon carbide is also classified as one of few light weight covalently bonded ceramics having the theoretical density of 3.210 g/cm$^3$ for β-SiC and 3.208 g/cm$^3$ for α-SiC (6H). Lightweight properties combined with strong covalence and excellent properties as described earlier has made SiC as material of choice for replacing conventional metals and alloys.

1.1.2 Mechanical Properties and Application of SiC

Due to its capability to provide various properties required for structural materials like resistance to abrasion, corrosion and heat, SiC has been the material of choice for many high thermal and corrosion-resistance applications. **Table 1** provides the properties of α-SiC including the mechanical and thermal properties in several sintering temperature.

Due to properties like high hardness and strength, good thermal and chemical stability and high melting point, SiC based ceramic has also been used as technical ceramics **[6-9]**, semiconductors material, ceramic bearing, brake disc, abrasive materials as well as processing materials **[10-11]**. Most importantly, owing to its superior resistance to

**Table 1** Properties of α-SiC in several sintering temperatures **[5]**.

| Property [unit] | 20°C | 500°C | 1000°C | 1200°C | 1400°C | 1500°C |
|---|---|---|---|---|---|---|
| Bulk modulus [Gpa] | 203 (3%) | 197 | 191 | 188 | 186 | 184 |
| Creep rate[$10^{-9}s^{-1}$] at 300 MPa | 0 | 0 | 0 | 0.004 | 0.27 | 1.6 |
| Density[$g/cm^3$] | 3.16 (1%) | 3.14 | 3.11 | 3.1 | 3.09 | 3.08 |
| Elastic Modulus [GPa] | 415(3%) | 404 | 392 | 387 | 383 | 380 |
| Flexural Strength [MPa] | 359(15%) | 359 | 397 | 437 | 446 | 446 |
| Fracture Toughness[MPa $m^{1/2}$] | 3.1(10%) | 3.1 | 3.1 | 3.1 | 3.1 | 3.1 |
| Friction coefficient[ ] at 0.2m/s, 5N | 0.7(21%) | 0.4 | 0.4 | | | |
| Hardness (Vickers, 1kg) [GPa] | 32(15%) | 17 | 8.9 | (6.9) | (5.3) | (4.6) |
| Lattice Parameter, *a* [A] (polytype 6H) | 3.0815 (0.01%) | 3.0874 | 3.095 | (3.0984) | (3.1021) | (3.104) |
| Lattice Parameter *c* [A] polytype 6H | 15.117 (0.02%) | 15.144 | 15.179 | 15.194 | 15.21 | 15.218 |
| Poisson Ratio [ ] | 0.16(25%) | 0.159 | 0.157 | 0.157 | 0.156 | 0.156 |
| Shear modulus [GPa] | 179(3%) | 174 | 169 | 167 | 166 | 165 |
| Sound velocity, longitudinal [km/s] | 11.82(2%) | 11.69 | 11.57 | 11.52 | 11.47 | 11.44 |
| Sound velocity, shear [km/s] | 7.52(2%) | 7.45 | 7.38 | 7.35 | 7.32 | 7.31 |
| Specific Heat [$Jkg^{-1}K^{-1}$] | 715(5%) | 1086 | 1240 | 1282 | 1318 | 1336 |
| Tensile Strength[MPa] | 250(6%) | 250 | 250 | 250 | 250 | 250 |
| Thermal conductivity [$Wm^{-1}K^{-1}$] | 114(8%) | 55.1 | 35.7 | 31.3 | 27.8 | 26.3 |
| Thermal Diffusifivity [$cm^2/s$] | 0.5(12%) | 0.16 | 0.092 | 0.079 | 0.068 | 0.064 |
| Thermal expansion from 0°C [$10^{-6}K^{-1}$] | 1.1(10%) | 4.4 | 5.0 | 5.2 | 5.4 | 5.5 |
| Wear coefficient($Log_{10}$)[ ] at 0.2 m/s, 5N | -4.0(5%) | -3.6 | -3.6 | | | |
| Weibull modulus [ ] | 11 (27%) | 11 | 11 | 11 | 11 | 11 |

at, SiC compacts has also being widely used in various types of high-temperature applications such as core tubes, heating elements and refractory bricks in which high density sintered body is not necessarily required. It is convenient to classify structural SiC to two classes; (1) abrasion and corrosion resistant components and (2) heat resistance components **[12]**. **Figure 4** illustrates the applications of SiC sintered body in this regard.

| | Application | | Operating Environment |
|---|---|---|---|
| | Present | Future | |
| Abrasion and corrosion resistant components | Mechanical seals | | Acid/alkali/slurry, abrasion |
| | Pump shaftws and bearings | | |
| | Nozzles | | |
| | Liners | | |
| | Valves | | |
| | Bearings | | Abrasion, high loads |
| | Grinding media | | Abrasion ,shock |
| | Paper-making components | | Pulp slurry/alkali, Abrasion |
| Heat-resistant components | Heat exchangers | | High- Temperature oxidation |
| | Fans | | |
| | Heating elements | | |
| | Semiconductor jigs | | High Temperature |
| | High-Temperature test jigs | | |
| Engine components | | Gas Turbine (including those for power generation Turbochargers) | High Temperature, High loads |
| Other | Components for steel refining and manufacture | | Higth Temperature, corrosion |
| | Components for refining of non-ferrous metals | | |
| | catalyst carrier | | |
| | | | High temperature |
| | | MHD generators (insulation, electrode wallas) | High Temperature corrosion |
| | | Fusion reactors (cooling walls) | High Temperature radiation |

**Figure 4** Applications of SiC compacts **[12]**.

## 1.2 Introduction to Aluminum Alloy

### 1.2.1 Aluminum Alloy

Aluminum and its alloy are among important class of structural material and being used in many applications due to its versatility. Generally, aluminum alloy can be divided to two major categories namely: casting composition and wrought composition depending on its fabrication process as below **[13-14]**;

1) Casting alloy; which has to be re-melted and then casted
2) Wrought alloy; which has to be hot/cold worked (i.e extrusion, forging and drawing) without being re-melted.

Moreover, with respect to their reaction to heat treatment, aluminum alloys can also be classified to i) non-heat treatable alloy and ii) Heat treatable alloy. Aluminum alloy can also be classified according to its composition using the numerical designation as shown below **[14]**;

**Table 2** Aluminum alloy designation **[14]**.

| Aluminum Alloy Group | Designation |
|---|---|
| Aluminum-99% | 1xxx |
| Copper | 2xxx |
| Manganese | 3xxx |
| Silicon | 4xxx |
| Magnesium | 5xxx |
| Magnesium & Silicon | 6xxx |
| Zinc | 7xxx |
| Other Element | 8xxx |

### 1.2.2 Mechanical Properties and Applications of Pure Aluminum Alloy

As mentioned earlier, due to its versatility, aluminum and its alloy has been used in many industrial applications like aerospace, automotive, packaging and building industries. In this thesis, the mechanical properties improvement investigations are carried out using pure aluminum powder as the based material due to its relatively low strength but with a good ductility. Pure aluminum alloy is highly resistant to corrosion and thus the specific applications include cables, panels, ceilings and tanks **[14]**. The mechanical properties of Aluminum with several properties are shown in **Table 3**.

**Table 3** Mechanical properties of pure Aluminum at room temperature **[15]**.

| Tensile yield strength (0.2% offset) | | | Tensile strength | | Elongation |
|---|---|---|---|---|---|
| Purity, (%) | MPa | ksi | MPa | ksi | in 50 mm |
| 99.99 | 10 | 1.4 | 45 | 6.5 | 50 |
| 99.8 | 20 | 2.9 | 60 | 8.7 | 45 |
| 99.6 | 30 | 4.4 | 70 | 10.2 | 43 |

## REFERENCES:

**[1]** C.G. Carter and M.G. Norton, "*Ceramic Materials Science and Engineering*", Springer, 2007

**[2]** A.H. Rashed, "*Properties and Characteristics of Silicon Carbide*", Poco Graphite, Inc (2002) pp.1-19.

**[3]** R. Cheung, in: *Silicon Carbide Microelectromechanical Systems for Harsh Environments*, edited by R. Cheung, Imperial College Press, London, UK, pp. 1, 2006.

**[4]** W.D. Kingery et al, "*Introduction to Ceramics*", 2nd ed., Wiley, New York, 1976, pp. 63.

**[5]** R.G. Munro, J. Phys. Chem. Ref. Data, Vol. 26 (1997) pp.1195-1203.

**[6]** V.A. Izhevskyi, L.A. Genova, A.H.A. Bressiani, J.C. Bressiani, Mater. Res. 3 (2000) pp. 131–138.

**[7]** V.A. Izhevskyi, L.A. Genova, J.C. Bressiani, A.H.A. Bressiani, Ceramica 50, (2004) pp. 261–267.

**[8]** E.K. Polychroniadis, A. Andreadou, A. Mantzari, J. Optoelectron. Adv. Mater. 6 (2004) pp. 47–52.

**[9]** R. Singh, Microelectron. Reliab. 46 (2006) pp. 713–730.

**[10]** P. Forquin, C. Denoual, C.E. Cottenot, F. Hild, Mech. Mater. 35 (2003) pp. 987–1002.

**[11]** M.F. Zawrah, M. El-Gazery, Mater. Chem. Phys. 106 (2007) pp. 330–337.

**[12]** S. Somiya and Y. Inomata, "*Silicon Carbide Ceramic-1 Fundamental and Solid Reaction*", Elsevier Applied Science (1991) pp.37-38.

**[13]** J. R. Davis, "*Aluminum and Aluminum Alloys",* ASM Specialty Handbook (1993)

pp.1-3.

**[14]** J. G. Kaufman, "*Properties of Aluminum alloys Tensile, Creep and Fatigue Data at High and Low Temperatures*", ASM International (1999) pp.8.

**[15]** J.E. Hatch, "*Aluminum: Properties and Physical Metallurgy*", American Society for Metals (1984) pp.2.

# Chapter 2

# Literature Review

## 2.1 Particle Characterization

The sinterability of powders often depends on several factors such as processing technique, the packing structure of initial powder and mean particle size. Regarding the packing structure of a powder set, there are mainly two powders' aspects that can be considered in order to improve the packing structure of the powder prior to consolidation, namely particle size distribution and particle morphology. The following discussion revolves around these two factors and its effect to the packing structure of a powder set.

### 2.1.1 Particle Size Analysis

As mentioned earlier, particle size plays important role in dictating a packing structure of a powder set. In many particle size analysis techniques, a particle is generally assumed to be spherical due to the difficulties of comparing dimension of non-spherical particles. Due to the different specifications to each analysis technique, the physical attributes such as volume, mass and maximum length often varies within each technique. **Table 1** and **Figure 1** illustrate the comparison of particle size analysis technique, which provides the information about approximate size range, dynamic ratio and the measuring technique. Generally, it implies the best possible range measurement range obtainable for each technique. In present theses, a laser type particle size analyser (Shidmadzu SALD-2300, Japan) is used to analyze particle size data for both SiC and Al powders.

When a data of particle size is obtained, there are several methods which is used to

analysis the data. Most often they are present as histogram or frequency plot which shows the number/amount of particles in each size increment. In such plots, the mode is defined as the peak particle size while the median refers to the central tendency. **[1]**

**Table 1** Comparison of particle size analysis approaches **[1]**.

| Technique | size range,μm | dynamic ratio | sample size, g | basis* |
|---|---|---|---|---|
| **sieving (wet and dry)** | | | | |
| electroform | 5-120 | 20 | >5 | W |
| wire mesh | 38 and | 20 | >5 | W |
| **sedimentation** | | | | |
| gravity | 0.2-100 | 50 | 5 | W |
| centrifugal | 0.02-10 | 50 | 1 | W |
| **microscopy** | | | | |
| optical | 0.8 and | 30 | <1 | P |
| electron | 0.001-400 | 30 | <1 | P |
| **light scattering** | | | | |
| Mie | 0.1-3 | 30 | 1 | W |
| velocity | 0.5-200 | 400 | 1 | W |
| Brownian | 0.005-5 | 1000 | <1 | P |
| Fraunhofer | 1-800 | <200 | <5 | W |
| **light blocking** | 1-600 | 45 | 3 | P |
| **X-ray** | | | | |
| broadening | 0.01-0.2 | - | 1 | P |
| small angle | 0.001-0.05 | - | 1 | P |

*P= population basis, W= weight basis

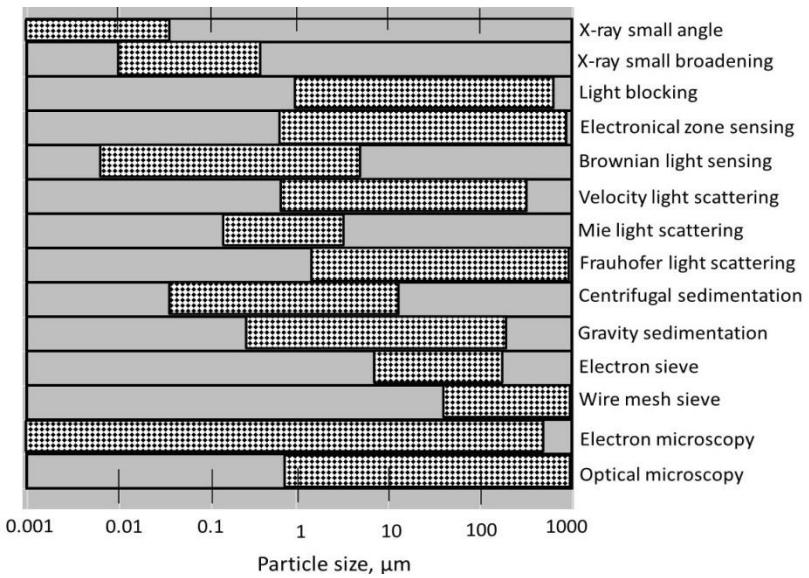


**Figure 1** A comparative plot of particle size analysis techniques and the nominal useful size ranges for each **[1]**.

2.1.2 Particle Size Distribution

**Figure 2** illustrates the common types of particle size distribution in commercial powder in both frequency and cumulative modes. It is worth noting that, normal powder fabrication method does not form single sized powder. It is common practice to define particle size distribution by 3 values as shown in **Figure 3**. These three numbers are taken from the cumulative particle size based on particle size at 10, 50 and 90 % (termed $D_{10}$, $D_{50}$ and $D_{90}$).

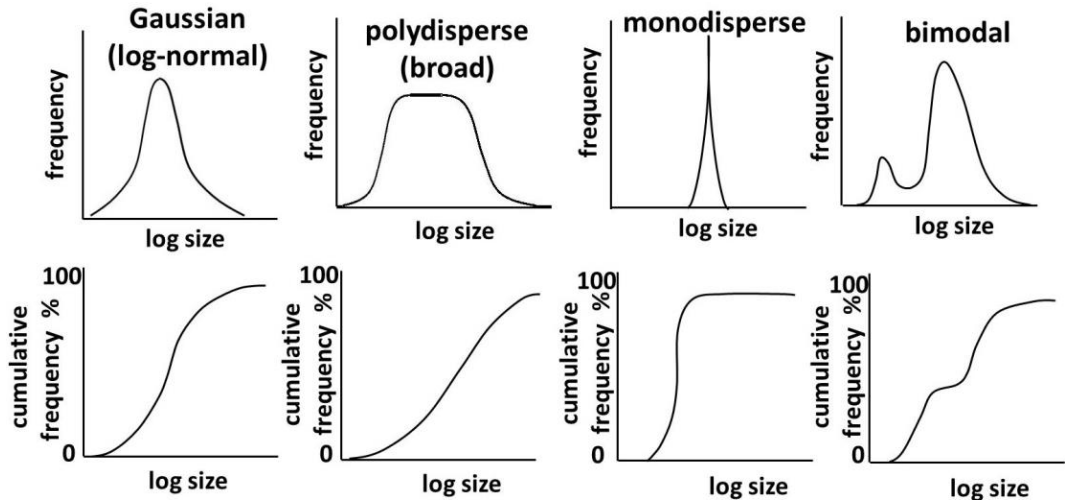


**Figure 2** Common types of particle size distributions in both frequency and cumulative modes **[1]**.

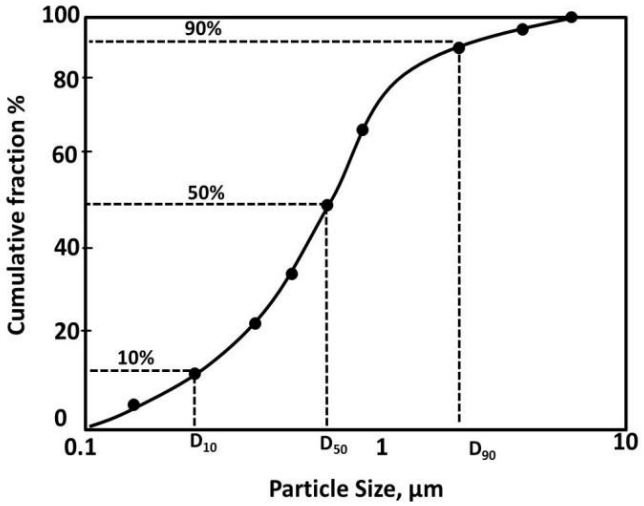


**Figure 3** Cumulative particle size distribution defined into three number based on particle size at 10, 50 and 90% ($D_{10}$, $D_{50}$, $D_{90}$) **[1]**.

2.1.3 Particle Shape

Particle Shape is one of important factors in determining packing structure, flow and compressibility. It is often difficult to describe particle shape and thus the qualitative descriptor is often used. **Figure 4** shows the possible types of particles and the suggested qualitative descriptors. In general, the qualitative measures of particles are developed from the observation under microscope. Genuine descriptor for particle shape is the aspect ratio which is defined as the maximum particle dimension divided by the minimum particle dimension. For example, a spherical particle will have an aspect ratio of 1 while for a ligament-like particle it will have an aspect ratio of 3 to 5**[1].**

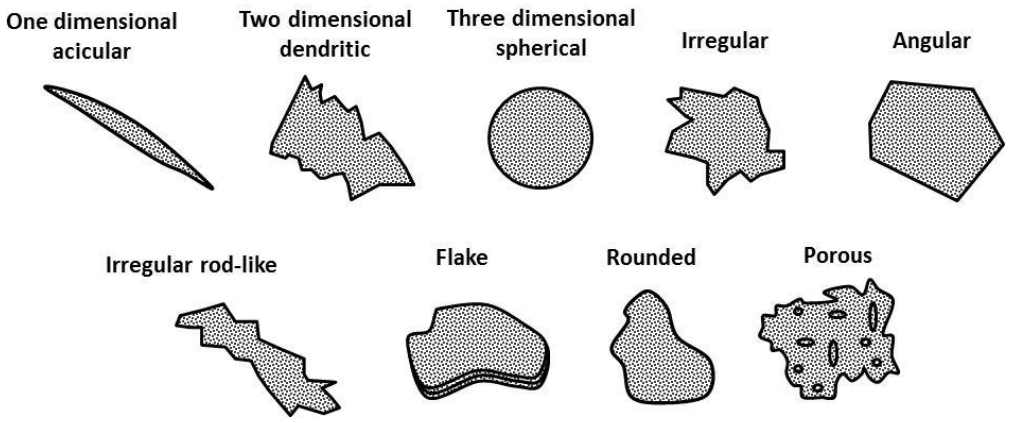


**Figure 4** Types of particle shape and its qualitative descriptors **[2]**.

2.1.4 Particle Packing Structures and Improved Packing Techniques

Particle packing is important aspect that control the sinterability of a powder set because it controls the binder, shrinkage during sintering and die fill and for commercial powder the random packing is typical. With regard to packing density, it relies on the several characteristics mainly being the particle size and particle shape. For irregular particles, the packing density is lower and even lower as the particles get smaller, more irregular and spongier resulting in a lower coordination number. Lower packing density implies that the particles do not slide easily amongst them due to the inter-particle

friction, as the more irregular the particle shape is, the more surface area it has leading to a lower packing density.

To attain a higher packing density, it is possible to tailor the particle size distribution. For example, bimodal particle size provides a higher packing density as compared to the monosized particles. Finer particles will enhance the packing density by filling the gaps between coarse particles while keeping them intact. **Figure 5** illustrates the packing density variation with composition for a bimodal structure, showing five possible structures. At the maximum packing composition, there are a greater volume of coarser particles than that of the finer particles. From this figure, it can be observed that the benefit of adding finer particles to coarser particles reach its maximum packing density at A* of coarse particles, in which the further addition of finer particle will only decrease the overall packing density **[1].**

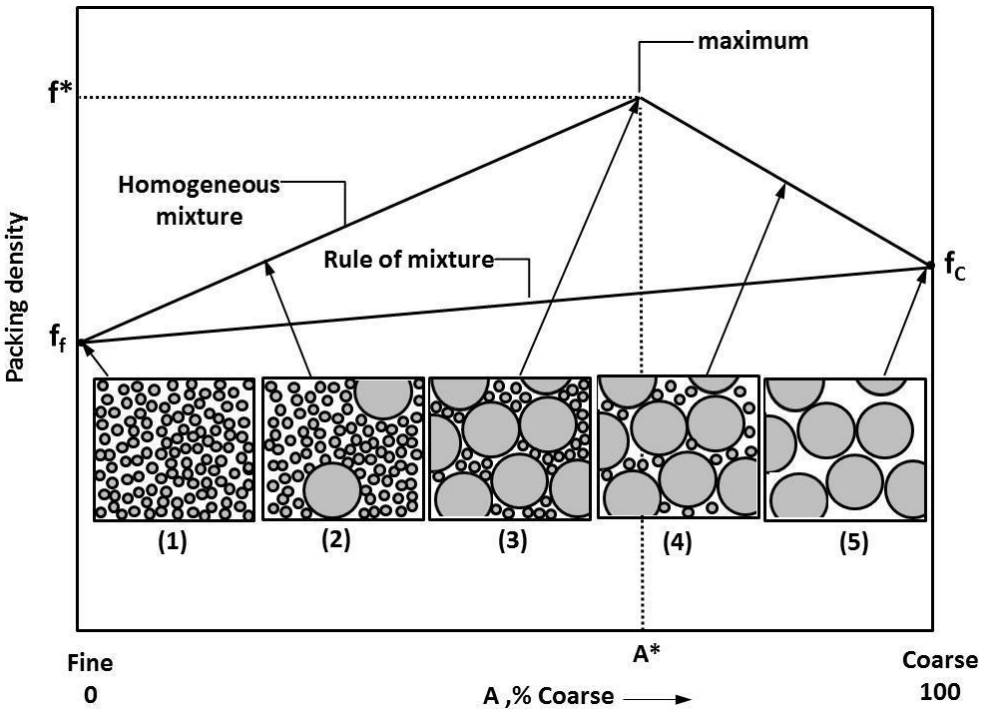


**Figure 5** The packing density variation with composition for a bimodal mixture, showing five possible structures **[3]**.

## 2.2 Strengthening Mechanism in Metals

2.2.1 Grain Refinement by Severe Plastic Deformation

In recent years, severe plastic deformation (SPD) has emerged as a very attractive method to produce ultrafine- grained with superior mechanical properties **[4,5].** Moreover, the strengthening degree via grain refinement can be predicted by Hall-Petch relation **[6]** making it a versatile method for many applications. The development of SPD method has attracted growing interest because the conventional plastic deformation such as intense rolling or drawing enhances the strength and other properties in the expense of ductility decrement **[7]**. In this section discussion will be made regarding the most established SPD method namely, high pressure torsion (HPT), equal-channel angular pressing (ECAP), mechanical milling (MM) and accumulative-roll bonding (ARB) **[8]**.

2.2.1.1 High Pressure Torsion (HPT)

High-pressure torsion (HPT) is a severe plastic deformation (SPD) technique in which a sample is subjected to torsional shear straining under a high hydrostatic pressure as shown in **Figure 6 [9]**.

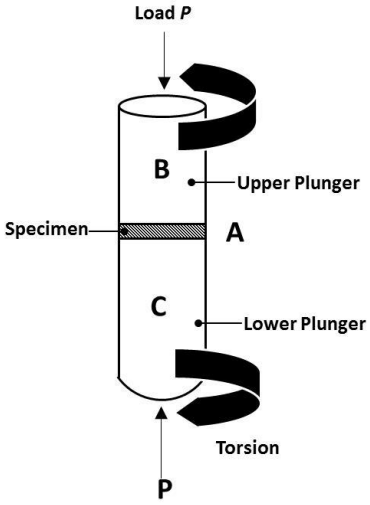


**Figure 6** Principle of HPT in ideal condition **[9]**.

As shown in Figure 6, a thin disc is squeezed between two anvils (A and B) under a high pressure, P, and intense shear strain is introduced by rotating the two anvils with respect to each other. The growing interest of processing material via HPT is not only limited due to its ability to attain grain refinement, but also for many other features such as twins, high density lattice defects and dislocations **[9].** One important advantage of HPT is its ability to control cumulative strain, applied pressure and strain rate. However, samples processed by HPT have important limitation; the sample is small in size thus limiting its application for industrial scale **[7]**.

2.2.1.2 Equal-channel Angular Pressing (ECAP)

Equal-channel angular pressing (ECAP) is a processing method in which a metal is subjected to an intense plastic straining through simple shear without any corresponding change in the cross-sectional dimensions of the sample **[10]**. **Figure 7** illustrates the schematic of a typical ECAP facility.

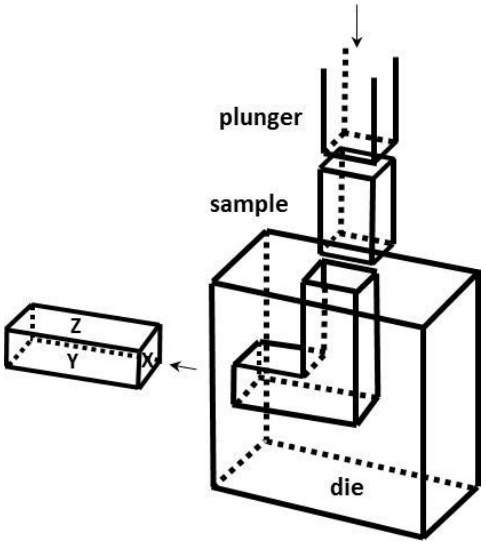


**Figure 7** Schematic illustration of a typical ECAP facility: the X, Y and Z planes denote the transverse plane, the flow plane and the longitudinal plane, respectively **[10]**.

ECAP is used to obtain ultrafine grain size for polycrystalline material. As compared top HPT, ECAP provides is a more promising method due to its ability to scale up the samples for industrial application.

2.2.1.3 Mechanical Milling

Mechanical milling is a powder processing method process generally used in powder metallurgy industries. When it is used for blending powders which is its traditional purpose, often the powders subjected to mechanical milling are either fragmented or underwent no significant morphological change. Later on, mechanical milling was found to be inducing excessive plastic deformation to the milled powders forming a new powder structure than its initial state, known as mechanically alloyed powder **[11]**.Mechanical alloy is a solid-state powder processing technique which produces a new powder structure than its elemental powder through the repeating process of welding, fracturing and rewilding during mechanical milling **[11, 12]**.

Essentially, there are several types of mechanical milling techniques namely vibratory ball mills, planetary ball mills, Attritor mills and commercial mills. In present thesis, vibratory and planetary ball mills have been used to mill SiC and Al powder. Since the purpose for SiC milling is to induce fragmentation for several particle size distributions, high energy vibratory ball mill has been used. In contrast, for Al/Si and Al/SiC powders, the main purpose is to blend the powder to make well dispersed SiC/Si particles around Al particles and thus planetary ball mill has been chosen. A more detailed explanation is discussed in chapter 3.

2.2.1.4 Accumulative-roll Bonding (ARB)

Accumulative roll bonding is a relatively new SPD process which used rolling

deformation and the principle of ARB is illustrated in **Figure 8.** In ARB process, the thickness of two sheets of the same thickness is reduced to the thickness of initial sheet by simultaneous rolling which is repeated several times resulting in the sheets of are bonded together forming a refined microstructure **[7].**

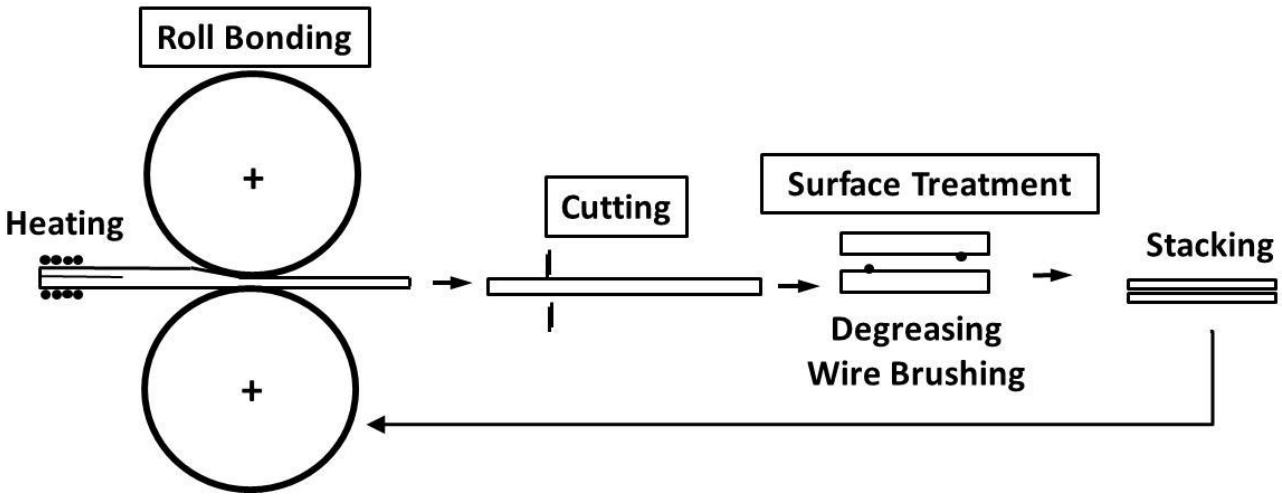


**Figure 8** Schematic illustration showing the principle of accumulative roll bonding (ARB) **[8]**.

2.2.2 Solid Solution Strengthening

Solid solution strengthening is a strengthening mechanism of metallic material in which impurities/solute atoms go into parent metal's host atoms to form either substitional or interstitial solid solution. These solute atoms impose lattice strain around the host atoms inducing either tensile or compressive strains around the dislocation and nullify the existing lattice strain (compressive/tensile), causing the overall strain energy to be reduced. As a result, the required stress to move the dislocation is increasing resulting in a higher stress required to deform the material **[13]**. **Figure 9** illustrates the representative tensile lattice strain induced by impurities atom.

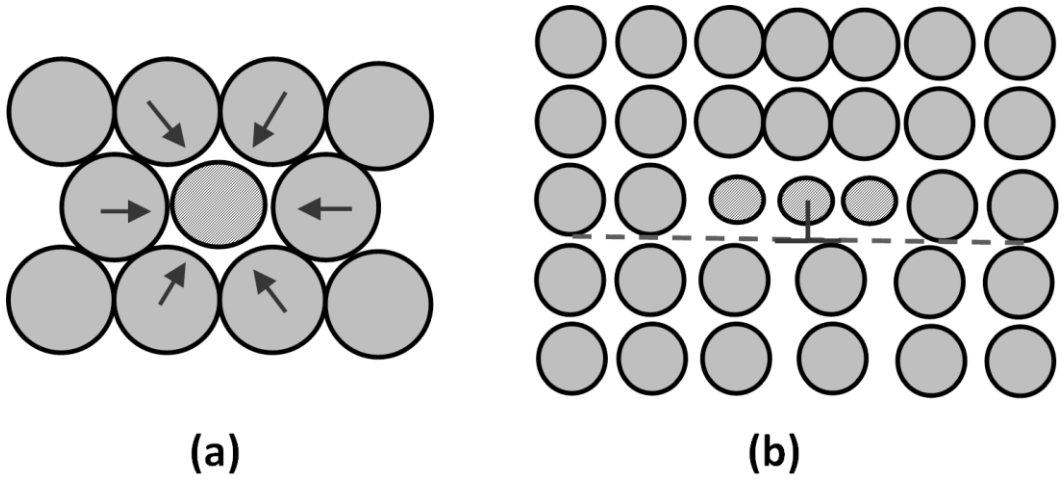


**Figure 9** (a) Representation of tensile lattice strains imposed of host atoms by a smaller substitional impurity atom (b) Possible locations of smaller impurity atoms relative to an edge dislocation such that there is partial cancellation of impurity- dislocation lattice strains **[13]**.

2.2.3 Precipitation Strengthening

Precipitation hardening has been long used to improve the strength of a wide range of commercial alloys system. Precipitation hardening strengthening is attained by producing obstacle to dislocation movement obtained by particulate dispersion. In general, the precipitation phase is the secondary phase obtained during precipitation process. The degree of strengthening obtained is highly dependent upon the metallic system involved, the volume fraction and size of the particles, and the nature of the interaction of the particles with dislocations. Precipitation strengthening is extensively used in ferrous systems but as well as in in non-ferrous system, in which the possibilities for grain refinement are restricted by the absence of allotropic changes Generally, precipitation hardening, involves the strengthening of alloys by coherent precipitates which are capable of being sheared by dislocations**[14]**.

Precipitation strengthening occurs when two segments of dislocations is pinned by sub-micrometer precipitates and subsequently extruded between two pinning points due to the additional applied shear stress $\Delta\tau$ as shown in **Figure 10**. The strengthening resulting from this mechanism is known as Orowan strengthening which can be defined by the following equation **[16]**:

$$\Delta \boldsymbol{\tau} = \frac{Gb}{L-2r} = \frac{Gb}{L'} \tag{2.1}$$

Where $G$ is the shear modulus, $b$ is the Burger's vector, $L$ is the center-to-center separation between the precipitates, $r$ is the particle radius and $L'$ is the effective particle separation, $L'=L-2r$.

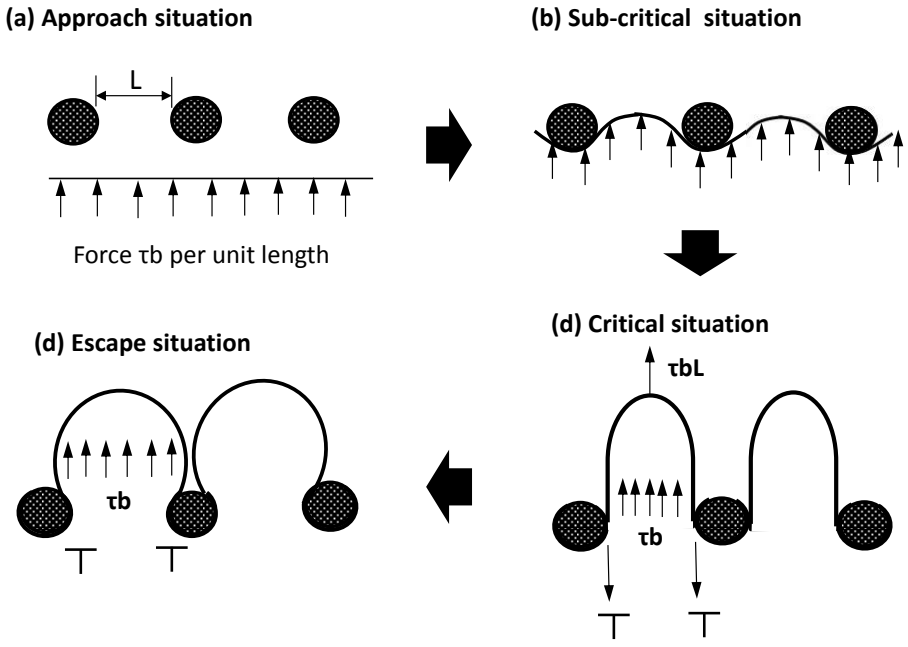


**Figure 10** Sequence when dislocation meets hard undeform able second phase particles: dislocation release at higher stresses occur by Orowan looping/ cross-slip (a) dislocation approaching particles; (b) dislocation extruding through particles; (c) critical situation when extruded dislocation reaches semicircular configuration; (d) escape situation **[15]**.

## 2.3 Strain Hardening Rate (SHR) Curve

When metallic materials undergo plastic deformation, the dislocation density increases with strain amount. The stress field containing the piling up of these dislocations inhibits the movement of another dislocation, resulting in a higher required stress to continue deforming the material. This phenomenon of material hardening due to piling up of dislocation is called strain hardening. In present theses, the strain hardening rate curve (SHR curve) is used in order to understand the behavior of the strain hardening phenomenon. Strain hardening rate is defined as below;

$$d\sigma_t/d\varepsilon_t \tag{2.2}$$

where $\sigma_t$ and $\varepsilon_t$ refers to true stress and true strain respectively. The true stress $\sigma_t$ and true $\varepsilon_t$ in the uniform elongation range is obtained by below equation **[13];**

$$\sigma_t = (1+\varepsilon_n)\,\sigma_n \tag{2.3}$$

$$\varepsilon_t = \ln(1+\varepsilon_n) \tag{2.4}$$

where, $\sigma_n$ and $\varepsilon_n$ refer to nominal stress and nominal strain respectively. **Figure 11** shows the schematic of SHR curve.

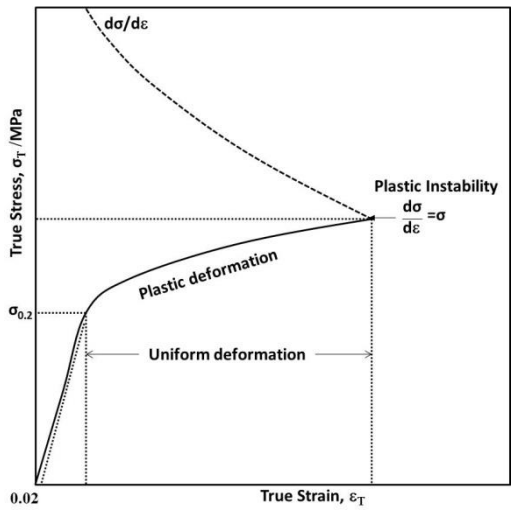


**Figure 11** Schematic of a true stress- true strain curve and the strain hardening rate (SHR) curve **[16]**.

## 2.4 Harmonic Structured Material and its Recent Progress

In recent years, extensive investigations have been conducted in order to meet the demand of structural materials with superior mechanical properties, as compared to those of the conventional materials, with an emphasis on improving the existent material's properties. The improved mechanical properties will not only reduce the cost by providing small sized components with high strength but also enable the generation of novel lightweight materials for a wide range of emerging industrial applications.

In past decades, mechanical performance improvement by obtaining ultrafine grain (UFG) of bulk metals has attracted significant attention. The fine grain structure has demonstrated significant enhancement in strength and hardness when compared to their coarse grain counterpart (CG). It was also reported that the refinement of grain also increases the wear resistance as well as resistance to cavitation. However, with the enhancement of strength of fine grain structure, it comes with an expense of ductility. This drawback has limited its widespread application for industrial purpose. The deterioration of ductility in homogenous fine grain material has long been associated with the early plastic instability under deformation which cause strain localization and the subsequent failure. Therefore, it is necessary to find a solution to the aforementioned issue by improving both of the strength and ductility by a microstructure control. Realizing this issue, considerable amount of attempts has been initiated through combining UFG and CG to form a bimodal grain size structure in order to improve both strength and ductility as mentioned above. In this bimodal structure, the UFG contributes to improvement of strength while the CG contributes to the improvement in ductility. However, the reproducibility of such microstructure remains a matter of concern as it depends to a great extent of many processing parameters such as grain size

and spatial distribution leading to inconsistent outcome properties due to the microstructural varieties.

To address the above mentioned issue, recently, Ameyama and co-workers have proposed a microstructural design to improve mechanical properties by obtaining both high strength and high ductility in metallic materials, through the formation of so-called "harmonic structured material". Essentially, it is an exquisite heterogeneous microstructural design, consisting of bimodal grain size distribution, in which ductile coarse grained regions (termed as "core") are enclosed in a continuously connected three-dimensional networks regions with high strength ultra-fine grained structure, known as "shell". The fabrication of conventional harmonic structured material includes the application of severe plastic deformation (SPD) by controlled mechanical milling to initially coarse grain structured metallic powder in order to obtain a bimodal structured powder having fine grained structure in the surface region (termed as "shell") while maintaining a coarse grained structure at the inner region (termed as "core"). The consolidation of the mechanically milled powder results in the formation of a three interconnected ultra-fine grain region enclosing the isolated coarse grain region. The schematic for fabrication method of conventional harmonic structured material is illustrated in **Figure 12**. Variety of pure metals and alloys demonstrate a winning combination of both strength and ductility when compared to its homogenous structure counterpart. Most importantly, the suggested approach also demonstrates a good reproducibility for both microstructure as well as mechanical properties. **Figure 13** shows the normalized proof stress and normalized absorbed energy in harmonic structured material for various metals and alloys. The absorbed energy, $E_{abs}$ of every sample is obtained by the area under the stress-strain curve by the below equation **[17]**:

$$E_{abs} = \int_0^{\varepsilon_{max}} \sigma \, d\varepsilon \tag{2.5}$$

Where, σ and ε are the nominal stress and nominal strain respectively. It is also worth to mention that the comparison is made with regard to its initial homogeneous counterpart, labelled as uniform structure in **Figure 13**.

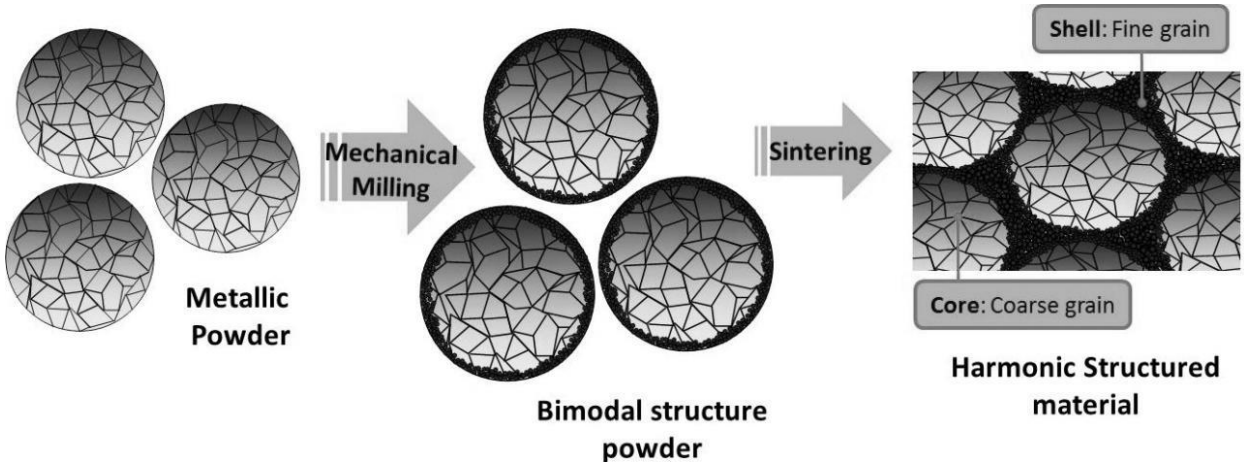


**Figure 12** Fabrication method of conventional harmonic structured material.

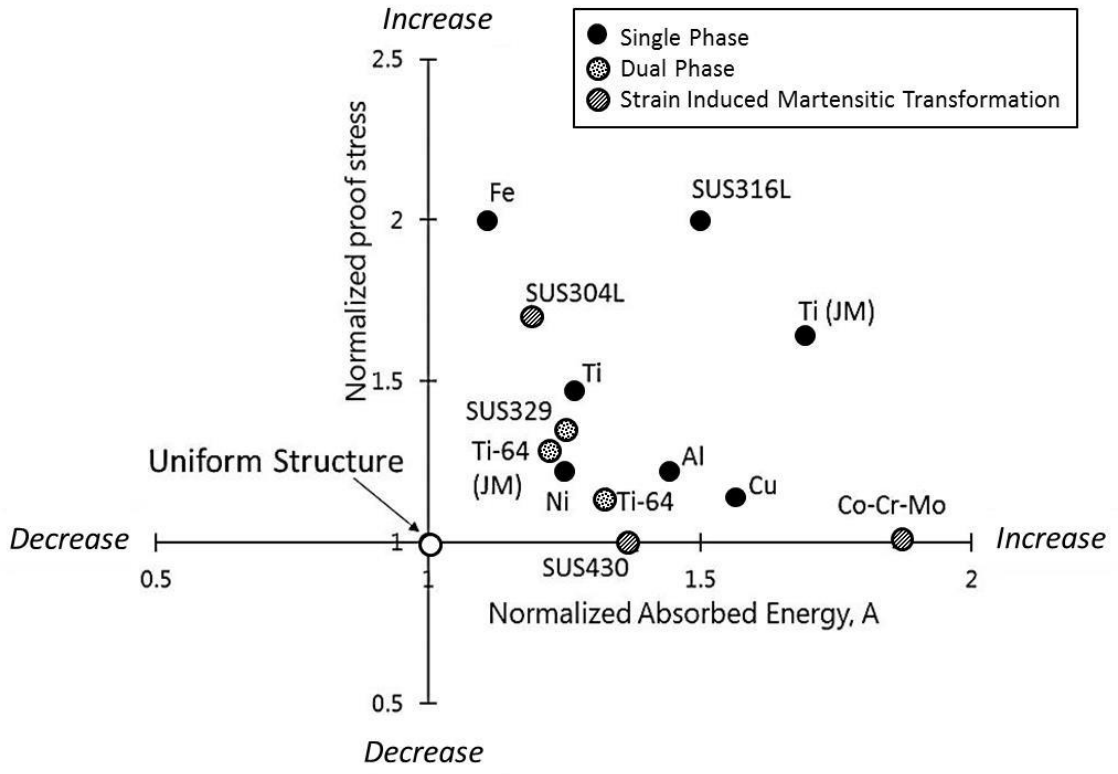


**Figure 13** Normalized proof stress and normalized absorbed energy in harmonic structured material for various metals and alloys **[18]**.

## 2.5 Research Objective and Approach

Owing to its many advantages like the ability to process high-melting point materials, synthesis alloy/composite materials, and ability to obtain a near net shape product for complex materials, powder metallurgy (P/M) has been utilized in many industrial fields. However, when compared to other route, (P/M) route suffers in terms of securing good toughness properties in the final product. There are various factors attributing to the lacking of toughness in structural material. For example in high-melting point materials, it can be attributed to the poor sinterability while for composite materials, the remaining pores due to the poor joining in the boundary of the involving elemental might be the contributing factor. Therefore, this thesis has described detailed information on the

works conducted to improve the mechanical properties in structural materials through controlling various processing parameters by focusing on the particle size of the base material.

Consequently, the broad objective of present thesis is on the mechanical properties improvement of structural material by particle size control. The aspect of particle size control in improving mechanical properties has been chosen because particle size is a fundamental and important aspect in powder metallurgy field in dictating mechanical properties of structural materials in general. To realize this objective, particle size control in specific approach has been applied to two classes of material namely ceramic and metallic material. **Figure 14** illustrates the work flow and the methodology proposed to tackle the specific issue in this thesis. As a ceramic material representative, SiC has been chosen due to its very attractive properties yet difficult sinter ability issue as discussed in chapter 1 and 2 of thesis. Therefore, the specific methodology proposed to tackle the sinter ability issue which will leads to mechanical properties improvement includes the clarification on the effect of particle size distribution to its sinter ability. On the other hand, for metallic material representative, Al alloy has been chosen and the specific methodology to improve the mechanical properties of this alloy includes the control of microstructure/particle size by applying the harmonic structure concept.

As described in chapter 1 of present thesis, Silicon carbide (SiC) is an important structural ceramic material owing to its exceptional properties like excellent thermal properties and high wear resistance. However, the main drawback for this material that limited its widespread application includes its hard-to-sintered nature, due to its highly covalent bonded characteristic, leading to extremely low a self-diffusion coefficient. The conventional solid state sintering requires a very high temperature coupled with a

longtime sintering to achieve full densification. This in turn deteriorates the final mechanical properties due to the grain coarsening during sintering. Therefore, in this work, an attempt has been made to improve the mechanical properties of SiC ceramic by enhancing the sinter ability of SiC ceramic through particle size distribution control.

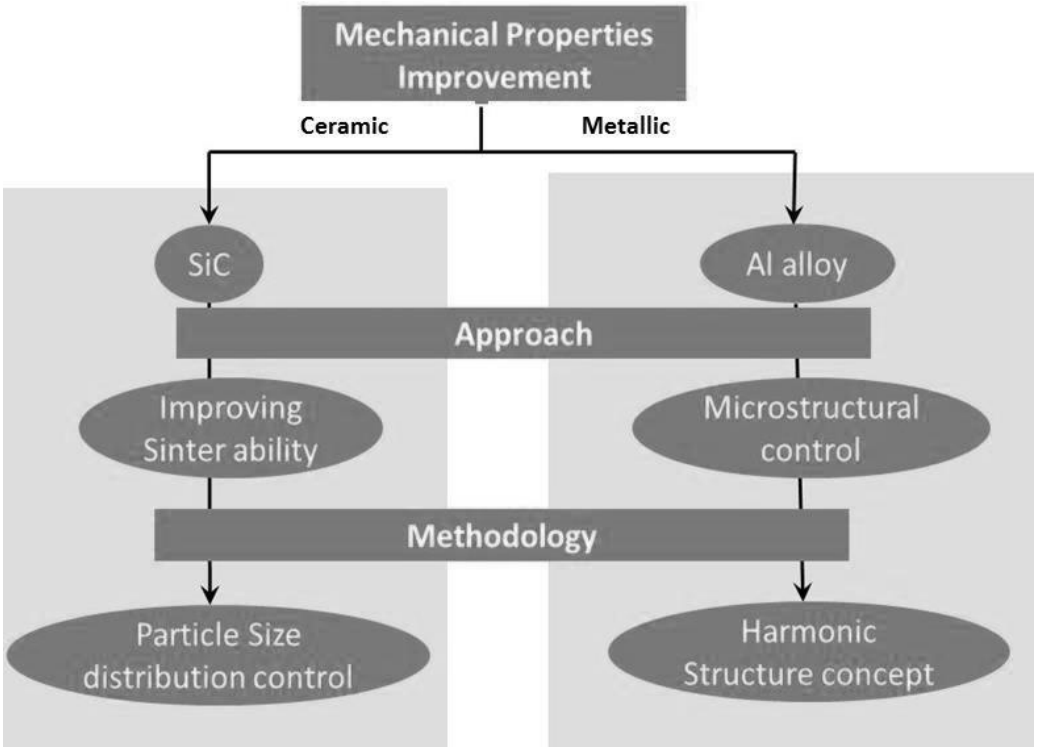


**Figure 14** Flowchart of the proposed methodology to improve mechanical properties in ceramic and metallic material.

Specifically, several sets of powder having different particle size distribution and different variables (e.g: mean particle size and standard deviation) were prepared by mechanical milling followed by subsequent spark plasma sintering to make a compact. The sinter ability of powder compacts were evaluated by relative density and flexural strength. An attempt has also been made to propose a convenient statistical parameter which can describe the relative dispersion in the initial powder having different

variables.

Aluminum alloy on the other hand is an important class of metals which is used in many structural applications such as aerospace industries due to its many excellent properties like high strength to weight ratio characteristic. The investigation to further improve the mechanical properties of this alloy is continuously demanded. As discussed in 3.2, Ameyama and co-worker has introduced harmonic structure concept fabricated by SPD method to improve both strength and ductility in metallic material. However, with regard to aluminum alloy, the formation and retention of fine grained structure on the "shell" region through the conventional MM-consolidation process is rather difficult to achieve and/or maintain due to the low melting point of aluminum. Thus, in present thesis, a new and more feasible concept for fabricating harmonic structured aluminum alloy has been proposed. In particular, an attempt has been made to explore the possibility to fabricate harmonic structured material to fabricate a network structure of soft phase, which is enclosed by three dimensional interconnected network regions of hard phase. In the proposed approach, the "shell" region with alternative strengthening mechanism than that of the conventional harmonic structured material, while maintaining the "core" region as the softer phase. **Figure 15** illustrates the schematic of the proposed approach. By subjecting pure Al powder and Si/SiC powder, to controlled mechanical milling followed by subsequent sintering, attempts has been made to form a network structure which the "core" region is composed of softer pure Aluminum phase while the "shell" is composed of hard phase region i.e dispersion of Si/SiC and/or the solid solution region. Si and SiC have been chosen as the secondary element candidate owing to their hard nature and the ability for Si and Al to form the Al-Si solid solution phase. The investigation has also been made with respect to their strain hardening

behavior to further understand the deformation behavior of the harmonic structured Al alloy.

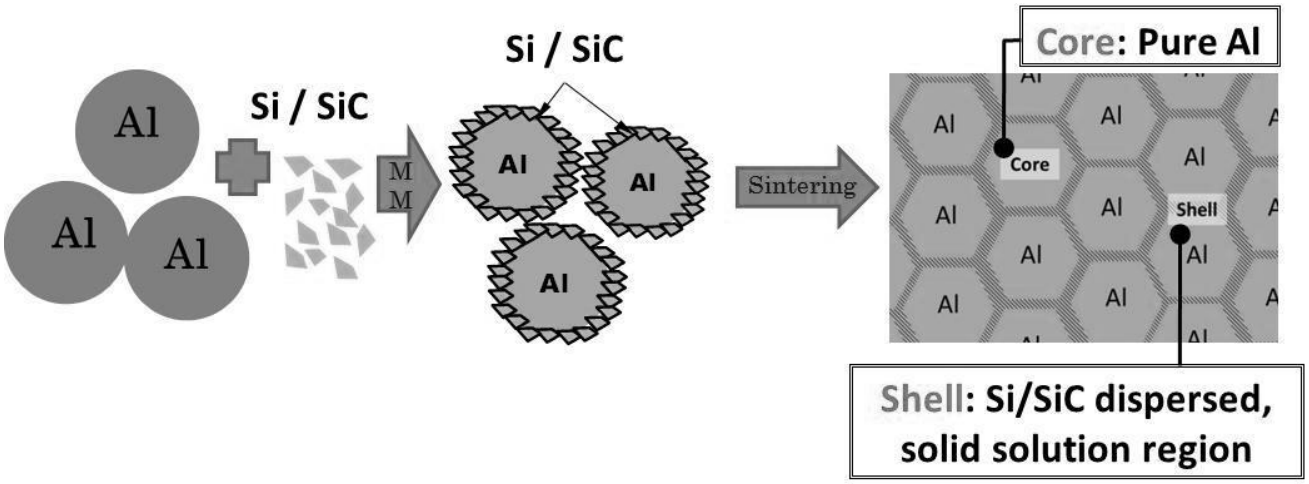


**Figure 15** Schematic of the proposed novel approach of fabricating harmonic structured in Al alloy containing hard phase in the "shell" region and soft ductile Al in the "core".

## REFERENCES:

**[1]** R.M. German, *Powder Metallurgy & Particulate Materials Processing*, Metal Powder Industries Federation (2005) pp.32-129.

**[2]** G.S. Upadhyaya, "*Powder Metallurgy Technology*", Cambridge International Science Publishing (2002) pp.19.

**[3]** R.M. German, Metallurgical Transactions A, Vol. 23A (1992) pp. 1455-1465.

**[4]** R.Z. Valiev, A.V. Korznikov, and R.R. Mulyukov, Mater. Sci. Eng. A, 186 (1993), pp.141.

**[5]** T.C. Lowe and R.Z. Valiev, JOM, 52 (April 2000), pp. 27.

**[6]** N. Hansen: Scripta Materilia 51 (2004) pp.801-806.

**[7]** T.C. Lowe, R.Z. Valiev JOM, 56 (2004), pp. 64.

**[8]** M.A. Meyers, A. Mishra and D.J. Benson: Progress in Materials Science 51 (2006) pp. 427-556.

**[9]** K. Edalati, Z. Horita: Mater. Sci. Eng. A, 652 (2016), pp. 325–352

**[10]** M. Furukawa, Z. Horita, M. Nemoto, T.G. Langdon J. Mater. Sci., 36 (2001), pp. 2835.

**[11]** C. Suryanarayana, Prog. Mater Sci., 46 (2001), pp. 1–184.

**[12]** D.L. Zhang, Prog. Mater. Sci., 49 (2004), pp. 537–560.

**[13]** W.D. Callister, *Materials Science and Engineering An Introduction*, John Wiley & Sons. Inc. (2007) pp. 190-191.

**[14]** T. Gladman: Mater. Sci. Tech., 15 (1999), pp. 30-36.

**[15]** W. Soboyejo, "*Mechanical Properties of Engineered Materials*", Marcel Dekker, Inc (2003) pp.235-236.

**[16]** T. Sekiguchi,*"Study on the Fabrication of Harmonic structured pure Ti and*

*Ti-64-4V alloy and its mechanical properties"* Doctoral Dissertation (2012).

**[17]** T. Daitoh and T. Takaai: Japan Inst. Light Metal 39 (1989) pp.873-877.

**[18]** Mie Ota: "*Study on harmonic structure design process in single and dual phase materials*" Doctoral Dissertation (2015).

# Chapter 3

# Experimental Procedures

## 3.1 Mechanical Milling (MM)

In powder metallurgy, mechanical milling is a traditionally used technique to blend and crushing powders. There are several types of high energy milling equipment and these include planetary ball mill, attritor mills, vibration ball mill and shaker mills. This equipment differs in their capacity, efficiency of milling and additional arrangement for cooling and heating **[1, 2]**. In the present thesis, mechanical milling process on Al and SiC powders were carried out using a planetary ball mill (Fritsch P-5) manufactured by Fritsch GmbH in Germany and a vibratory ball mill. The following discussions will be focusing on these two types of mill:

i) **Vibratory ball mill**- This type of mill is generally used to prepare very fine powders which require mechanical activation. Mechanical milling of solid by this type of mill usually requires a longtime milling and generally conducted in a batch process **[3]**. In this thesis, owing to its high energy advantage, vibratory ball mill has been adopted to fragment the hard-natured SiC powders particles.

ii) **Planetary ball mill**- this type of mill gets its name to the planet-like movement of its vials. The vials are arranged on a rotating support disc and force mechanism causes them to rotate on its axes. The vial content are subjected to both centrifugal force produce by the vials rotating around their axes combined with the rotating support disc, causing the vial contents to be ground by the grinding balls as shown in **Figure 1**. Because the vials and the supporting disc

and vials rotate in opposite direction, the centrifugal forces also act in as like in opposite direction causing the grinding balls inside the vial to run down the inside wall of vial inducing the effect of friction followed by the grinding of the material **[1]**.

The conditions of mechanical milling for each powder are listed in **Table 1.**

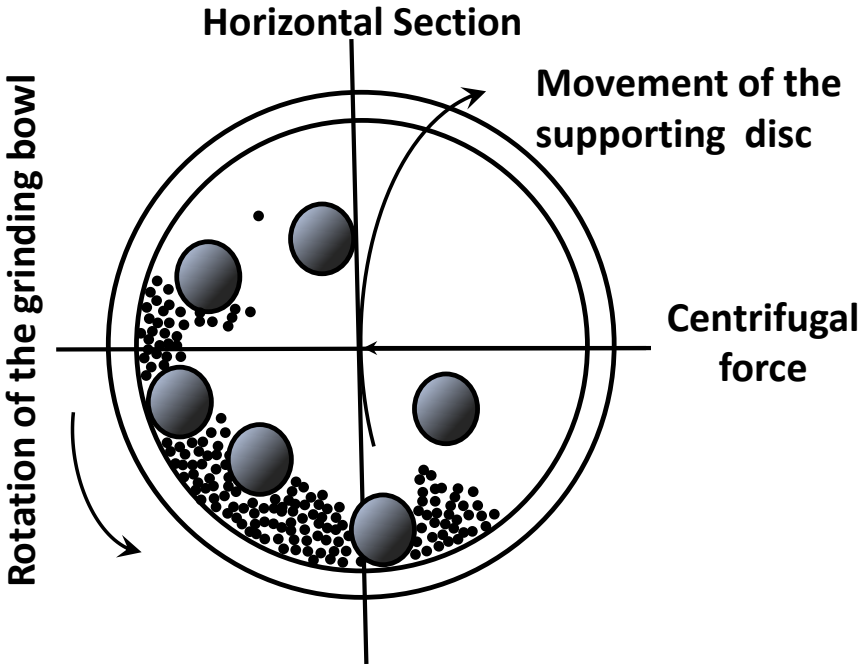


**Figure 1** Schematic illustrating the ball motion inside the ball mill **[1]**.

**Table 1** Mechanical milling conditions.

| Powders | SiC | | Al-SiC | | Al-Si | |
|---|---|---|---|---|---|---|
| | Fine | Coarse | Al | SiC | Al | Si |
| Average Particle Size(μm) | 0.3 | 2.5 | 300 | 0.3 | 300 | 45 |
| Mechanical milling | Vibratory ball-mill | | Planetary ball-mill | | | |
| Process Control Agent (PCA) | $C_2H_5OH$ | | $C_{18}H_{36}O_2$ | | | |
| Atmosphere | Air | | Ar | | | |
| Temperature | Room Temp. | | | | | |
| Ball size (mm) | 11 | | 3.2 | | | |
| Ball :Powder: PCA （Weight Ratio） | 5:1:1 | | 10:1:0.1 | | | |
| Time (ks) | 0-360 | | 36 | | | |
| Rotation Speed | 12.5Hz | | 150 rpm | | | |

## 3.2 Spark Plasma Sintering (SPS)

Spark plasma sintering (SPS) is a novel synthesis and processing technique -which enable sintering at low temperatures with short periods, by applying high temperature spark plasma generated momentarily in between powders. SPS is also regarded as a rapid sintering method because it utilizes self-heating action from inside the powder, similar to that of the self-propagating high temperature synthesis (SHS) and microwave sintering. SPS systems provide many merits as compared to the conventional systems using hot isostatic pressing (HIP), hot press (HP) sintering or atmospheric furnaces in such that this technique offers easier operational method combined with accurate control of sintering energy. Furthermore, a high sintering speed and reproducibility, reliability and safety can also be expected by using SPS. The SPS process is widely

used in the fabrication of many classes of materials such as fiber reinforced ceramics (FRC), functionally graded materials (FGMs) and metal matrix composites (MMC) which are difficult to sinter using the conventional sintering approach. It is due to this versatility also the SPS method has been chosen as the consolidation technique for sintering both SiC and Al composites powders in present theses. **Figure 2** illustrates the materials classes covered by SPS processing.

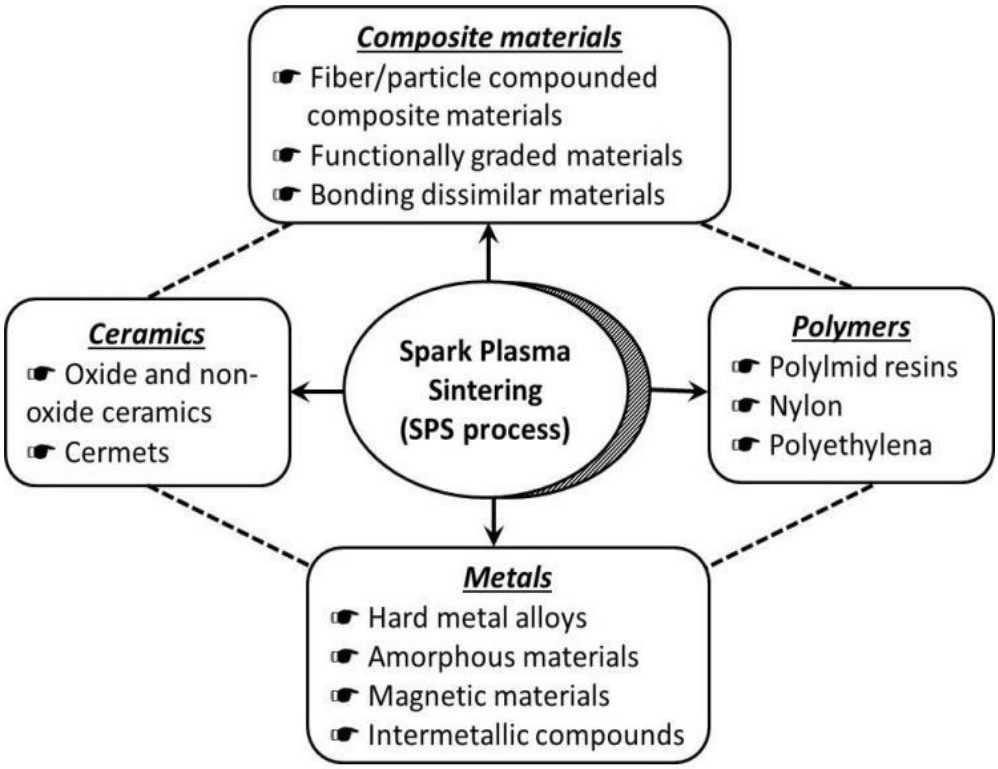


**Figure 2** Materials covered by SPS processing **[4]**.

The SPS process features a very high thermal efficiency because of the direct heating of the sintering graphite mold and stacked powder materials by the large spark pulse current. It can easily consolidate a homogeneous, high-quality sintered compact due to the the uniform heating, surface purification and activation made possible by dispersing the spark points **[4]**. **Figure 3** shows the schematic diagram of SPS process with die and

punch dimensions used in present work. In present work, (DR. SINTER 1020, Sumitomo) was applied to sinter both SiC and Al composites powder. The detailed SPS profile and sintering parameters are shown in **Figure 4** and **Table 2.**

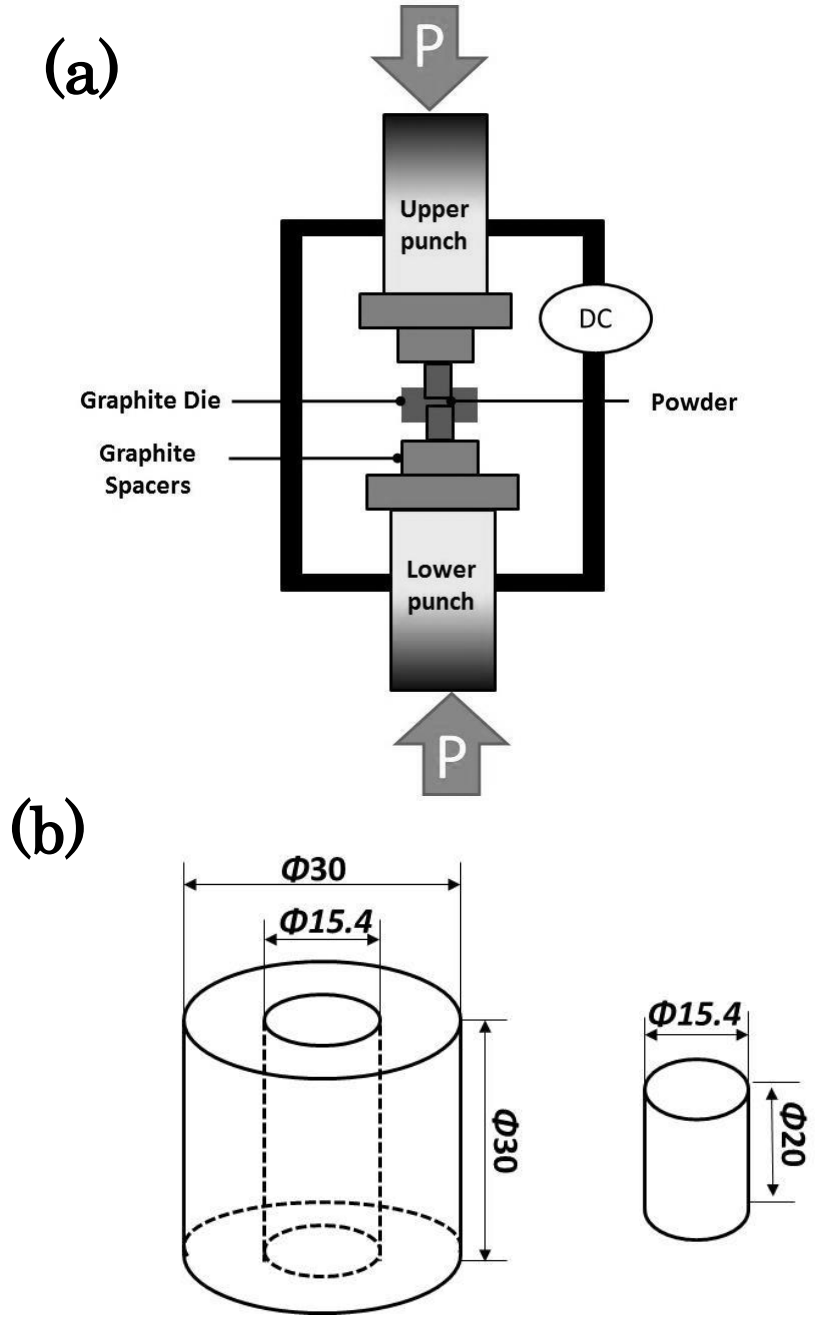


**Figure 3** a) Schematic diagram of SPS process **[12]** b) Die and punch dimensions.

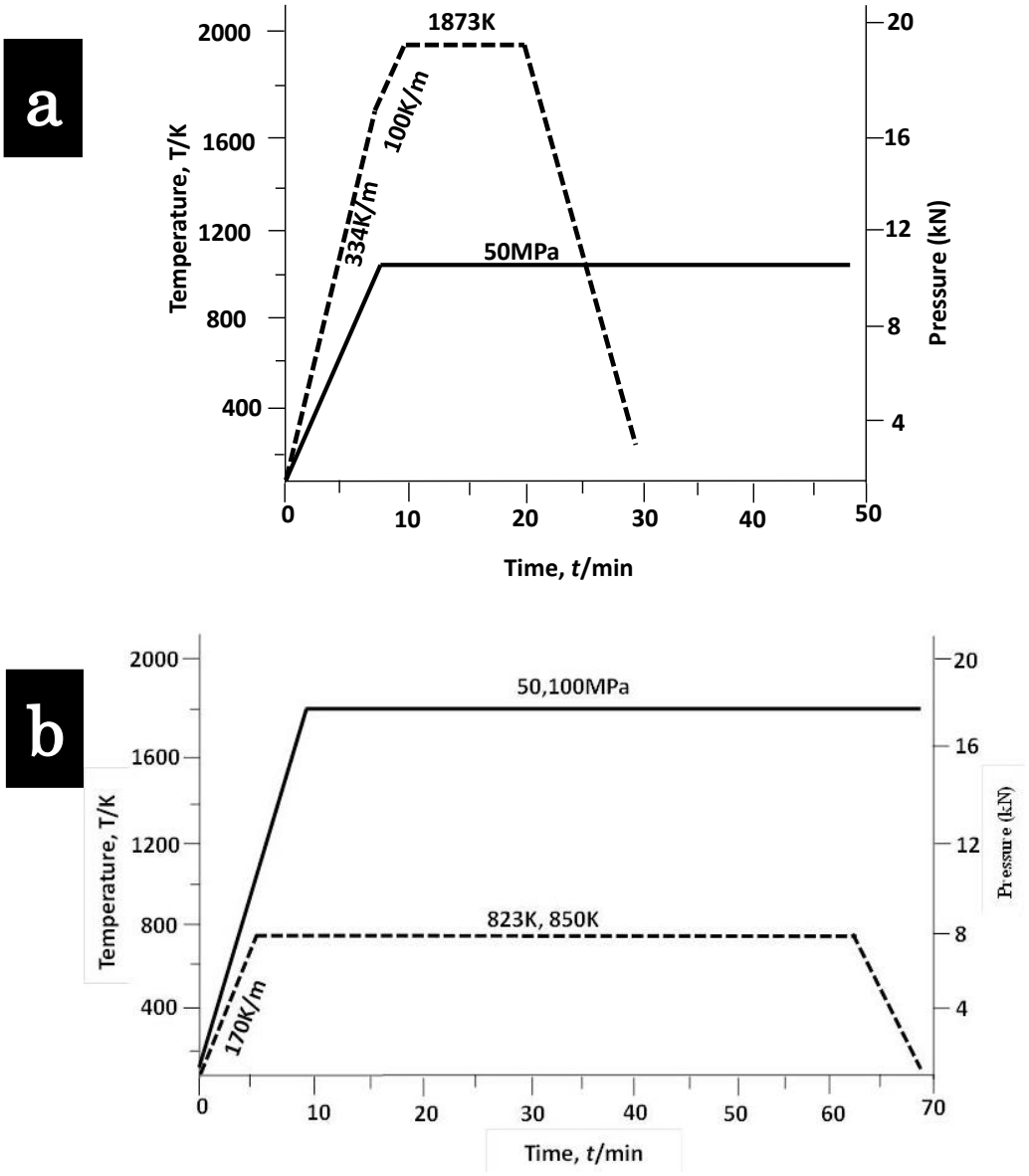


**Figure 4** SPS heat profile for a) SiC and b) Al-SiC, Al-Si powders compacts.

**Table 2** Spark plasma sintering conditions.

| Powders | SiC | Al-SiC | Al-Si |
|---|---|---|---|
| Temperature (K) | 1873 | 823 | 850 |
| Heating rate(K/min) | <1673K, 334 | 106 | 111 |
| | >1673K, 100 | | |
| Pressure (Mpa) | 50 | 100 | 50 |
| Holding time(ks) | 0.6 | 3.6 | 1.8 |
| Atmosphere | Vacuum | | |
| Cooling | Furnace | | |

## 3.3 Characterization

3.3.1 Particle Size Analyzer

The particle size analyzer is an apparatus meant to perform measurements on powders and to obtain size distribution of powders particle in real time. When compared to other methods, this method does not require a very low dilution, and the quantity of material used may vary greatly in proportion. The measurement range extends from 2 pAm to 100 pm or even to 500m depending on the specifications provided by manufacturer. The particle size distribution is calculated from the characteristics of the diffraction pattern when a coherent beam passed through a powder sample. As shown in **Figure 5**, a gas laser source emits a continuous beam of coherent light. Through the beam expander, the beam expanded and crosses the sample. A sample plane positioned beyond the samples measured, allows observation of the diffraction pattern at infinity in its focal plane **[5]**.

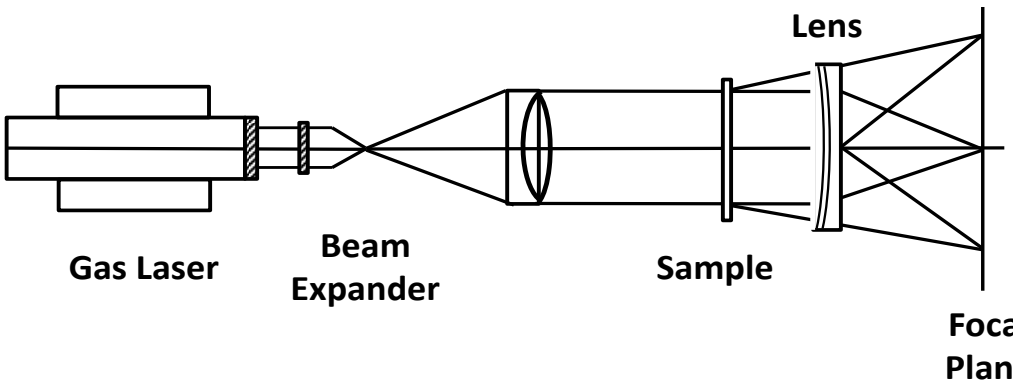


**Figure 5** Schematic diagrams illustrating the principle of particle size analyser **[5]**.

In this thesis, the particle size of each powder was measured using laser type particle size analyser (Shidmadzu SALD-2300, Japan). Prior to measurement, each powder was saluted in distilled water to enhance dispersions while avoiding agglomeration amongst powder particles. **Figure 6** illustrates the distribution data of as received Si powder obtained from Shidmadzu SALD-2300.

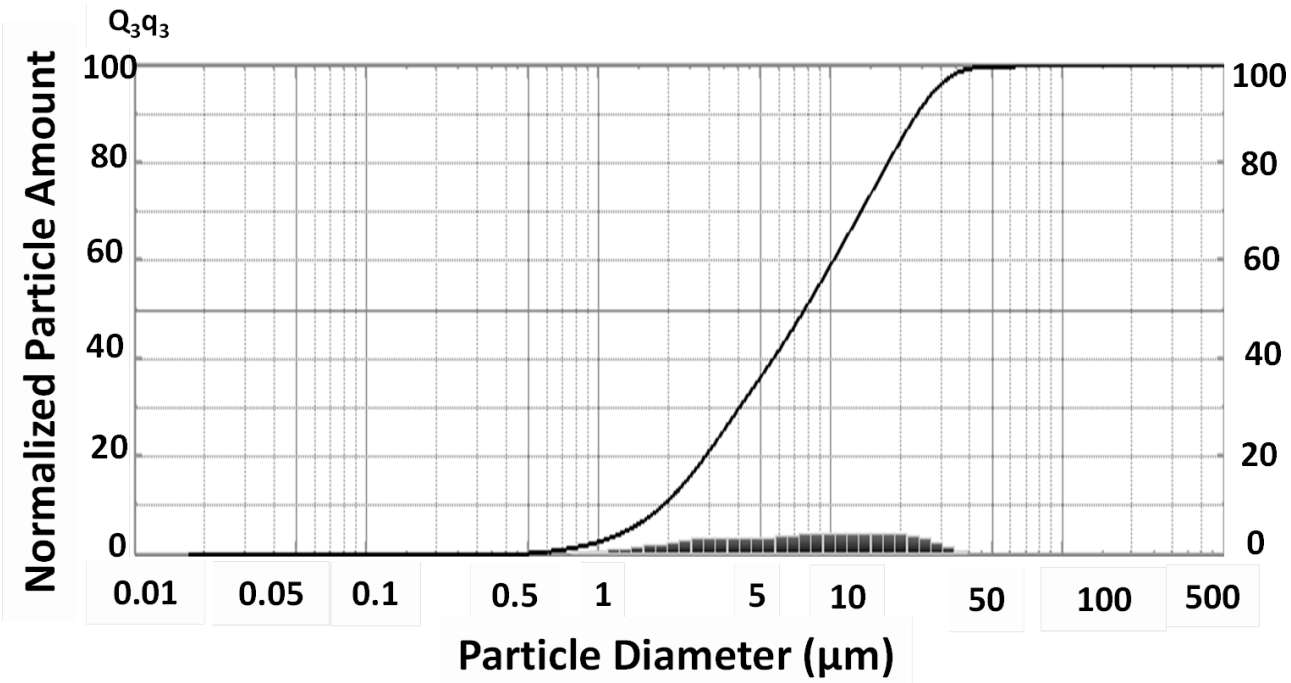


**Figure 6** Distribution data of as received Si powder obtained from Shidmadzu SALD-2300.

### 3.3.2 Scanning Electron Microscope (SEM)

The Scanning electron microscope (SEM) is an important and essential research and tool extensively used in many phases of industry especially in research and development field. The SEM provides higher resolution analysis and inspection than that afforded by current techniques using the optical microscope. Furthermore, unlike the optical microscope the SEM offers a wide variety of analytical modes, each contributing unique information regarding the physical, chemical, and electrical properties of a particular specimen. The SEM is being used in many applications in many fields especially research activities because of recent developments that eliminate or minimize sample damage and contamination, enabling continuous nondestructive in process inspection. In SEM, a finely focused beam of electrons is moved or scanned from point to point on the specimen surface in precise patterns**.**

The primary beam electrons originate from an electron source and are accelerated toward the specimen by a voltage usually between 200V (0.2kV) and 30,000(30kV). The electron beams travels down the column where it undergoes a multistep electron optical demagnification by one or more condenser lenses. This demagnification reduces the diameter of the electron beam from as large as several micrometers to nanometers dimensions. Depending on the application, magnification range, resolution required and specimen nature, the operator optimizes the image by choosing the proper accelerating voltage and amount of condenser lens demagnification.

One of major characteristics of the SEM, in contrast to the optical microscope is its great depth of field which is 100 to 500 times greater than that of an optical microscope, which enables the SEM to produce completely in-focus micrographs of relatively rough surfaces even at high magnifications **[6]**. In present work, SEM Hitachi SU6600 has

been used to observe and analyze both SiC and Al specimens.

Prior to observation using SEM, each specimen was subjected to polishing specific to its material type. For SiC specimens, they are polished using diamond and SiC papers on the STRUERS polishing unit. Firstly, the specimen surface was polished using 80 and 320 grit SiC paper disks. Subsequently, the specimens were polished in 120 grit diamond paper. Finally, the polished specimens were soaked in acetone and cleaned with in an ultrasonic bath. For Al samples, they are mechanically polished using SiC papers on the polishing unit (Strues). Firstly, the specimen surface was ground from 80~2000 grit SiC paper. Next, the specimens were buffed with 0.1μm $Al_2O_3$ followed by mechanical grinded by OP-S suspension (Strupers). OP-S suspension is a colloidal silica suspension for final polishing, which consists of negatively charged particles. Following this, the sample surface is slightly etched using Kellers etchant. The specific composition of the etchants is shown in **Table 3**.

**Table 3** Kellers etchant composition.

| Composition | Volume [ml] |
|---|---|
| $H_2O$ | 20 |
| HCl | 20 |
| $HNO_3$ | 20 |
| HF | 5 |

3.3.3 Energy Dispersive X-ray Spectroscopy (EDS)

Energy Dispersive Spectroscopy (EDS, also called EDX or Energy Dispersive X-ray Analysis) is the most widely used chemical analysis tool. It is generally used as an attachment to the Scanning Electron Microscope (SEM) and offers very significant advantages such as speedy analysis of specimen combined with the easier interpretation

of spectra. In general, the interaction of an electron beam with a sample generates a host of useful radiation types for analysis namely secondary and backscattered electrons, characteristic X-rays I and Auger electrons. The characteristic X-ray is used for EDS. EDS is commonly used for qualitative or semi-quantitative analysis **[7]**. **Figure 7** and **Figure 8** illustrate the qualitative analysis of a specimen indicating the concentration of selected elements and spectral analysis indicating elements present in Al sample.

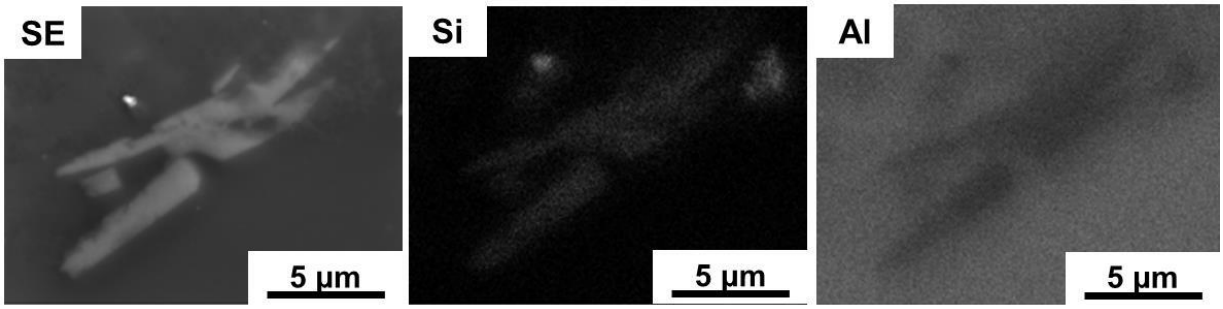


**Figure 7** SE image and corresponding dot maps of the specific elements indicating the concentration of Si and Al elements.

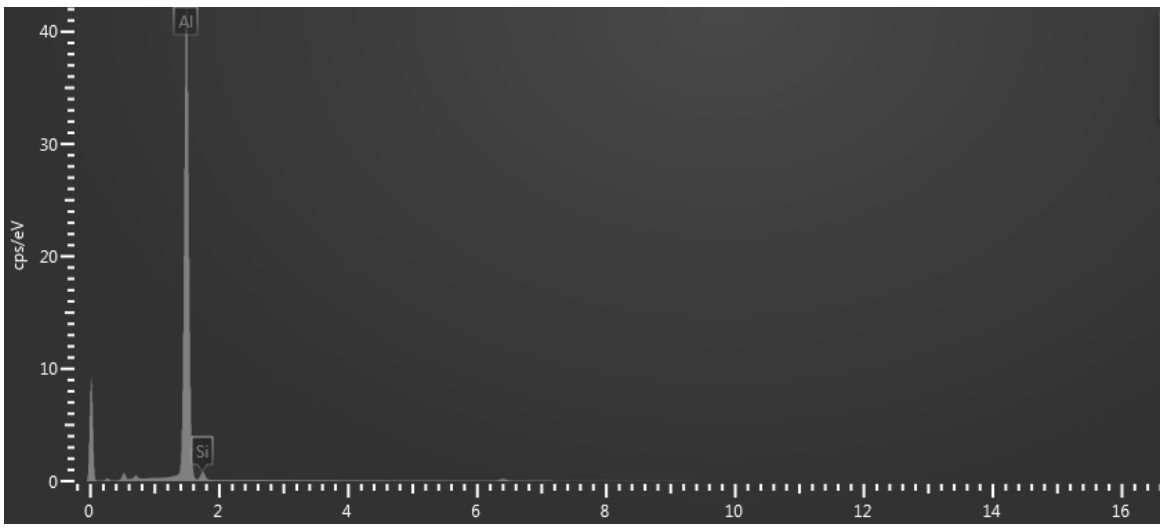


**Figure 8** Spectral analysis indicating the elements present in sample shown at Figure 7.

### 3.3.4 Electron Backscatter Diffraction (EBSD)

Electron backscatter diffraction (EBSD) is generally utilized as additional characterization technique to a scanning electron microscope (SEM). It does not only enables the characterization of individual grain orientations but also local texture of the grain, point-to point orientation privilege, combined with phase and distributions to be determined from surfaces of bulk polycrystals. The application offers many advantages such as the ease of sample preparation, high speed of data analysis combined with detailed information about the microstructure in submicron scale. For example, from the same specimen area, the characterization of the microstructure surface structure in detailed manner is enabled by the means of relief and orientation contrast in secondary and backscatter electron images. EBSD patterns are generated on a phosphor screen by backscatter diffraction of a stationary beam of high energy electrons from a volume of crystal material approximately 20 nm deep in the specimen, times the projected area of the incident beam. The characteristic feature of a backscatter Kikuchi pattern is the regular arrangement of parallel bright bands on a steep continuous background as shown in **Figure 9 [8]**.

**Figure 10** illustrates the essential elements of the instrumentation necessary to obtain Kikuchi patterns. An electron beam is incident as a stationary probe on the specimen at a glancing angle of less than 35°. A phosphor screen is placed close to the specimen to collect the backscattered electrons. A normal to the screen drawn from the point of electron incidence must subtend an angle greater than 70° and less than 120° with the incident beam. The screen is normally viewed using a low light sensitive television camera. In some instances a mechanism for inserting cut film in front of the screen has been adopted so that high quality patterns can be recorded **[9]**.

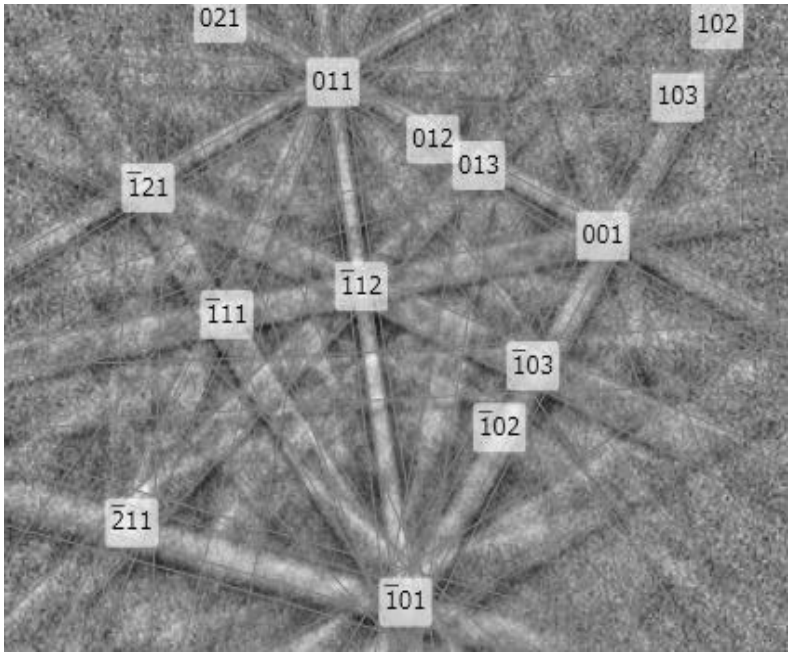


**Figure 9** Backscatter Kikuchi pattern and orientation for Al.

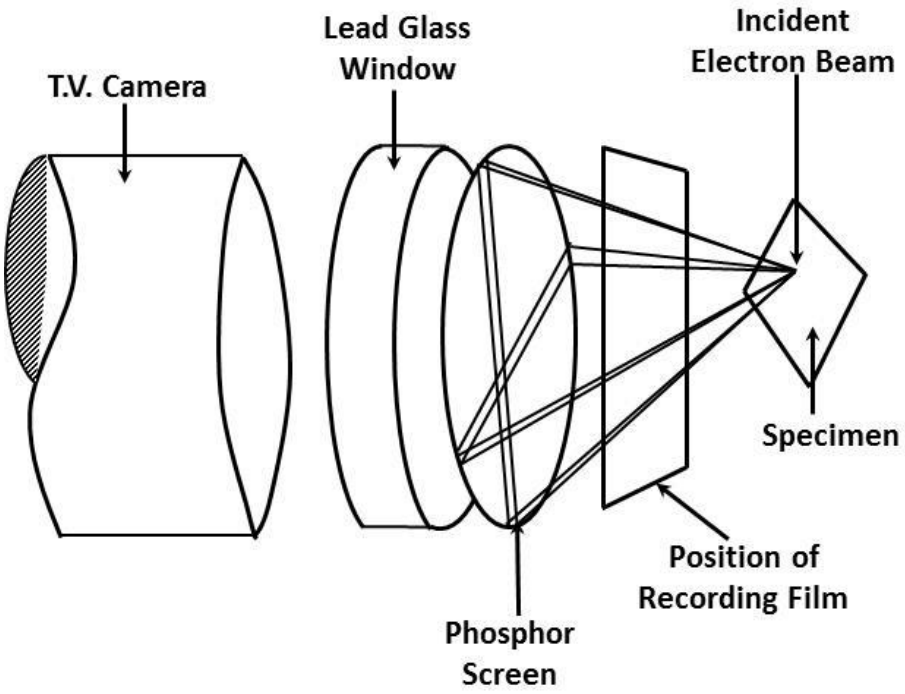


**Figure 10** Schematic diagram for detection of electron backscatter diffraction (EBSD) patterns **[9]**.

3.3.5 X-ray Diffraction (XRD)

X-ray diffraction is the definitive method for identifying minerals and other crystalline compound. X-rays are diffracted by the regular three-dimensional arrangements of atoms in crystals, and the resulting diffraction patterns are recorded by an imaging plate or detector. A diffraction pattern is diagnostic for a particular material, and can be used as a "fingerprint" for its identification. The diffraction patterns are compared against those in a computerized database to find a match. Additionally, X-ray diffraction can be used to determine unit-cell parameters and other structural details, and for quantitative analyses of mixtures of minerals and other crystalline phases.

**Figure 11** shows a schematic of an apparatus used to determine the angles at which diffraction occurs, known as diffractometer. A specimen in the form of a flat plate is supported so that rotations about the axis labeled O are possible; this axis is perpendicular to the plane of the page. The monochromatic x-ray beam is generated at X-ray source, and the intensities of diffracted beams are detected with a counter at detector. The specimen, x-ray source, and counter are all coplanar. The counter is mounted on a movable carriage that may also be rotated about the O axis; its angular position in terms of is marked on a graduated scale.4 Carriage and specimen are mechanically coupled such that a rotation of the specimen through is accompanied by a rotation of the counter; this assures that the incident and reflection angles are maintained equal to one another. **[10]**

In present work, XRD analysis for powders and powder compacts has been conducted using XRD-600 (Shidmadzu). Prior to XRD analysis, each sample is polished to have even and flat surface to obtain accurate data from XRD instrument. XRD conditions and parameters are shown in **Table 4.**

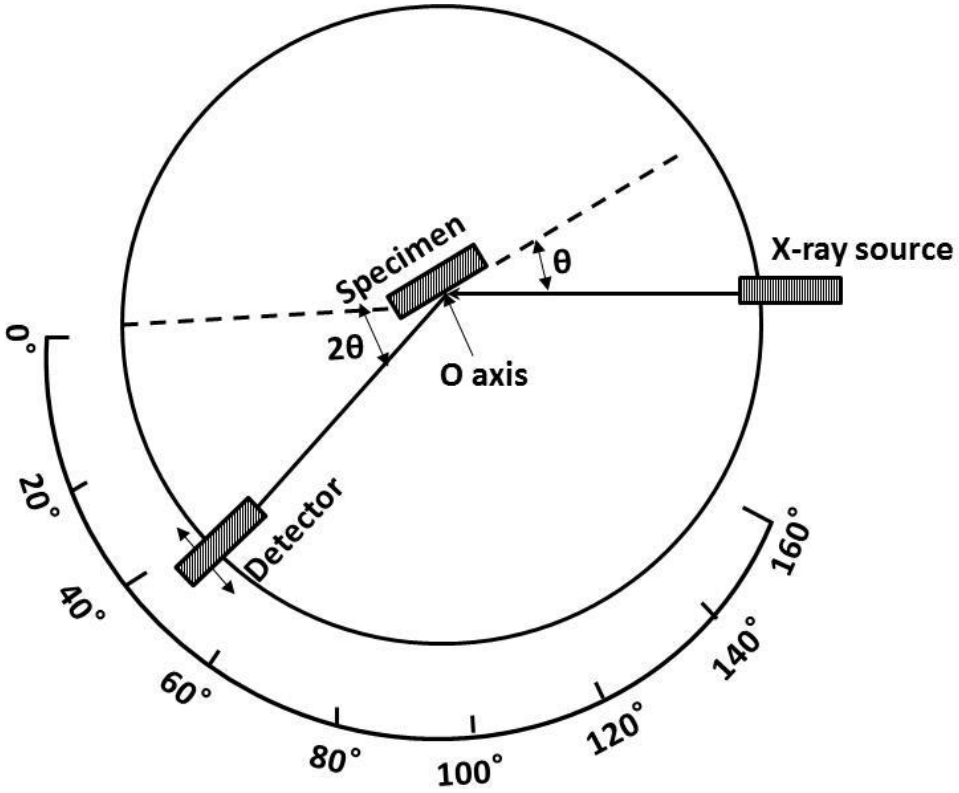


**Figure 11** Schematic diagram of an x-ray diffractometer **[10]**

**Table 4** X-ray diffractions conditions

| Target | CuKα |
|---|---|
| measuring mode | continuous |
| X-ray tube voltage | 40kV |
| X-ray tube current | 30mA |
| Scan range | 20°~100° |
| Sampling pitch | 0.02[deg] |
| Scan speed | 2deg/min |

3.3.6 Differential Scanning Calorimetry (DSC)

DSC is a method of thermal analysis that is widely used to study thermal transitions, i.e., solid-solid transitions as well as solid-liquid and various other transitions and reactions. A solid-solid phase transition would be if the material had its structure altered, but do not gain enough energy to become a liquid. By utilizing thermal analysis, understandings of material which do not demonstrate physical/ visual changes are possible. By understanding the technique and instrumentation of DSC, it is possible to understand what the materials go through during energy gain or loss.

Generally, in a DSC component, there are two pans isolated from the ambient environment in a chamber. One pan contains the sample to be analyzed, and the other pan is empty and is used as a reference pan. Both pans have heaters underneath them which are used to raise or lower the supplied temperature. Each pan also has a sensor that indicates what the temperatures of the pans are at any given moment. Using computer controlled sensors; the heaters are set to heat the pans at a constant rate (T/t) that is the rate of temperature change is the same **[11]**. **Figure 12** illustrates DSC profile of an exothermic reaction, when measured as heat flow a function of temperature

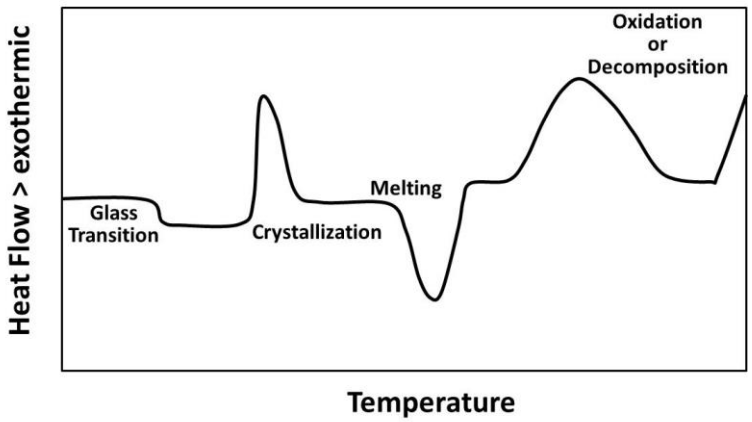


**Figure 12** Example of DSC profile illustrating exothermic heat flow is measured versus temperature **[11]** .

## 3.4 Mechanical Properties

3.4.1 Vickers Hardness Test

Hardness of specimens was measured using micro hardness tester (HMV-1, Shimadzu) based on Vickers indentation. As illustrated in **Figure 13**, Vickers ranges use a 136° pyramidal diamond indenter that forms a square indent. The indenter is pressed into the sample by controlled test force for a specific dwell time, normally being around 10~15s.After the dwelling time is over; the indenter is removed leaving an indent in the sample leaving a square shape on the samples surface and subsequently the size of the indent is determined optically by measuring the two diagonals of the square indent. The Vickers hardness value is obtained by the quotient of the test force, F and the indentation surface of the remaining indentation surface **[13]**. In present thesis, the Vickers indentation conditions were differed according to material type and hardness. The detailed conditions are shown in **Table 5**.

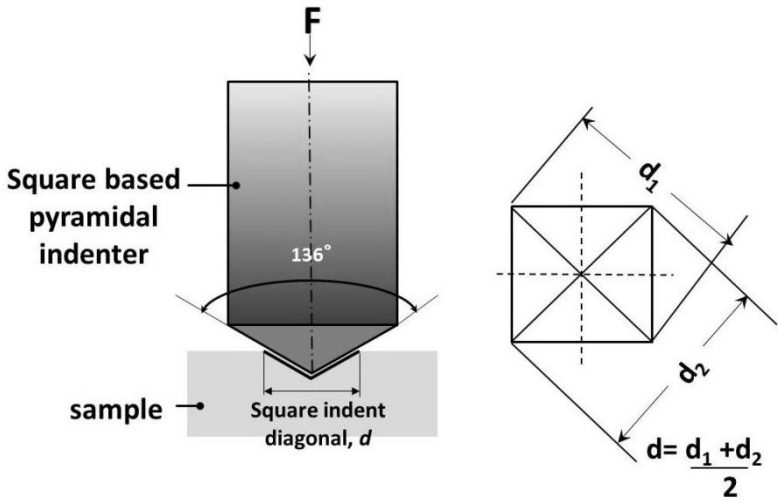


**Figure 13** Principle of Vickers hardness test **[13]**.

**Table 5** Vickers Hardness indentation conditions.

| Material | SiC | Al-SiC | Al-Si |
|---|---|---|---|
| Time[s] | 5 | | |
| Load N [Hv] | 9.807 [1] | 0.09807 [0.01] | |

3.4.2 Four Point Bend Test

Unlike metallic materials, stress-strain behavior of brittle ceramic is not usually obtained by tensile test for three reasons; 1) difficulty to grip brittle material without fracturing them, 2) difficulty to prepare and test specimens having the required geometry and 3) usually ceramics fails after only about 0.1% strain which necessitates that tensile specimen to be perfectly aligned to avoid any presence of bending strength which is difficult. For these reasons, the three or four point bend test is usually applied to determine the strength of brittle ceramic**[9]**. In this thesis, to evaluate the strength of SiC powder compacts, 4-point bend test has been conducted using Shimadzu Autograph AG-50kNXplus machine. **Figure 14** illustrates the schematic of four point bend test. Flexural strength, $\sigma$ was calculated from equation (3.1) **[14]**. The bend test conditions are shown in **Table 6.**

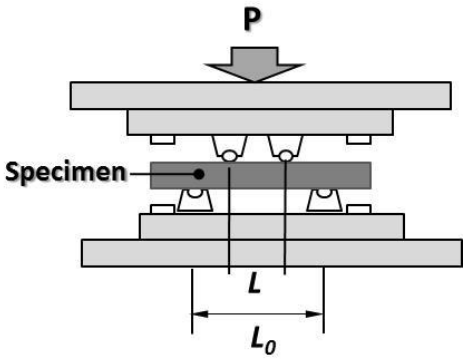


**Figure 14** Schematic of four point bending test.

$$\sigma = \frac{3P\,(L_0 - L)}{2WD^2} \quad \cdots (3.1)$$

*P*: fracture load [N],
$L_0$: Specimen length [mm],
*L*: Loading Span Length [mm]
*W*: Specimen width [mm],
*D*: specimen thickness [mm]

**Table 6** Four point bend test conditions.

| | |
|---|---|
| Load [N] | 500 |
| Crosshead [mm/min] | 0.1 |
| Specimen dimension | 13mm x 4mm x 2mm |

3.4.3 Tensile Test

In present work, to determine the stress strain behavior of Al-SiC and Al-Si composite compacts, mini tensile test has been conducted using universal testing machine (Autograph AGS-10k ND, Shidmadzu) under displacement control. The specimen for tensile test was prepared to be having dimensions as shown in **Figure 15**. For every powder compacts conditions, at least 3 samples each were evaluated. The detailed conditions for tensile evaluation are shown in **Table 7**.

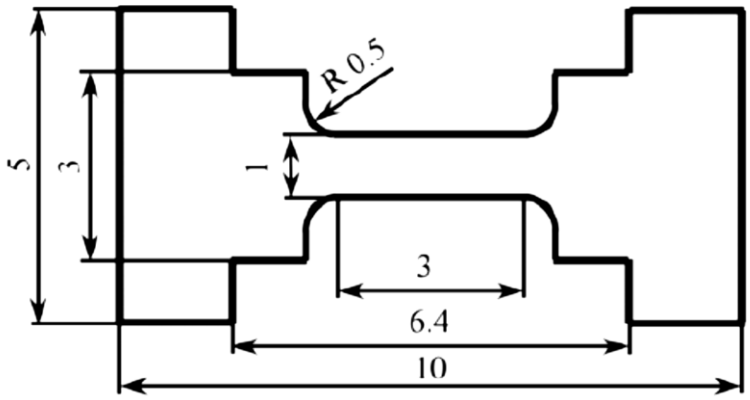


**Figure 15** Dimension of tensile test specimen (in mm).

**Table 7** Tensile test conditions.

| | |
|---|---|
| Gauge Length[mm] | 3 |
| Gauge width[mm] | 1 |
| Gauge thickness[mm] | 1 |
| Cross-head speed[mm/min] | 0.1 |
| Nominal strain rate[$s^{-1}$] | $2.7 \times 10^{-3} s^{-1}$ |

## REFERENCES:

**[1]** C. Suryanarayana, Mechanical alloying and milling, Progress in Materials Science, 46 (2001) pp.1-184.

**[2]** D.L. Zhang, Prog. Mater. Sci., 49 (2004), pp. 537–560.

**[3]** P. Balaz, "*Mechanochemistry in Nanoscience and Minerals Engineering*", Springer-Verlag Berlin Heidelberg (2008) pp. 103-132.

**[4]** M.Tokita, Mechanism of Spark Plasma Sintering, Proceeding of NEDO International Symposium on Functionally Graded Materials Vol.22 (1999) pp.1-2.

**[5]** J. Cornillault, Particle Size Analyzer, Applied Optics, Vol.11, No.2 (1972) pp.265.

**[6]** J. Orloff, Handbook of Charged Particle, (1997) Optics, pp.364-365.

**[7]** P.D. Ngo, Failure Analysis of Integrated Circuits, (1999), pp.205-212.

**[8]** A.J. Schwartz *et al*, Electron Backscatter Diffraction in Material Science 2nd ed,(2009), pp.1-2.

**[9]** D.J. Dingley *et al*, Electron backscatter diffraction and orientation imaging microscopy, Materials Science and Technology Vol.13 (1997) pp.69-70.

**[10]** W.D. Callister, Jr, Materials Science and Engineering, 7th ed, (2007), pp.66-69.

**[11]** K. Lukas et al, Differential Scanning Calorimetry: Fundamental Overview, Vol.14 Issue 8, (2009), pp.807-817.

**[12]** V.N. Chuvildeev, D.V. Panov, M.S. Boldin, A.V. Nokhrin, Yu.V.

Blagoveshchensky, N.V. Sakharov, S.V. Shotin, D.N. Kotkov, Acta Astronaut. 109 (2015), pp. 172-176.

**[13]** K.Herrmann: *"Hardness Testing: Principles and Applications"*, ASM International (2011) pp.44.

**[14]** Kantesh Balani et al., "*Biosurfaces: A Materials Science and Engineering Perspective"*, 1st ed, John Wiley & Sons, Inc (2015), pp.51-52.

# Chapter 4

# Improvement of SiC Ceramic Sinterability via Particle Size Distribution (PSD) Control

## 4.1 Introduction

Owing to its exceptional thermal and mechanical properties, Silicon Carbide (SiC) is an excellent candidate for high temperature applications **[1-5]**. Nevertheless, it's highly covalent bonded nature which results into the low self-diffusion coefficient has made sintering of SiC a rather intriguing topic **[6, 7]**. The conventional solid state sintering of SiC includes the sintering in extremely high temperatures up to 2200°C combined with prolonged sintering time in order to attain full densified compacts **[7, 8]**. In general, the conventional solid state sintering which include prolonged sintering with high temperature will induce the grain growth phenomenon, which deteriorates the final properties of sintered products. Considering the particle size distribution (PSD), in order to attain dense, uniform and fine-grained microstructure, the emphasis has been made by earlier researchers on the usage of mono-sized powder of narrow distribution **[9-12]**. Patterson and Griffin **[13]** has demonstrated that the increasing of PSD leads to the better densification in coarse spherical powder. On the other hand, in fine tungsten powder, when compared to the intermediate distribution, the widest and narrowest distribution appears to have the most rapid densification. Later on, Yeah and Sacks **[14]** have reported that, due the higher starting green density, broader distribution is preferred for better sinterability pertaining to commercial alumina powder. In other work, Ma and Lim **[15]** claimed that narrow PSD provides better sinterability due to the

microstructural homogeneity of the green compact and thus is preferred for practical use, provided that the initial powder is agglomerate-free. It is also mentioned that the optimum PSD for a given powder system vary with regard to its consolidation technique and condition used. In recent work, Andreas et. al **[16]** have simulated the effect of PSD on solid state sintering for several patterns of PSD (normal, log-normal and bimodal) . It has been demonstrated that the densification rate is decreasing with the increasing of the distribution width with polydispersity in PSD. This is associated with the higher average contacts coupled with lower coordination number in the initial packing structure. From these literatures, it appears that the dependence of sinter ability on the PSD is rather complicated and inconsistent to interpret since it varies to a great extent depending on the sintering mechanism and material used. Therefore, this work is aimed to investigate the effect of dispersion in particle size distribution on sinterability in SiC ceramic. Present work also discusses the appropriate dispersion measure for distributions having different variables, namely mean and standard deviation. In this work, SiC powders were subjected to mechanical milling to produce various kinds of particle size distributions. In order to increase the dispersion in the milled powder, wet milling is adopted while mechanical milling is conducted **[17]**. The milled powders were subsequently subjected to spark plasma sintering to make a compact and the sinter ability was evaluated by measuring the relative density and flexural strength. Moreover, the evolution of powder particles morphology is also discussed.

## 4.2 Experimental Procedures

In present work, coarse α-SiC powder of 2.5 μm and fine SiC powder of 0.3μm were used as starting material. In order to produce various particle size distribution patterns, each powder were subjected to vibratory mechanical milling for total of time 0ks~360ks.

The wet milling was adopted using ethanol in the ratio of 1:1 to minimize the agglomeration during milling. The vibration of the vibratory milling was kept at a constant frequency of 12.5Hz and the ratio of the ball to milled powder was 5:1 by weight. The milled powder was sieved to eliminate the hard agglomerates. The particle size was subsequently measured by laser diffraction particle size analyser (Shidmadzu SALD-2300, Japan) using 10 different powder samples to get the average distribution pattern for each powder. The morphology of the milled powders were observed using Field Emission Scanning Electron Microscope (FE-SEM S-4800, Hitachi Japan) and subsequently milled powders were subjected to SPS at 1873 K for 0.6ks under an applied pressure of 50 MPa. Density of the sintered compacts was measured by the quotient of the weight and its dimension. The sintered compacts were carefully polished and microstructural observation was conducted by SEM and the mechanical properties were evaluated by 4-point bend test. The dimension of the bend test specimen was 13mm x 4mm x 2mm specimens, with crosshead of 0.1mm/min.

## 4.3 Results

### 4.3.1 Effect of Mechanical Milling to Particle Morphology and PSD

**Figure 1** illustrates the morphology of both as received and milled coarse SiC powders at low and high magnifications. As shown in Fig.1 (a), as received coarse powder has angular morphology. It is worth mentioning that the initial coarse powder also consists of significant amount of nano-sized particles, as shown in Fig.1 (b). Hence, the initial SiC coarse powder appears to consist of two different size regimes, namely coarse micron-sized and fine nano-sized particles. As shown in Fig. 1 (c), it can be observed that after milling for 144ks, the coarse particles have fragmented to smaller particles. This can be attributed to the intense impact of ball while milling was

conducted. As the particle morphology is concerned, it can be observed that in the milled powders, a wide range of particles exists and the particles demonstrate somewhat a mixture of angular and partially rounded. Figure 1(d) shows the remained coarse particle after milling and it shows a partially rounded morphology. Moreover, the existence of many nano-sized particles after milling was also observed. As shown in Fig. 1(e) further milling up to 360 ks results in further fragmentation of SiC particles, resulting in the formation of nano-sized particles. The final shape of the particles is somewhat rounded, as shown in Fig. 1 (f). Similarly, **Figure 2** illustrates the morphology of both as received and the milled fine SiC powders at low and high magnifications .From Fig. 2 (a), it can be observed that as received fine powder particles have angular morphology. It is worth mentioning that this powder initially consists of many nano-size particles as shown in Fig. 2 (b). As can be observed from Fig. 2 (c), after milling for 144 ks is conducted, the fragmentation occurred to most of the particles. Nonetheless, the powder particles do not demonstrate any significant change as the powder particles remained angular (Fig. 2 (d)). It is to justify that these morphological observations also indicate that there are no obvious agglomeration observed. This might be associated with the adoption of ethanol as PCA in the mechanical milling process. It is well known that, fine-sized particles are prone to induce agglomeration due to its higher interparticle attractive forces, which is associated with poor resistant to dispersion. This is undesirable due to the poor flow of powder during compaction, leading to decreased packing density. The usage of ethanol in this work induces the particle-particle dispersion, hindering the agglomeration amongst the SiC particles.

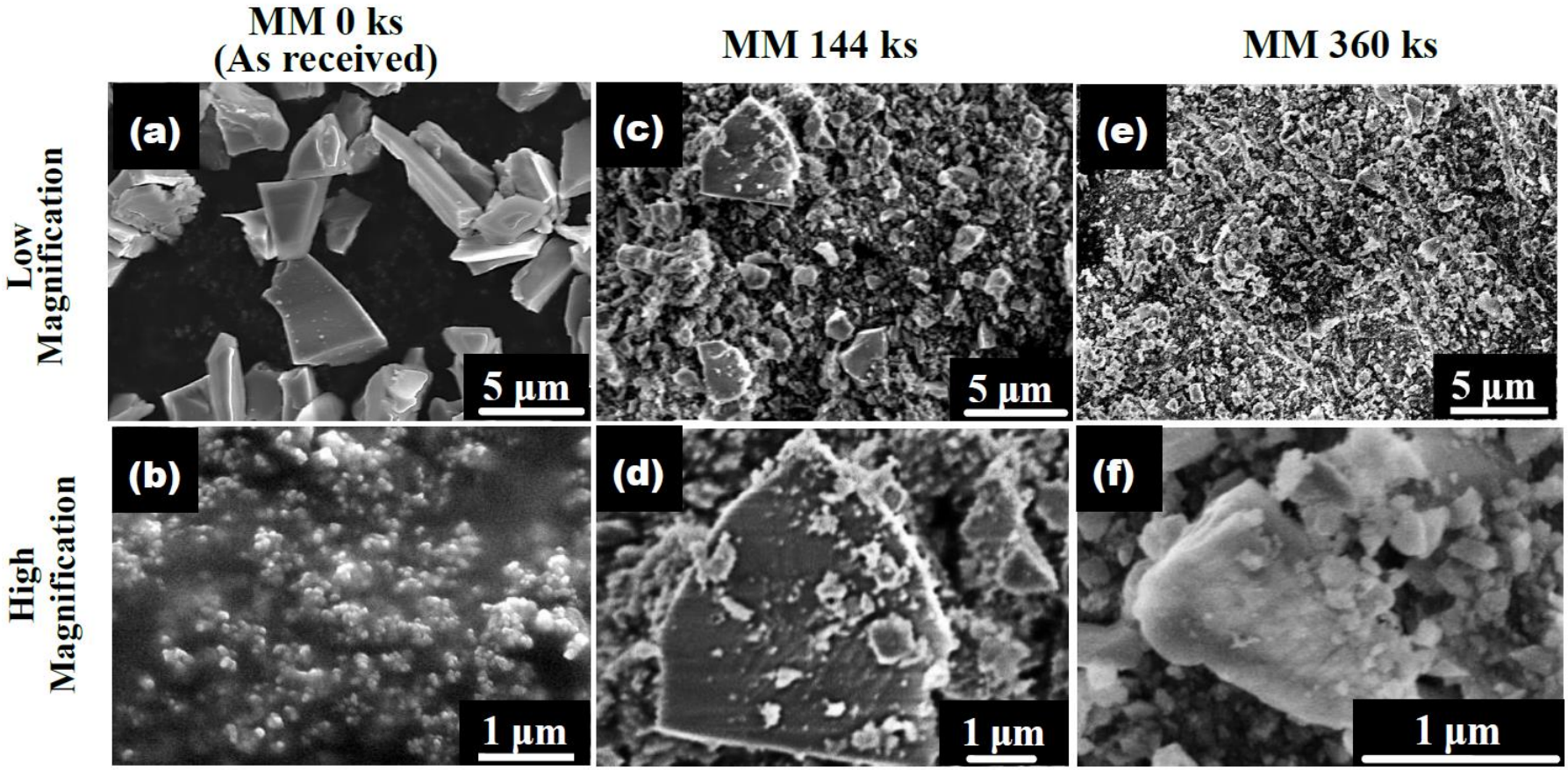


**Figure 1** SEM micrographs of coarse SiC powders in low and high magnifications (a) and (b) are as received powders, (c) and (d) are MM 144 ks powders , (e) and (f) are MM 360 ks powders.

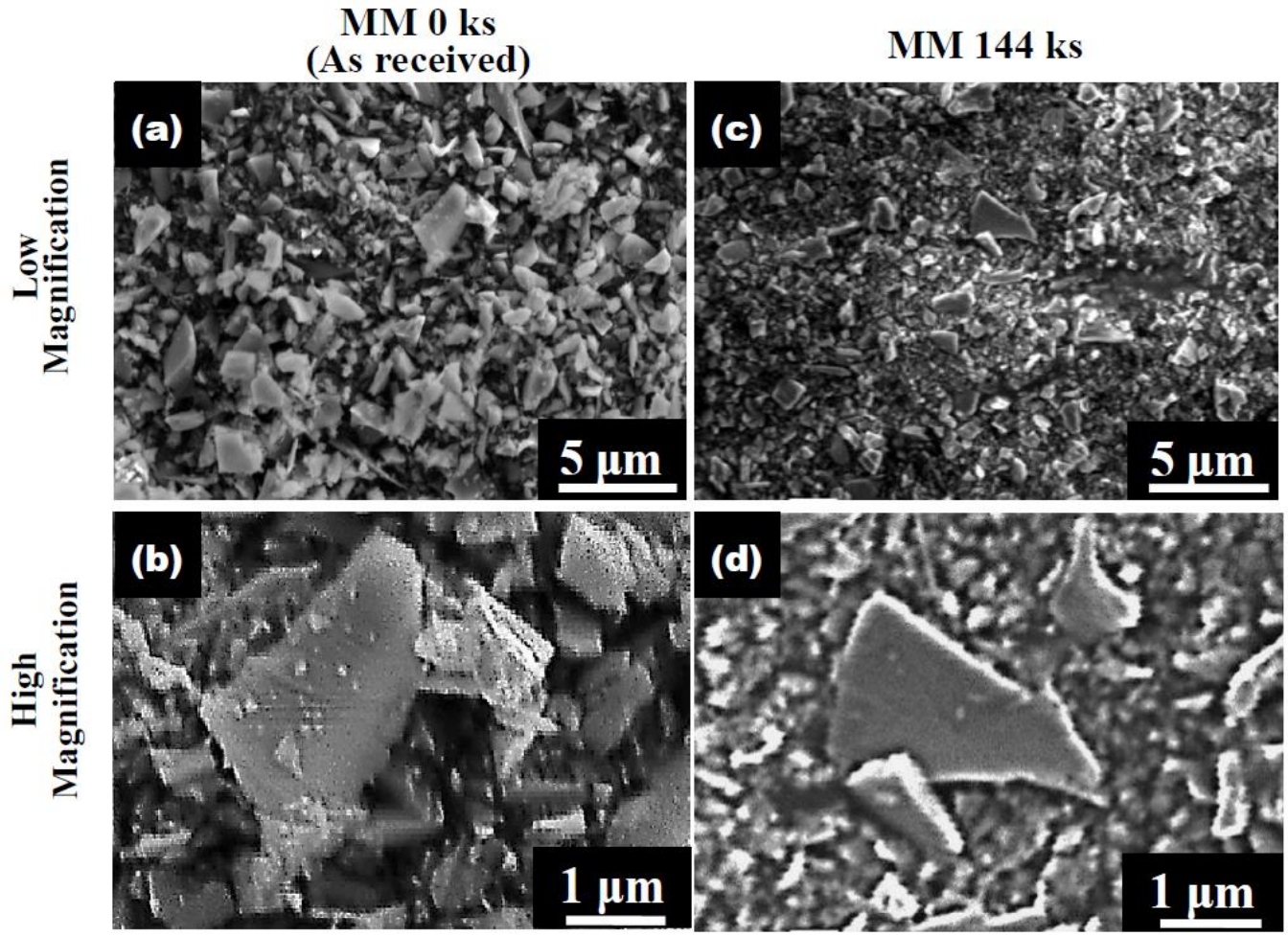


**Figure 2** SEM micrographs of fine SiC powders in low and high magnifications (a) and (b) are as received powders, (c) and (d) are MM 144 ks powders.

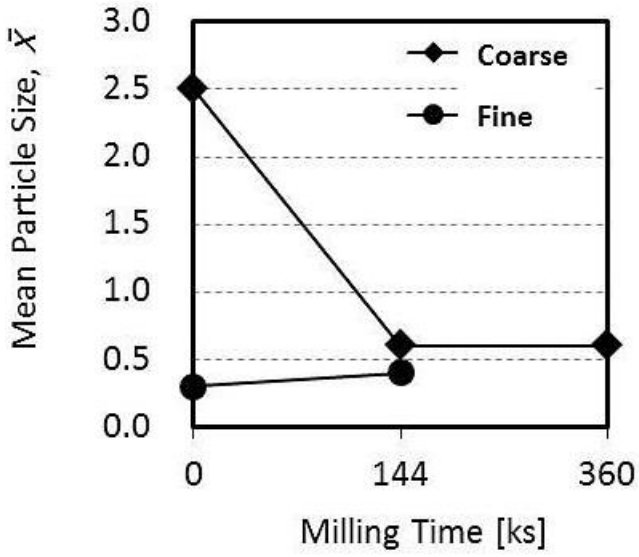


**Figure 3** Relationship between mean particle size and milling time.

Relationship between mean particle size and milling time for both coarse and fine powders is shown in **Figure 3**. With regard to coarse powder, it is observed that mechanical milling results in significant reduction in particle size as the milling time is increasing in the initial stage. However, as the milling time reaches 144 ks, the particle size remains constant and no further fragmentation was observed. However, it is interesting to mention that regardless of the significant particles fragmentation as observed in SEM for powders milled between 144ks and 360ks (Figs. 1(c)-1(f)), the mean particle size remains unchanged. This is due to the existence of significantly larger number fraction of finer particles as compared to the coarser particles in the MM 144 ks powder which results in no significant effect of coarser particles to the overall powder mass. It is to justify that the variation of particles size is expected to have more significant effect on the densification rather than the slight variation in the mean particle size of the overall powder. Accordingly, with regard to fine powder, mechanical milling resulted in no significant effect to the mean particle size and this might be associated to the particle fragmentation under present milling condition.

The PSD for both as received and milled SiC powders is illustrated in **Figure 4**. Apparently, the as received coarse powder demonstrates a bimodal distribution consisting of two distinct peaks namely coarse and fine peaks (Fig. 4(a)). From Fig. 4(b), as the milling time increases to 144ks, it is noted that the peak corresponding to coarse particles decreased significantly and is shifted toward relatively smaller particle size. These observations indicate that the fragmentation occurred to the particles with size larger than 1 μm. Furthermore, the PSD is observed to be broadened while retaining somewhat a bimodal distribution. Further milling up to 360 ks results in a complete disappearance of the coarser peak, which indicates that particles with size

larger than 1 μm are subsequently fragmented leading to a broadened unimodal distribution. It is also interesting to note that the final PSD exhibits a skewed right distribution. In this context, skewed distribution is a frequently used statistical term in which used to describe distribution in which one of its tails is stretched out longer than the other. Moreover, the skewness direction takes the side of the longer tail **[18]**.

The PSD of as received and milled SiC fine powder is shown in **Figure 5**. From Fig. 5(a), it is observed that initial fine powder had a narrow bimodal distribution. As shown in Fig. 5(b), mechanical milling up to 144 ks results in formation of a broadened unimodal distribution. These observation again confirms that the fragmentation under present milling condition is only limited to particle with size larger than 1 μm. Similarly, the final PSD also demonstrates a skewed right distribution. From these observations, the effect of mechanical milling to particle morphology and PSD can be summarized as follows; (1) With regard to coarse powders, mechanical milling results to significant reduction of particle mean size and reduction of particle aspect ratio while for fine powders, mechanical milling results in no significant reduction in both mean particle size and particle aspect ratio (3) mechanical milling induce the fragmentation of particle size larger than 1 μm, which results in a broadened unimodal size distribution for both coarse and fine powders.

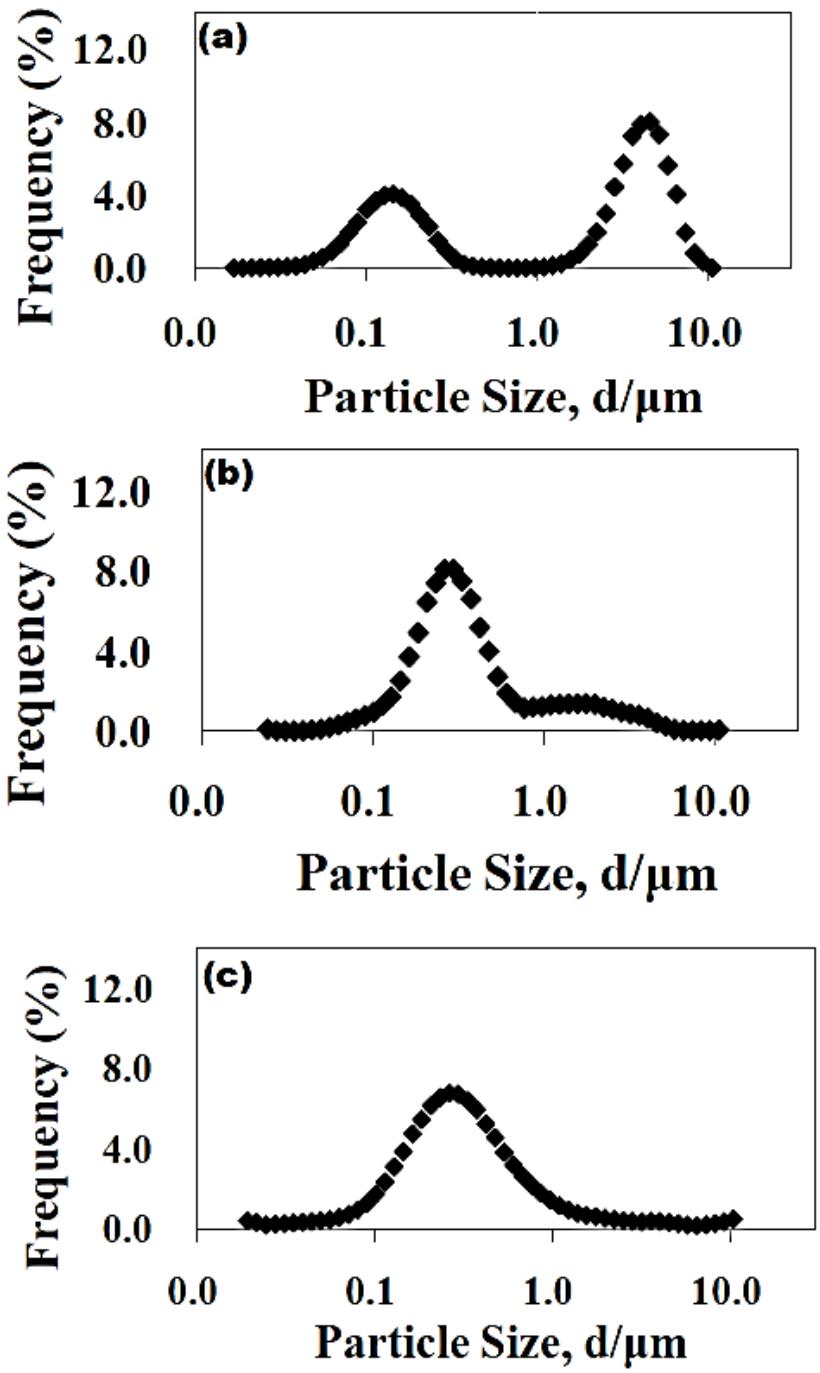


**Figure 4** Particle size distributions of coarse SiC powders (a) As received (b) MM 144 ks (c) MM 360 ks.

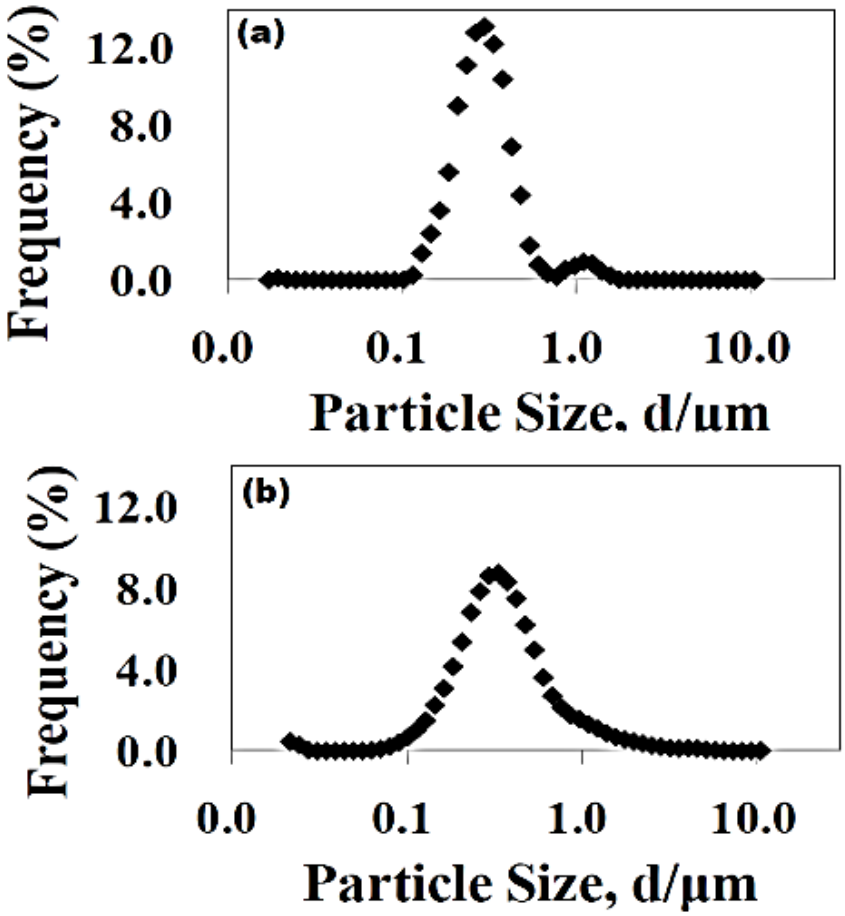


**Figure 5** Particle size distributions of fine SiC powders (a) As received (b) MM 144 ks.

4.3.2 Relative Density and Mechanical Properties

The relation between relative density and flexural strength of powder sintered compacts with milling time is shown in **Figure 6** and each value is summarized in **Table 2**. The density of sintered powder was calculated by the dividing the weight of the compact by its dimensions, while the mechanical properties were evaluated by 4-point bend test using three samples for each powder condition. As the milling time increases, it can be noted that both the relative density and flexural strength also increases. This can be associated with the increase in specific surface area in the mechanically milled powder, leading to a more surface energy resulting in a quicker sintering. Furthermore, mechanically milled powders consist of various particle sizes which improve the packing structure in the powder compacts, resulting in a higher densifications by providing shorter diffusions distances for atoms **[19, 20]**. In contrary, it is noted that the flexural strength and the relative density for the fine powder compacts do not demonstrate any significant changes with milling time. This can be explained in such that under present milling condition, the fragmentation of SiC powders is limited, resulting in no significant increase to the surface energy and the subsequent densification rate as mentioned above.

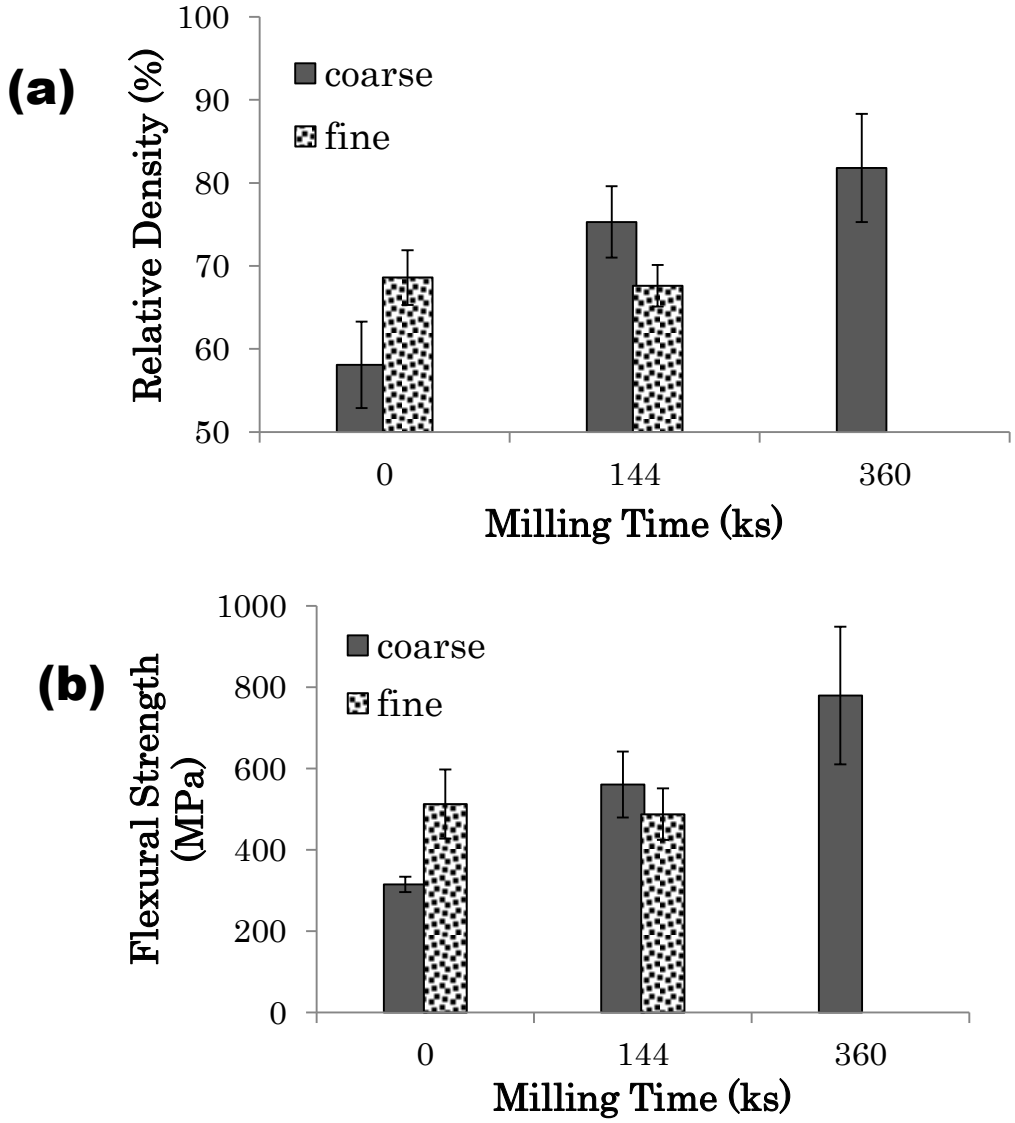


**Figure 6** Relationship between (a) relative density and (b) flexural strength as a function of milling time.

**Table 2** Relative density and mechanical properties of SiC compact.

| | Milling Time (ks) | Relative Denisty (%) | Flexural Strength(MPa) |
|---|---|---|---|
| Coarse | 0 (As received) | 58.1±5.2 | 315±18.8 |
| | 144 | 75.3±4.3 | 561±80.9 |
| | 360 | 81.8±6.5 | 780±169.3 |
| Fine | 0 (As received) | 68.6±3.3 | 513±84.8 |
| | 144 | 67.6±2.5 | 488±63.3 |

## 4.4 Discussions

4.4.1 Dispersion Measures in PSD

4.4.1.1 Variance and Standard Deviation

In present work, the typical dispersion measures for frequency distribution namely sample standard deviation, $s$ and sample variance, $s^2$ are used to define the dispersion level in PSD. Those measures are calculated using the equation (4.1) and (4.2) shown below 18);

$$\text{Sample standard deviation, } s = \sqrt{\Sigma x^2 f - ((\Sigma xf)^2/\Sigma f) / \Sigma f - 1} \qquad (4.1)$$

$$\text{Sample variance, } s^2 = \Sigma x^2 f - ((\Sigma xf)^2/\Sigma f) / \Sigma f - 1 \qquad (4.2)$$

In above equations, $x$ indicates the particle size while $f$ refers to the frequency of particle on the specific $x$ values.

4.4.1.2 Coefficient of Variation, Cv

It is already mentioned in 4.4.1 that the most commonly used dispersion measure in statistic is variance and standard deviation. While variance measured in the square units of the variable under study, standard deviation on the other hand is expressed in the same units as the respective variable, leading to an easier interpretation of the standard deviation. However, when all the variables do not pose the identical mean values and are not expressed in the same measurement, the standard deviation is not the most appropriate dispersion measure to compare several distributions having different variables. In this context, the Coefficient of variation, Cv provides a more reliable solution by measuring the relative dispersion, which is expressed by the quotient of

standard deviation and its arithmetic mean. The equation is shown below;

$$\text{Coefficient of variation, } C_v = s/\bar{x} \qquad (4.3)$$

where $s$ and $\bar{x}$ represent sample standard deviation and sample mean respectively. $\bar{x}$ value is calculated using the following equation;

$$\text{Sample mean, } \bar{x} = \Sigma xf/n \qquad (4.4)$$

where $n = \Sigma f$

The distribution with largest Cv value implies that it has the highest relative dispersion around mean. Furthermore, Cv is also a practical and dimensionless measure in order to compare several distributions having different variables, as it is a normalized statistical measure **[21-22]**. However, it is important to note that value is only applicable when the expected values are not negative or zero. Thus, Cv is introduced as an alternative dispersion measure for PSD because the mean size of PSD range investigated in present work is not identical.

### 4.4.2 Correlation between PSD Parameters and Sinterability

The relation between relative density and when plotted using three dispersion parameters namely standard deviation $s$, variance $s^2$ and coefficient of variation Cv are shown in **Figure 7**. Similarly, **Figure 8** shows the relation of flexural strength when plotted with those dispersion measures. It is important to mention that, density and flexural strength are used as indicator to determine the preciseness of those dispersion measures. In general, flexural strength is dependent on the relative density in such that, higher relative density leads to higher flexural strength due to the stronger interparticle bonding which inhibit the crack propagation in compact with higher relative density. From these observations, it can be noted that when experimental results namely

relative density and flexural strength are plotted using standard deviation, *s*, and variance, $s^2$, a clear and reliable correlation between these dispersion measures and those experimental results. At this juncture, it is worth mentioning that this is expected, because standard deviation and variance are not the most appropriate dispersion measure for describing dispersion level in several distributions having different mean size. Generally, in order to compare several distributions, it is essential to set the mean particle size constant so that the dispersion measure will be reliable. However, when the experimental results are plotted using the coefficient of variation Cv, it is observed that the experimental data exhibit a positive linear relation. As mentioned above, it is expected that the higher Cv value which implies higher relative dispersion will lead to improvement of relative density and flexural strength. This is attributed to the improvement of the packing density owing to the gap filling ability of finer particles, leading to enhancement of the particle average coordination number and particle rearrangement which subsequently favors the sintering. It is already mentioned in the introduction of present paper that several significant efforts have been devoted to investigate the dependence of dispersion in PSD to sinter ability **[9-15]**. However, in these works, it is reported that the mean particle size of the initial powders have to be made constant before comparison. It is obvious that this practice is not always practical especially for commercial powder. In this context, Cv as a normalized dispersion measure provides a more practical and reliable solution for comparing powder distributions having different mean particle size. Thus, in the PSD range investigated, it is justified that Cv is the most appropriate dispersion measure, owing to its ability to describe relation between dispersion in initial powder and sinter ability relatively accurate.

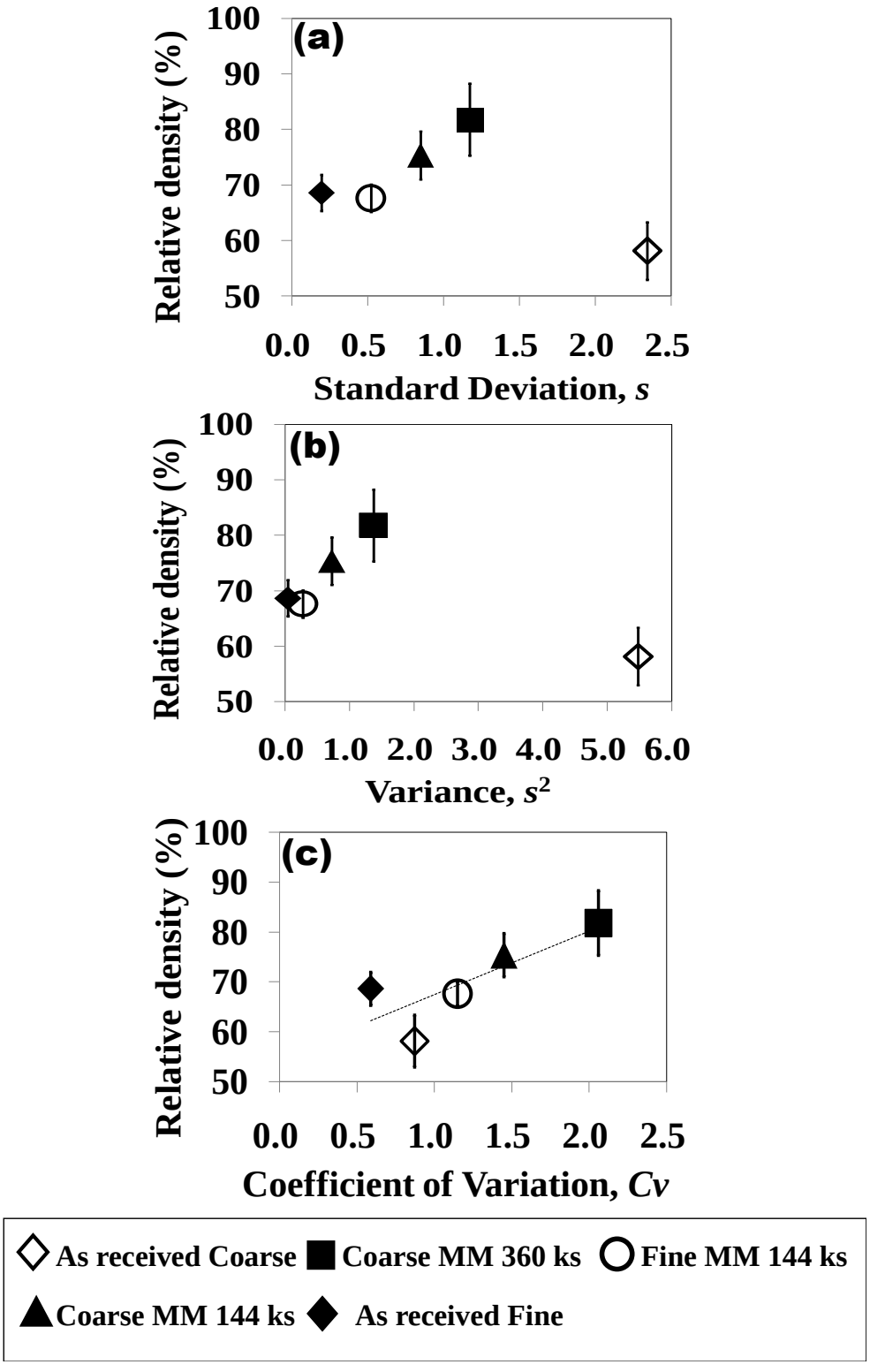


**Figure 7** Relative density plotted with dispersion measures (a) Standard Deviation (b) Variance (c) Coefficient of Variation.

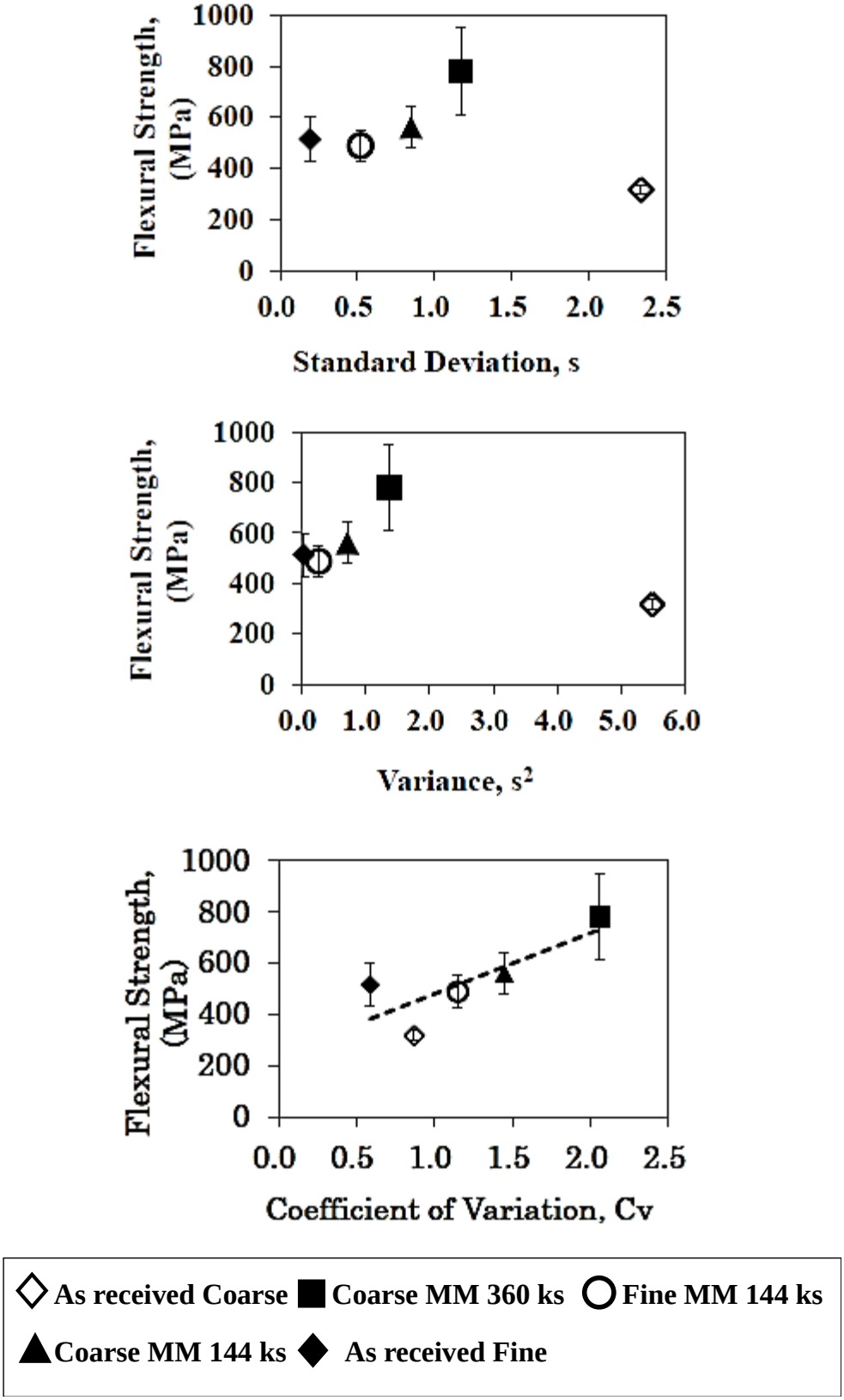


**Figure 8** Flexural Strength plotted with dispersion measures (a) Standard Deviation (b) Variance (c) Coefficient of Variation.

4.4.3 Relationship between Dispersion in PSD with Sinterability

**Figure 9** illustrates the microstructure of as received fine and milled 360 ks coarse powder compact with Cv value of 0.59 and 2.06 respectively in the initial powder. As can be observed from Figs.9 (a)-(b) with regard to as received fine powder compact, the sintered region is very minimum with obvious porosity, indicating the poor sinter ability in this compact. On the contrary, as observed in Fig.9 (c), milled 360 ks powder compact demonstrates a significant improvement in sinterability where the sintered region is increased significantly. These observations imply that the higher Cv value in the initial powder results in enhanced sinterability of powder compact. It is well known that sinterability of powder compact is dependent on several factors like packing structure, mean particle size and size distributions. With regard to mean particle size, when compared to coarser particles, finer particles provides larger specific surface area, leading to increased surface energy which results in enhanced sintering. Nevertheless, considering this factor alone is insufficient because the dispersion of initial PSD is also important to determine the initial packing structure as mentioned above. When considering several powders having not similar dispersion and mean particle size, it is always difficult to determine powder which will exhibit best sinter ability. In this context, the usage of Cv which both mean size and dispersion factors into account, the sinterability of respective powder can be predicted more accurately and holistically.

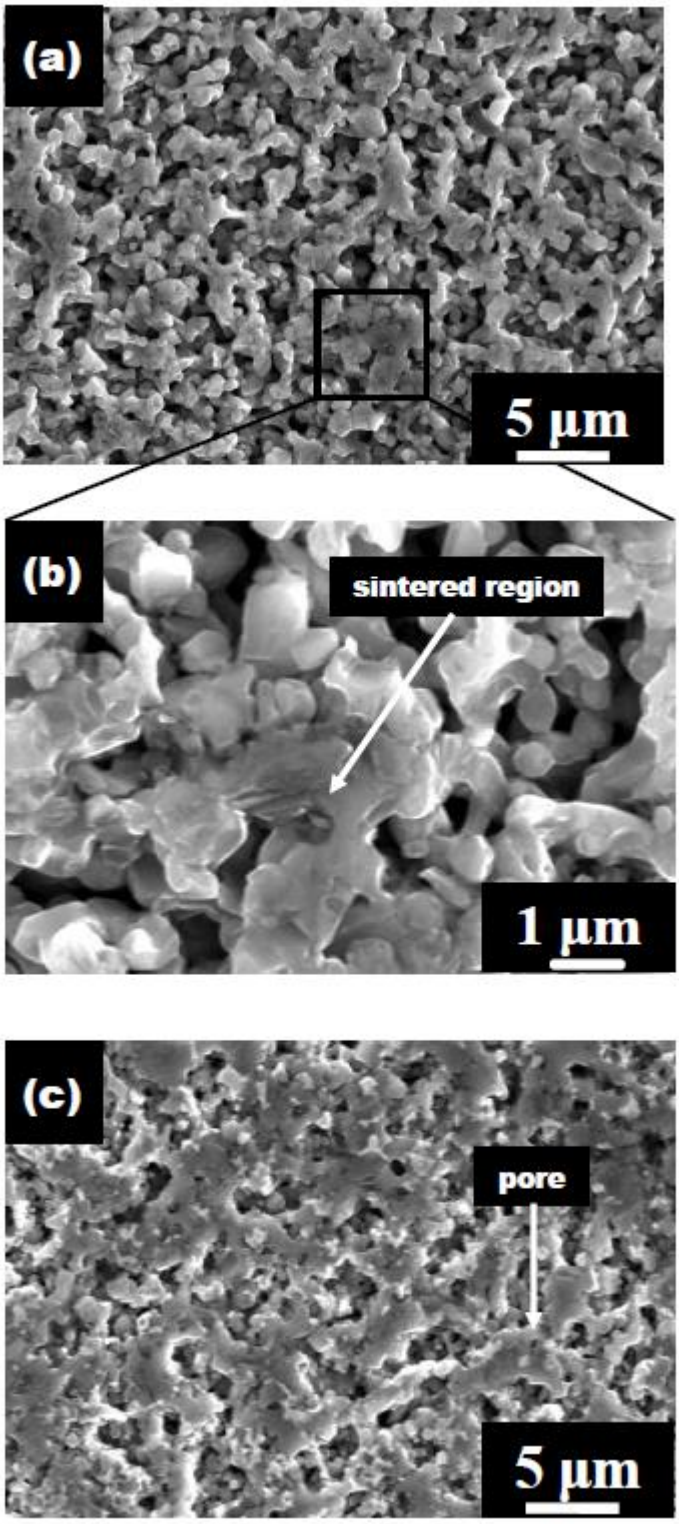


**Figure 9** Microstructure of sintered compacts (a) As received fine powders compact, Cv= 0.59 (b) enlargement from black rectangle in (a) ,(c) Coarse MM 360 ks powders compact, Cv= 2.06.

## 4.5 Conclusions

This work has investigated the effect of dispersion in Particle Size Distribution (PSD) to sintering ability of SiC ceramics under constant sintering temperature. Mechanical milling was adopted to create various patterns of PSD. Mechanical milling has resulted in the reduction of particles aspect ratio for coarser particle and no significance change in finer particles. The usage of Coefficient of variation, Cv, has demonstrated a reliable correlation for SiC sinter ability and thus was suggested as the most appropriate dispersion measure for PSD which do not hold identical mean values. In the range PSD investigated, the result showed that the sinterability of SiC ceramic improved with the increase of Cv value under constant sintering conditions.

## REFERENCES:

**[1]** F. M. Varela-Feria, J. Martinez-Fernandez, A.R.de Arellano- Lopez and M. Singh: *J. Eur. Cera. Soc*., **22** (2002) 2719-2725.

**[2]** M. Singh and J. A. Salem: *J. Eur. Cera. Soc*., **22** (2002) 2709-2717.

**[3]** Q.-W. Huang and L.H. Zhu: *Mater. Lett.*, **59** (2005) 1732-1735.

**[4]** J. Sanchez-Gonzalez, A.L. Ortiz, F. Guiberteau and C. Pascual: *J. Eur. Cera. Soc*., **27** (2007) 3935-3939.

**[5]** A. Maitre, A. Vande Put, J.P. Laval, S. Valette and G. Trolliard: *J. Eur. Cera. Soc.*, **28** (2008) 1881-1890.

**[6]** S.H. Lee: *J. Cera. Soc. JPN*., **119[8]** (2011) 640-644.

**[7]** A. Lara, A.L. Ortiz, A. Muñoz and A. Domínguez-Rodríguez: *Ceram. Int.*, **38** (2012) 45-53.

**[8]** A. Can, M. Hermann, D. S. McLachlan, I. Sigalas and J. Adler: *J. Eur. Cera. Soc.*, **26** (2006) 1707-1713.

**[9]** M. F. Yan: *Mater. Sci. Eng*., **48** (1981) 53–72

**[10]** E. A. Barringer and H. K. Bowen: *J. Am. Ceram. Soc.*, **65** (1982) pC-199–C-201.

**[11]** M. D. Sacks. and T. Y. Tseng, : *J. Am. Ceram. Soc.*, **67** (1984) 532–537.

**[12]** D. J. Sordelet and M. Akinc: *J. Am. Ceram. Soc*., **71** (1988) 1148–1153.

**[13]** B. R. Patterson, V.D. Parkhe and J. A. Griffin: *Mod. Des. Pow. Metall*., **15** (1984) 279-288.

**[14]** T. S. Yeh and M. D. Sacks: *J. Am. Ceram. Soc*., **71** (1988) C484–C487.

**[15]** J. Ma and L.C Lim: *J. Eur. Cera. Soc*., **22** (2002) 2197-2208.

**[16]** A. Wonisch, T. Kraft, M. Moseler and H. Riedel: *J. Am. Ceram. Soc*., **92[7]** (2009) 1428-1434.

**[17]** M. Hussain, Y. Oku, A. Nakahira and K. Niihara: *Matt. Lett.*, **26** (1996) 177-184.

**[18]** R. Johnson and P. Kuby: Elementary Statistics, (Thomson Brooks/Cole., California, 2007), pp. 118-119.

**[19]** Y. Han, J. Fan, T. Liu, H. Cheng and J. Tian: *Int. J. Ref. Met. H. Mat.* **29** (2011) 743-750.

**[20]** I. J. Shon and S.M. Kwak: J. *Ceram. Proc. Res*., **14** (2013) 694-699.

**[21]** J. D. Curto and J. C. Pinto: *J. Appl. Stat*., **36** (2009) 21-32.

**[22]** J. Sappakitkamjorn and S. Niwitpong: *Int. J. Math. Compu. Nat. Phys. Eng*., **7** (2013) No.9.

# Chapter 5

# Microstructure and Mechanical Properties of Al-SiC Composite with Harmonic Structure

## 5.1 Introduction

Al based alloys are among important structural material used in many applications such as electronics, aerospace industries and automotive field, due to its versatility and exceptional properties. Currently, among the most the most common production of Al based alloys are mainly based on casting and powder metallurgy route (PM). With regard to PM technique, it is well established that this technique is a near-net-shape manufacturing process, in which metallic powders are pressed and sintered into components. PM technique is also attractive in terms of its ability to fabricate material having superior properties due to the capability to process small particles. This is coupled with its potential to produce low cost parts which enable the generation of novel lightweight materials with high strength **[1]**. Although there are numerous works which have been devoted to improve the properties and performance of Al based alloy, the continuous demand of obtaining material with better mechanical properties has always been main focus for materials' researchers. Recently, Ameyama and co-workers have proposed an approach to obtain both high strength and ductility in metallic material through the formation of so-called "harmonic structured material" **[2-14].** Essentially, it is a peculiar heterogeneous microstructural design, consisting of bimodal grain size distribution, in which coarse grained region (or "core") having lower hardness are enclosed in a continuously connected three-dimensional networks regions with high strength fine grained structure known as "shell". It has been reported that

variety of metals and alloys with harmonic structure demonstrate higher strength with retention of ductility, compared to its coarse grain counterpart. In present work, an attempt has been made to propose a novel concept of harmonic structured material to Al based alloy, in which the typical feature of the harmonic structured material, which is hardness distribution in the core and shell regions is endorsed. As mentioned earlier, in the common harmonic structured material, the shell region which is formed from the fine grain structure, exhibit grain size strengthening effect, in contrast with its core region counterpart which consists of softer coarser grain region. Meanwhile, in present work we attempted to design the shell region with different strengthening mechanism, which is composed of dispersion of secondary hard phase element, while maintaining the softer phase in the core region. In this particular design, the shell region is made to be the dispersion strengthened phase of as silicon carbide (SiC) while the core region remains as softer region which is composed of pure aluminum matrix phase. Therefore, present work is aimed to investigate the possibilities of formation the above mentioned harmonic structured design in Al based alloy. In this work, the harmonic structure is fabricated through powder metallurgy approach, which comprises of mechanical milling of pure aluminum and SiC powder, followed by consolidation by spark plasma sintering (SPS). To understand the effect of such design to mechanical properties, the phase analysis and microstructural evolution are also presented and discussed.

## 5.2 Initial Powders and Experimental Procedures

In present work, commercially pure Al prepared by plasma rotating electrode process (PREP), supplied by Fukuda Metal Foil & Powder Co., Ltd and α-SiC powder were used as starting material. **Figure 1** shows the morphology and particle size distribution

of as received Al and SiC powders. It can be noted that Al particles has smooth surface with spherical morphology as shown in Fig.1 (a). It is also noted that the Al particles have more or less uniformed particle size. **Table 1** shows the chemical composition of as received Al powder. During gas atomization process, molten metals are being disintegrated by a high speed inert gaseous i.e helium and nitrogen which later form droplets and solidify into particles in the solidification process. Generally, metal powders obtained from this technique are spherical in shape with a high purity. **[1]** The particle size distribution of as received Al powders demonstrate somewhat a narrow distribution as shown in Fig.1 (b), and the average particle size is 283μm.Meanwhile, as received SiC powders demonstrate an irregular morphology with a wide range of particle size as shown in Figs.(1 (c)-2(d)). The mean particle size is 0.3 μm. The SiC content was varied from 1~10wt% of the total powder mass during mechanical milling under Ar atmosphere and room temperature. A constant rotation of 150 rpm and a total time of 36 ks were used to mill the powders and the ratio of the grinding ball to powder mixture was 10: 1 by mass. WC-Co vial and high carbon chromium steel balls (SUJ2) of 3 mm in diameter were used as grinding media. The vial and balls are pre-coated with aluminium powders to minimize the possible contamination caused by vial and balls. Stearic acid ($C_{17}H_{35}CO_2H$) in 1.0wt% of the total powder mass was used as process control agent to minimize the agglomeration amongst Al powder and to the milling media. The milled powders was inserted in a graphite die with external and internal diameter of 30 mm and 15.5 mm, respectively, with graphite punch having a diameter of 15mm and 20mm height. Subsequently, the powders were sintered by Spark Plasma Sintering (SPS) using DR.SINTER 1020 apparatus SPS Syntex Inc., Japan at 823K for 3.6 ks under an applied pressure of 100 MPa and carried out in a vacuum. The

temperature was measured using thermocouple wire inserted in the die. After the powders were soaked in the desired temperature, the pressure was released and the specimen is cooled down to room temperature. Microstructural and phase characteristics of both milled and sintered compacts were observed using SEM equipped with EDS detectors. The mechanical properties of sintered compacts were evaluated by vickers indentation and tensile tests. The initial strain rate for tensile test is $2.7 \times 10^{-3} s^{-1}$ at room temperature. The tensile specimens were prepared with a gauge length of 3 mm, with measurement width of 1 mm and thickness of 1 mm.

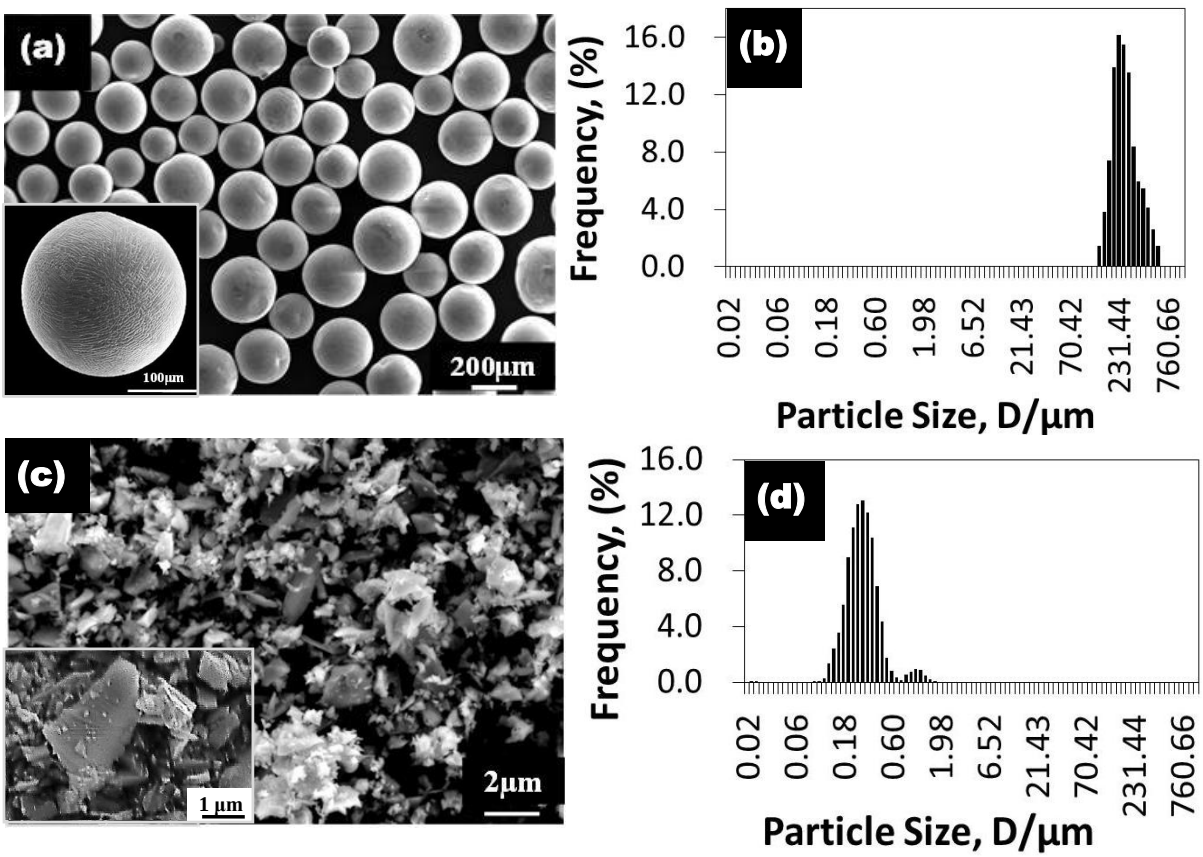


**Figure 1** Morphology and particle size distribution of as received powders for (a), (b) Al and (c), (d) SiC.

**Table 1** Chemical composition of as received Al powder.

| Com. | Si | Fe | Cu | Ti | Al |
|---|---|---|---|---|---|
| wt% | 0.07 | 0.14 | 0.01 | 0.01 | Bal. |

## 5.3 Results and Discussions

5.3.1 Morphological Characterization of Mechanically Milled Al-SiC Powder

**Figure 2** shows the morphology of mechanically milled (MMed) powders and its particle size distribution (PSD) in different SiC content. From this figures, it can be observed that regardless of SiC content, the MMed powders retains more or less of its initial shape without appreciable distortion as shown in Figs. 2(a), (c) and (e). It is important to emphasize that this is due to the optimization made to mechanical milling parameters and condition, including the usage of stearic acid, so that it will not lead to any agglomeration and/or sticking and fractures to the final milled Al particles. Moreover, it is also noted that, after mechanical milling is conducted, it can be observed that the Al powders particles surface demonstrates the absence of dendritic morphology together with formation of a deformed rough surface, as shown in the high magnifications of SEM micrographs in Figs. 2(a), (c) and (e). This suggests that, plastic deformation is induced while mechanical milling was conducted. Apparently, it appears that the plastic deformation is only limited to the powders' surface. Similar morphological observations have been reported also in literatures **[14]**. With regard to the PSD, it is observed that the as the silicon content increases, the PSD retains its unimodal distribution as observed present in the initial Al powder. However, it is also noted that the PSD demonstrates a broadened distribution with increment of SiC content. **Table 2** shows the mean particle size of the MMed powders. It can be noted that the mean particle size demonstrates a slight decrement as the SiC content increases. This might be attributed to the higher number fraction of the SiC particles as compared to number fraction of Al particles when SiC content increases, leading to the smaller mean particle size of the overall powder mass.

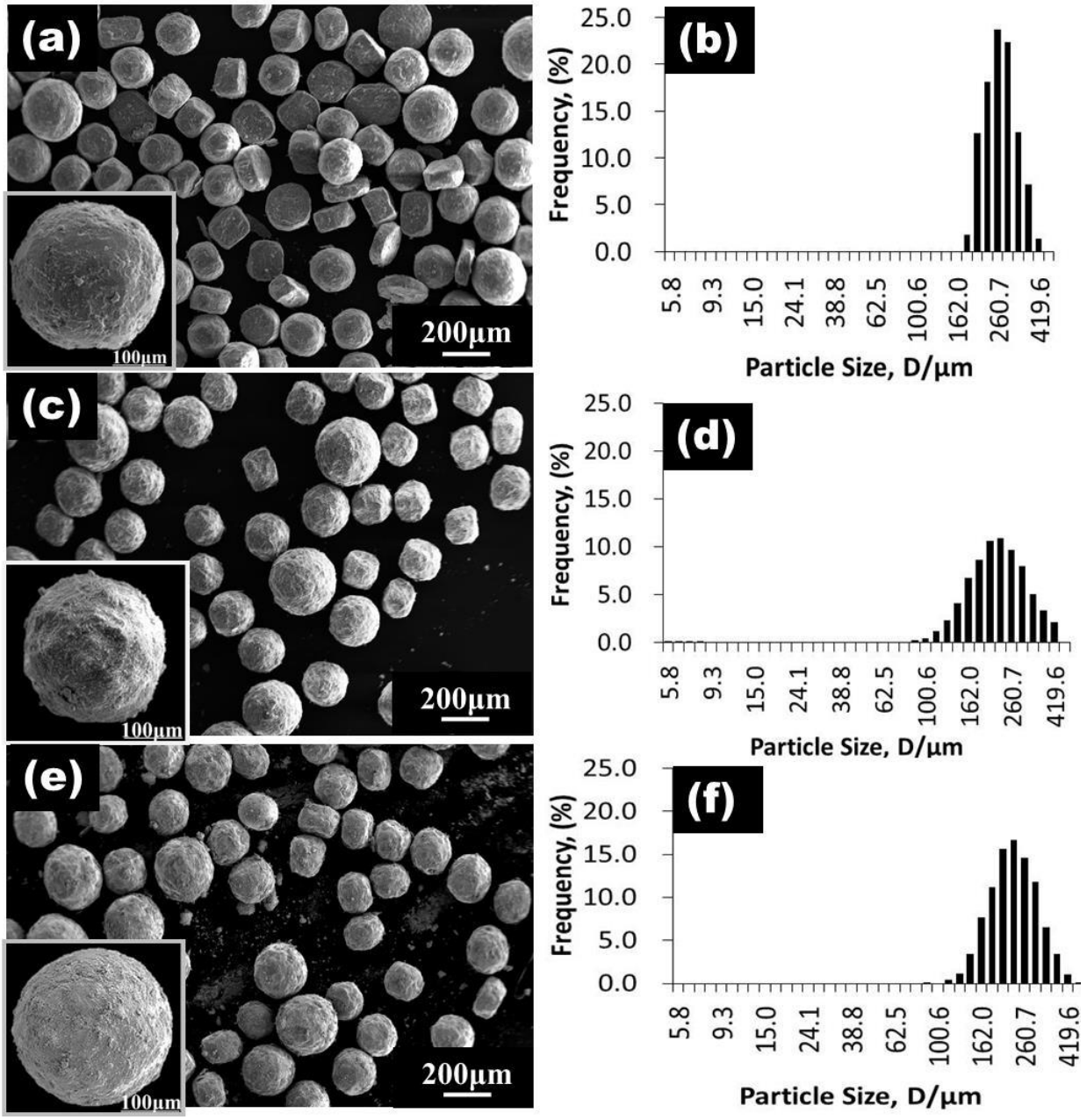


**Figure 2** SEM micrographs and particle size distribution of milled powders (a), (b) Al-1wt%SiC, (c), (d) Al-5wt%SiC (e), (f) Al-10wt%SiC.

**Table 2** Mean particle size of the initial and MMed powders.

| SiC content (weight %) | 0 | 1 | 5 | 10 |
|---|---|---|---|---|
| Mean Particle Size (µm) | 283.4 | 273.6 | 230.5 | 237.2 |

5.3.2 EDS Analysis of the Mechanically Milled Al-SiC Powders

**Figures 3-5** illustrate the cross section of the MMed powders at different SiC content, together with its EDS mapping results in both low and high magnifications. From these observations, it can be noted that regardless of the SiC content, the SiC is uniformly distributed on the surface of Al particle. It is also observed qualitatively that the higher SiC content result in the thicker SiC layer around Al particle. Moreover, it also appears that the SiC distribution is only limited to the particles surface in every SiC content. At this stage, it is worth emphasizing that the anticipated distribution of SiC around Al particles has been achieved.

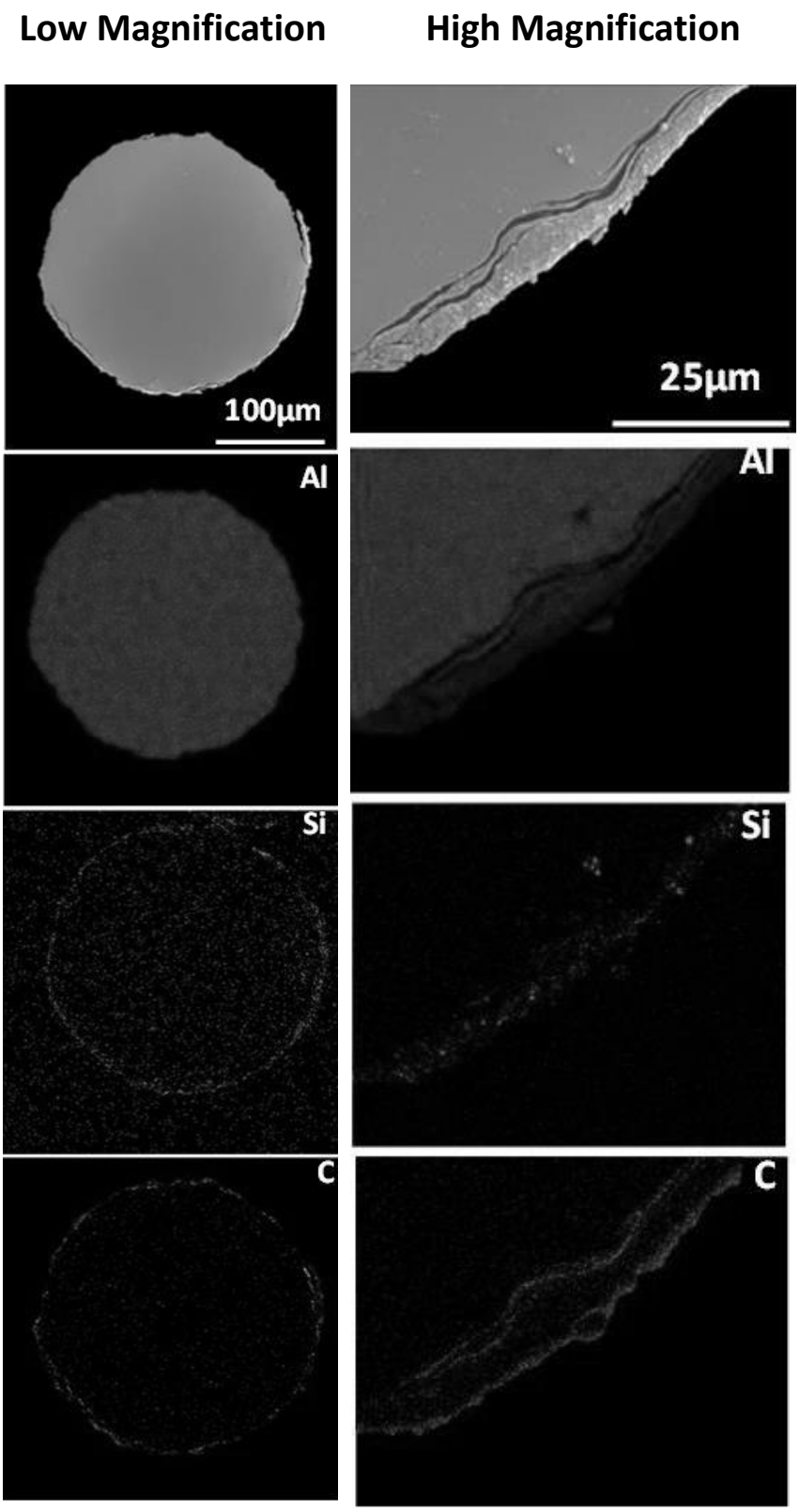


**Figure 3** SEM micrograph of the MMed Al-1wt%SiC powder and its EDS results illustrating distribution of Al, Si and C elements in low and high magnifications.

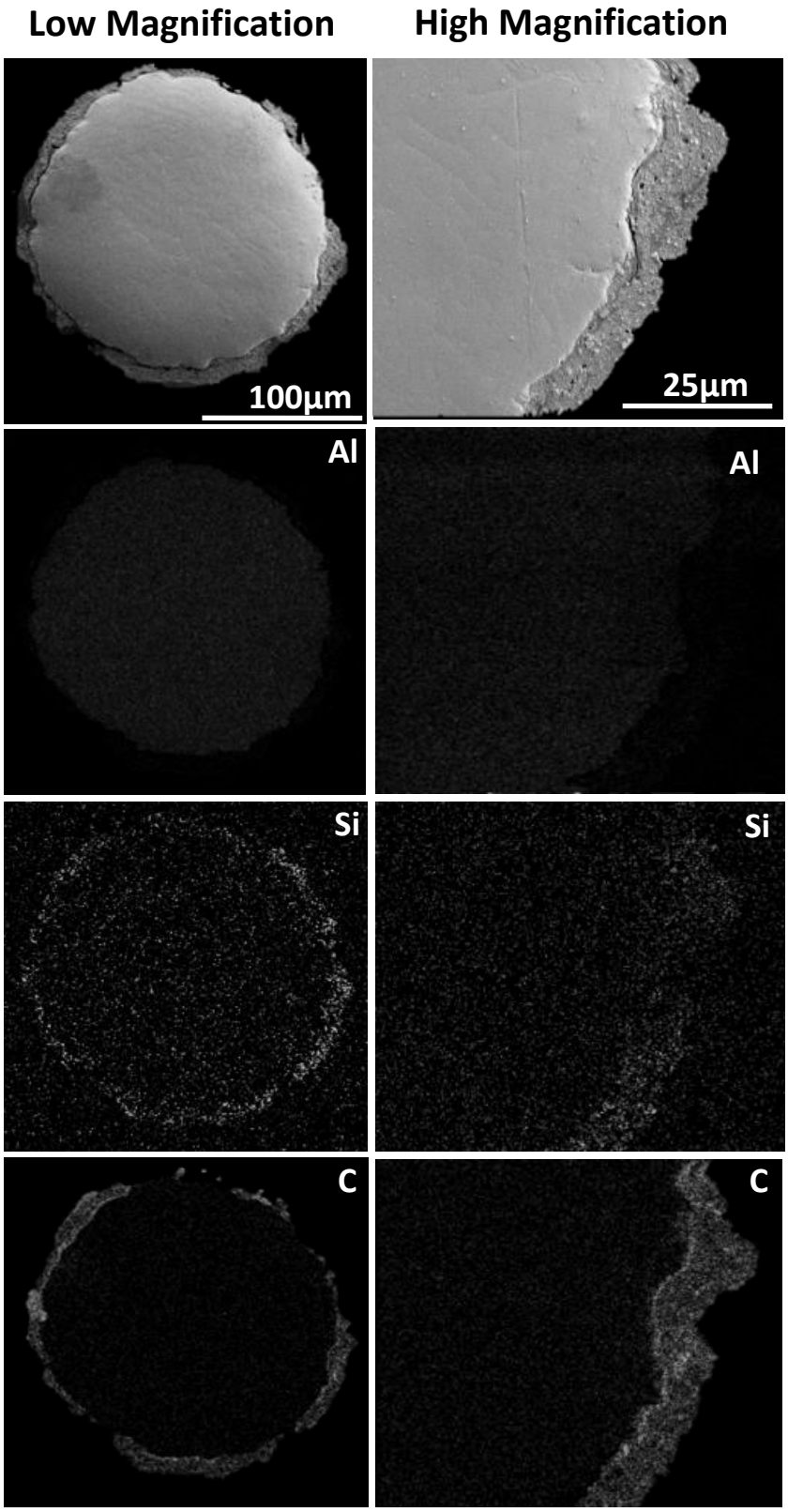


**Figure 4** SEM micrograph of the MMed Al-5wt%SiC powder and its EDS results illustrating distribution of Al, Si and C elements in low and high magnifications.

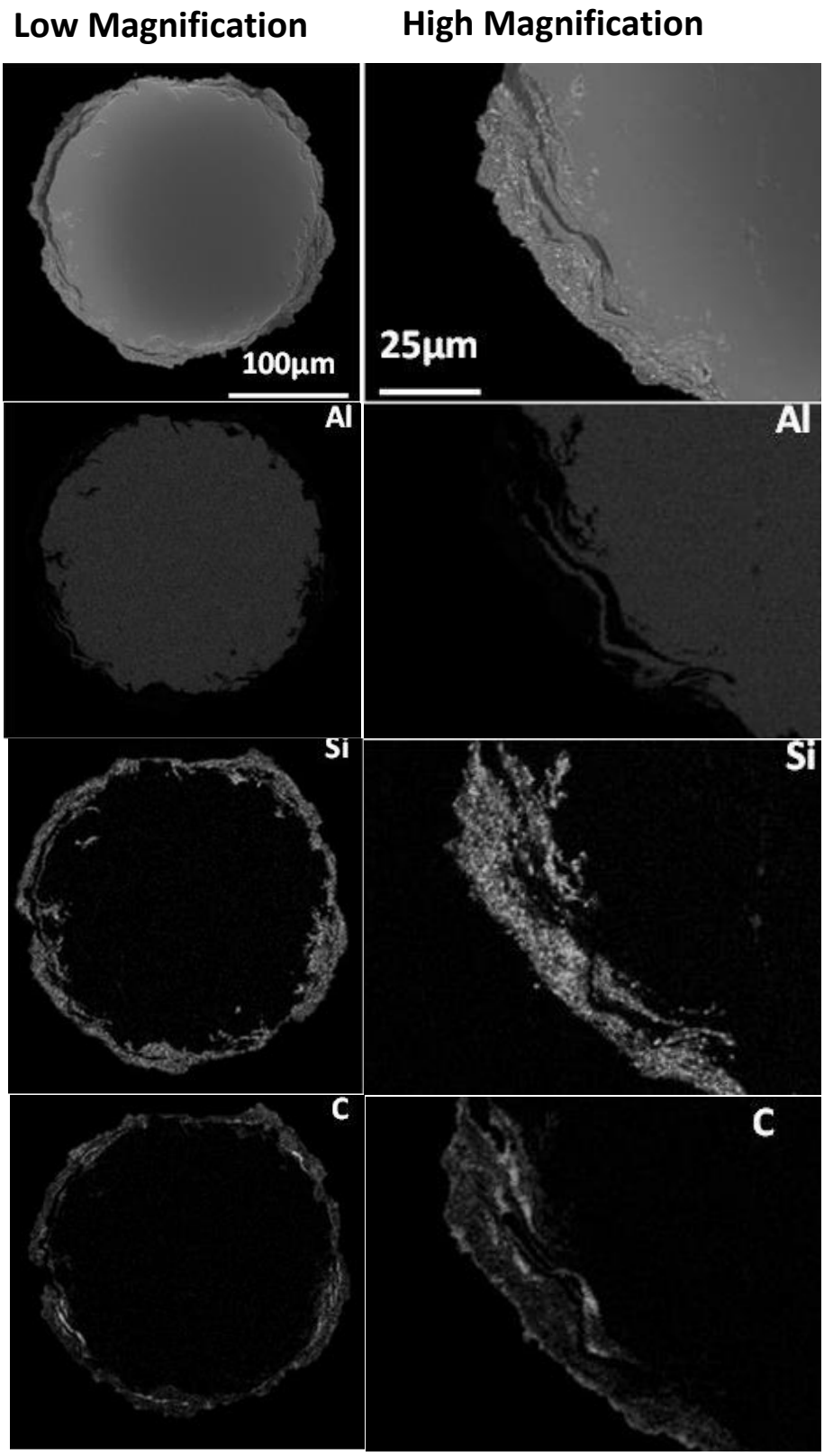


**Figure 5** SEM micrograph of the MMed Al-10wt%SiC powder and its EDS results illustrating distribution of Al, Si and C elements in low and high magnifications.

5.3.3 XRD Profile of Mechanically Milled Al-SiC Powders

**Figure 6** illustrate the XRD profile for the mechanically milled Al-SiC powders at different SiC content. From this figure, it can be observed that there is no emergence of new peaks corresponding to new elements. Furthermore, the peak corresponding to Al also do not demonstrate any shifting to higher/lower angle, suggesting that there are no mechanical alloying takes place during controlled mechanical milling. It is also worth mentioning that in the milled Al-1wt%SiC powder, the peak corresponding to SiC is almost undetectable. This might be attributed to the content of SiC particles in this powder mixture that is so small that in falls in the undetectable range of XRD instrument.

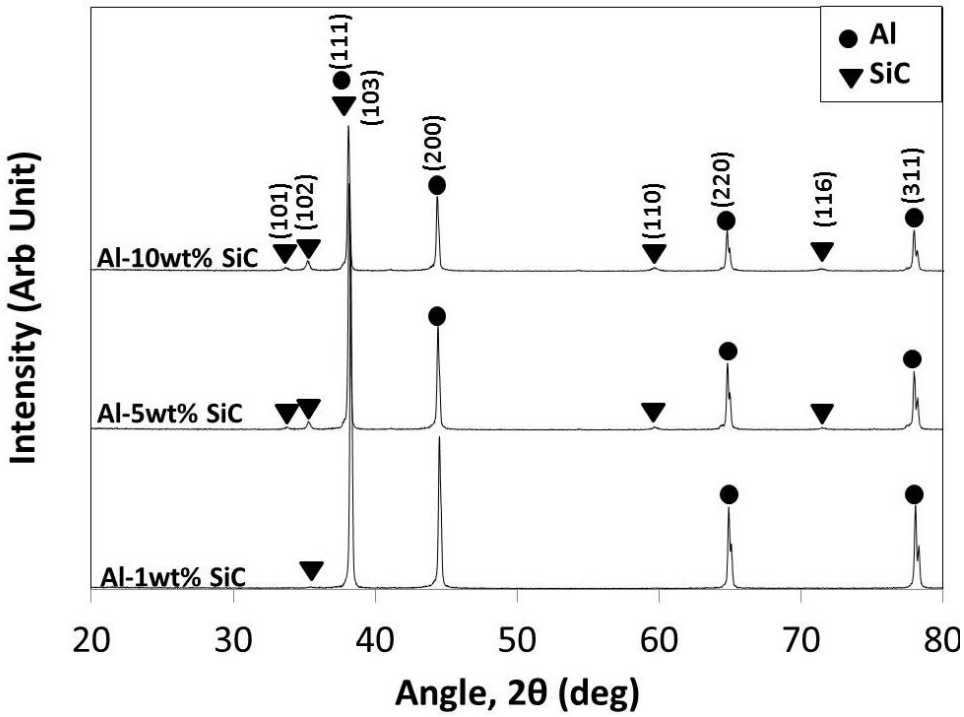


**Figure 6** XRD patterns of milled Al-SiC powders at different SiC content.

5.3.4 Vickers Hardness of Mechanically Milled Powders

**Figure 7** illustrates the hardness result for mechanically milled powder for every SiC content taken in two different regions, namely core and shell. The indentation was made at 98.07 mN for 5 seconds of holding time. For shell region, the measurements were conducted approximately 25μm from the surface of Al particles. Meanwhile, for center region, the measurements were taken at the center of the respective particles. The measurement was made at different powder particles for each region to avoid any possible work hardening effect due to indentation. When the SiC content=0% (i.e initial powder), it can be observed that the hardness of the shell region is slightly higher than that of the core region. As mentioned in section 5.2 of this chapter, in the PREP powder, molten metals are disintegrated using high speed inert gaseous before solidify into particles. Generally, during the solidification, faster cooling occurs on the particles surface moving towards the center of the respective particles. This usually results in smaller dendritic arms spacing resulting in a slightly higher hardness of the surface area of particles when compared to the inner region **[1]**. This explanation provides the possible justification on the higher hardness of the shell region as compared to core region in the initial powder. However, as the SiC content is varied from 1~10wt%, , it can be observed that regardless of SiC content, the hardness of shell region of the MMed powder shows a slight increment as compared to the core region. The increment of hardness in the MMed powder particle can be attributed by strain hardening that is caused by plastic deformation, while mechanical milling was conducted. In the ball milling process, work hardening is caused by interaction of dislocations with each other due to the continuous mechanical impact of the balls on the powder particles **[15].**In particular, controlled mechanical milling introduces continuous plastic straining, which

results in piling up of dislocations on the vicinity of powder particles' surface. This results in dislocation entanglement, which impedes the motion of other dislocations and any further deformation. Hence, the hardness in the MMed powder is increased.

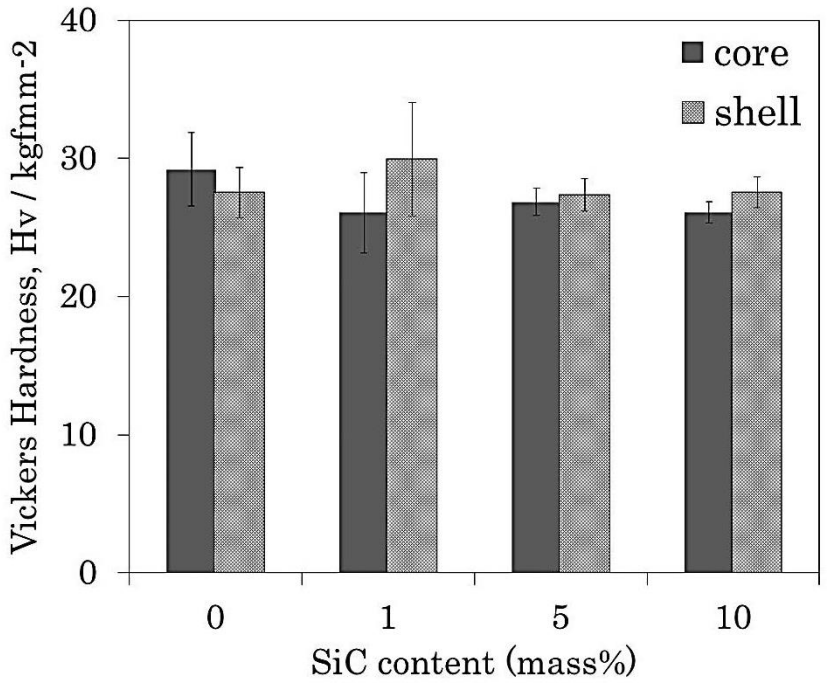


**Figure 7** Vickers hardness of the MMed powder with different content of SiC.

5.3.5 Phase Analysis in the Sintered Harmonic Al-SiC Compacts

**Figures 8-10** show the micrograph of sintered harmonic compact and EDS mapping images at both low and high magnification. Apparently, from these results it can be observed that at very SiC content, network structure of SiC-rich region (i.e shell) enclosed by pure aluminum region(i.e core) is formed, indicating that at this stage, the formation of desired harmonic structure consisting three- dimensional network of interconnected SiC dispersed region surrounding isolated aluminum matrix region has been successfully achieved. Moreover qualitatively, the variation of SiC content results in the variation of thickness of "shell" region, in which the higher SiC content leads to a

thicker "shell" region. Furthermore from high magnification image in Figs.9-10, it is also observed that, as SiC content increased more SiC particles is distributed/removed to the "core" region also. It is already elaborated in Chapter 4 that essentially SiC has a poor sinterability due to its highly covalent bonded nature. The sintering of SiC generally requires extremely high temperature (up to 2200°C) and longtime sintering in order to achieve full densification. Considering the sintered temperature and time in present work (i.e.550°C and 3.6ks) is significantly lower than that of the required temperature for high densified compacts, the increased SiC content in the "shell" region results in the more number of non-sintered SiC particles. Therefore during polishing of specimens. the overall increased of SiC content results in the more removal of non-sintered SiC particles in the "shell" region, resulting in the high amount removal of SiC particles to the extent of "core" region also. This explanation provides the possible justification on the existence of significant amount of SiC particles observed on the "core" region as the overall SiC content increased.

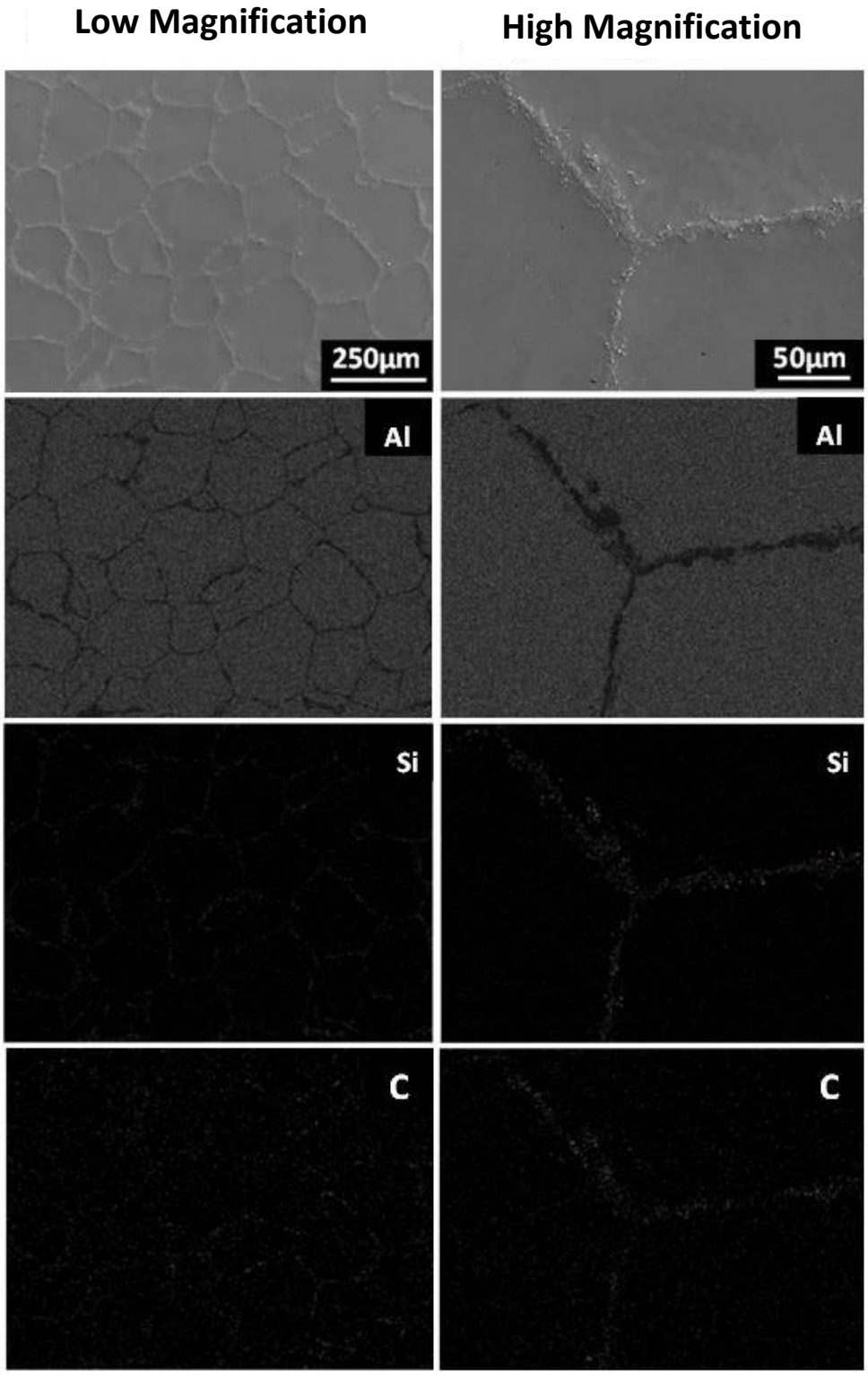


**Figure 8** SEM micrographs in the sintered Al-1wt%SiC powder compact with its EDS analysis results illustrating the distribution of Al, Si and C elements in low and high magnifications.

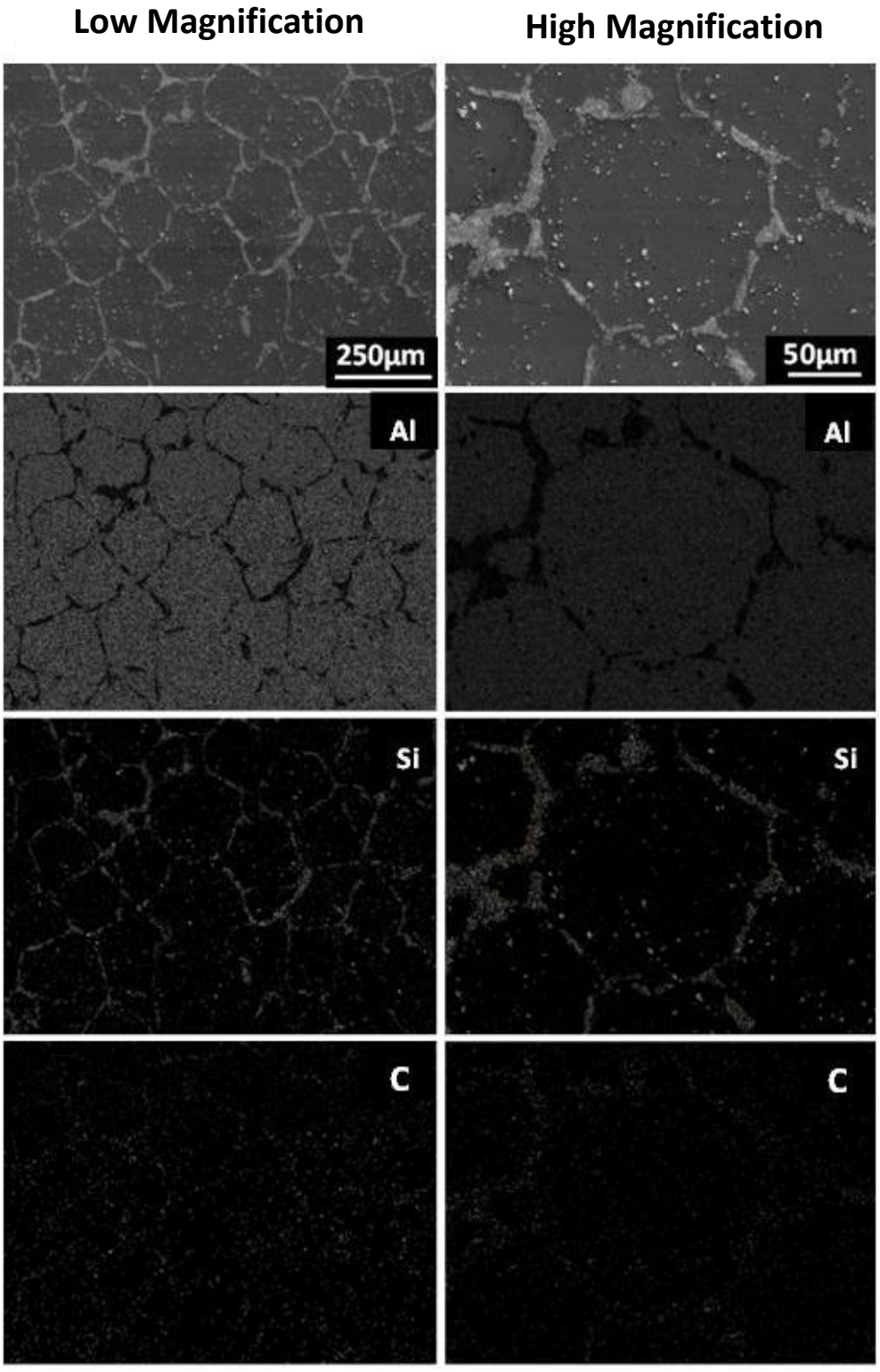


**Figure 9** SEM micrographs in the sintered Al-5 wt% SiC powder compact with its EDS analysis results illustrating the distribution of Al, Si and C elements in low and high magnifications.

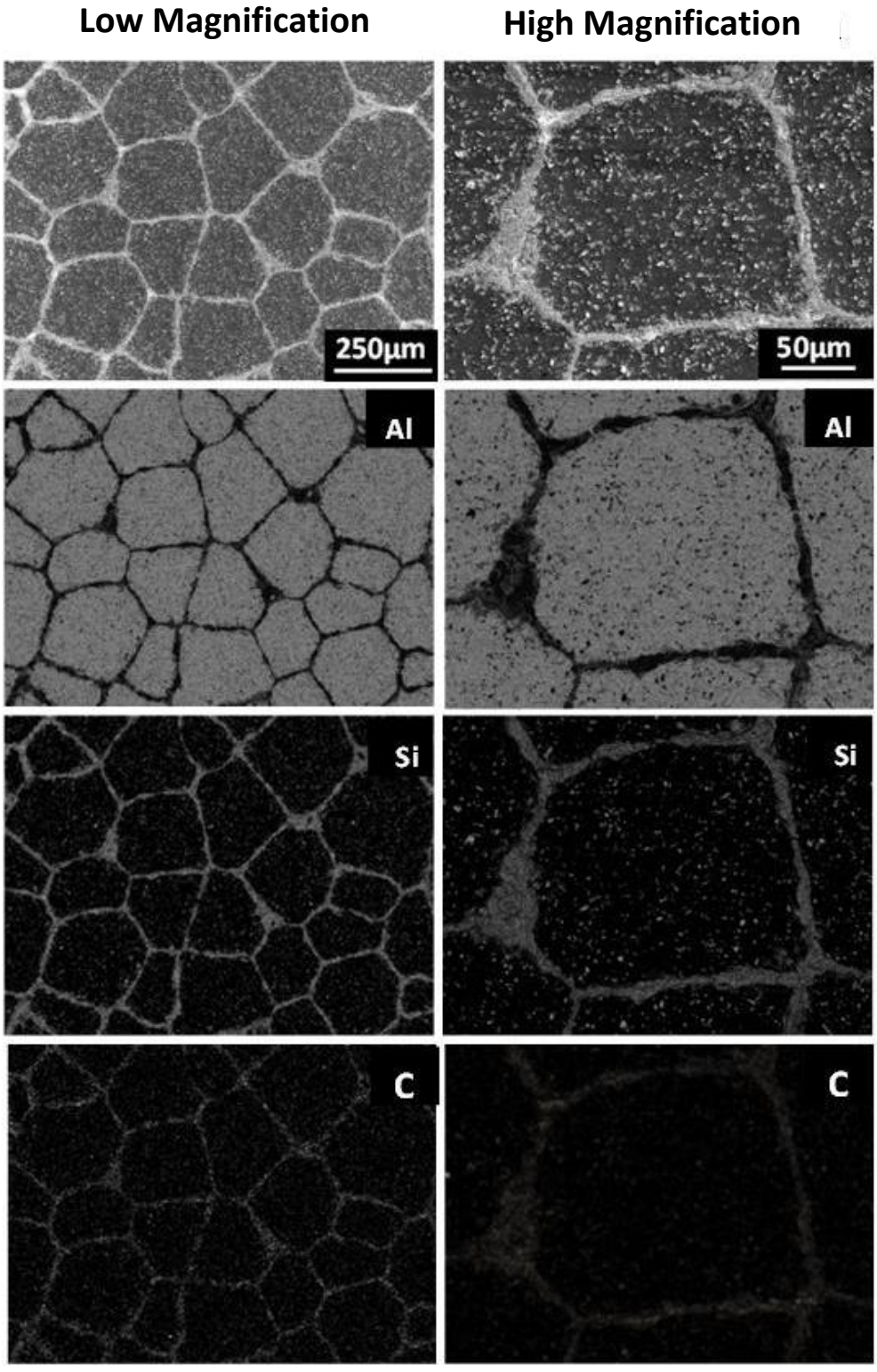


**Figure 10** SEM micrographs in the sintered Al-10 wt% SiC powder compact with its EDS analysis results illustrating the distribution of Al, Si and C elements in low and high magnifications.

5.3.6 XRD Profiles of Sintered Compacts

**Figure 11** illustrates the XRD profile for the milled Al-SiC powder compacts with different SiC content. From this result, it can be observed that there is no emergence of new peaks corresponding to new phase elements. It is also worth pointing out that in the Al-1wt%SiC powder compact, the peak corresponding to SiC is almost undetectable. As already mentioned in 5.3.3, this might be attributed to the content of SiC particles in this powder mixture that is so small that in falls in the undetectable range of XRD instrument. From these observations, it can be concluded that under present sintering conditions, sintered powder compacts do not demonstrate any emergence of new phase.

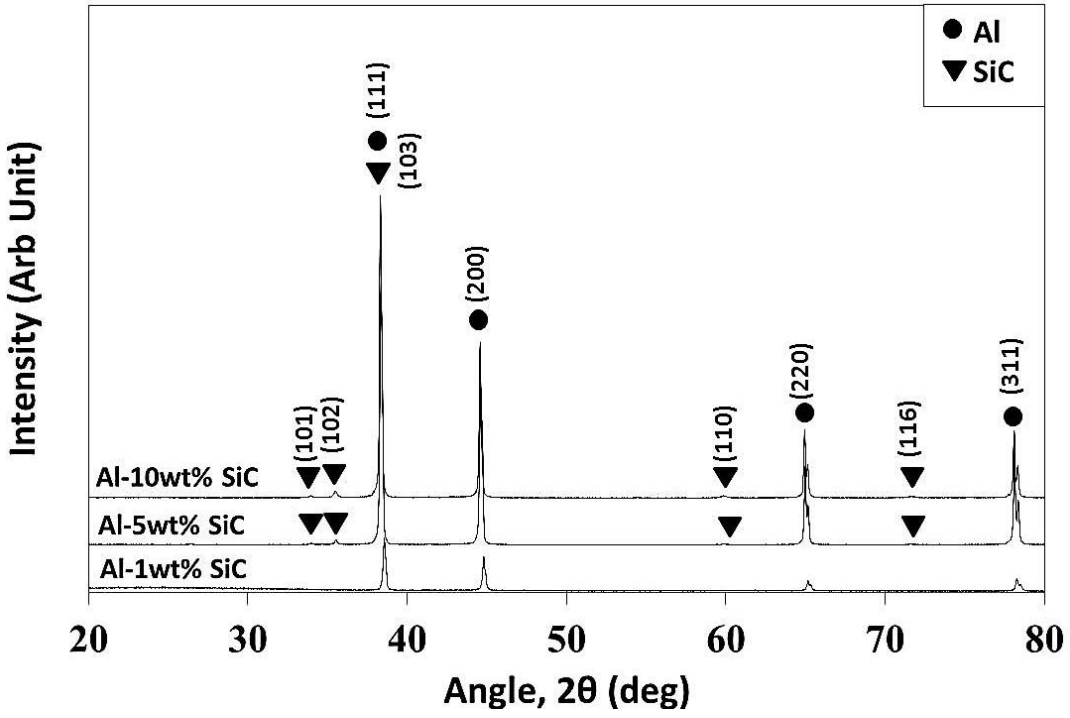


**Figure 11** XRD patterns of milled Al-SiC powder compacts at different SiC content.

5.3.7 Hardness of Sintered Compacts

**Figure 12** illustrates the hardness result for milled powder compacts in every SiC content taken in two different regions, namely core and shell. The indentation was made at 98.07 mN for 5 seconds of holding time. With regard to core region, it can be observed that in SiC content ranging from 1to 5wt%, there are no significant increment observed with SiC content, while when the content is increased up to 10wt%, a slight increment is observed. As already discussed in 5.3.5, as SiC content is increased to 10wt%, significant amount of SiC removal was observed to the extent of core region due to the poor sinter ability amongst SiC particles, leading to a higher average hardness in the core region when the indentation was made. On the other hand, for shell region, it is observed that for every SiC content, the average shell hardness demonstrates a higher average hardness value than that of the core region. Moreover, it is also observed that as the SiC content increases, it can also be noted that the standard deviation increases to a large extent leading to a higher average hardness value. This variation might be attributed to the difference in thickness of the shell region with SiC content in such that the higher content of SiC leads to thicker shell region, providing a broader SiC region for indentation resulting in the higher standard deviation in the shell region.

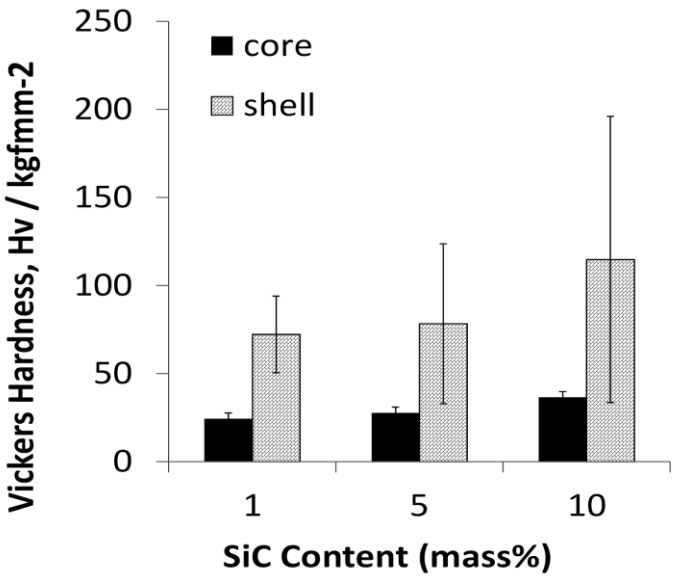


**Figure 12** Vickers hardness of the MMed powder compacts with different content of SiC.

5.3.8 Tensile Properties of Harmonic Al-SiC Compacts

**Figure 13**(a) illustrates the representative nominal stress-nominal strain curves of the sintered Al-SiC compacts having different SiC content. Figs.13 (b) - (c) summarize the relation between stress and elongation a function of SiC content. Firstly, it can be observed that as the yield strength increase as the SiC content increase. However, the most optimum combination of strength and ductility is observed when the content of SiC is 1. Further increment of SiC content results is observed to result in the deterioration of ductility. It is envisaged that the deterioration of ductility as the SiC content increases might be due to the poor sinterability amongst SiC particles in the "shell" region, resulting in the weak interparticle bonding leading to fracture in the sintered compact. Moreover, it is worth noting that harmonic compact with 5% silicon content demonstrates a brittle fracture behavior without any appreciable elongation. From this result, it can be concluded that, the effect of harmonic structure is not observed for harmonic structured Al-SiC fabricated via recent fabrication technique and it is envisaged that it is due to the poor sinterability amongst SiC particles at the shell

region.

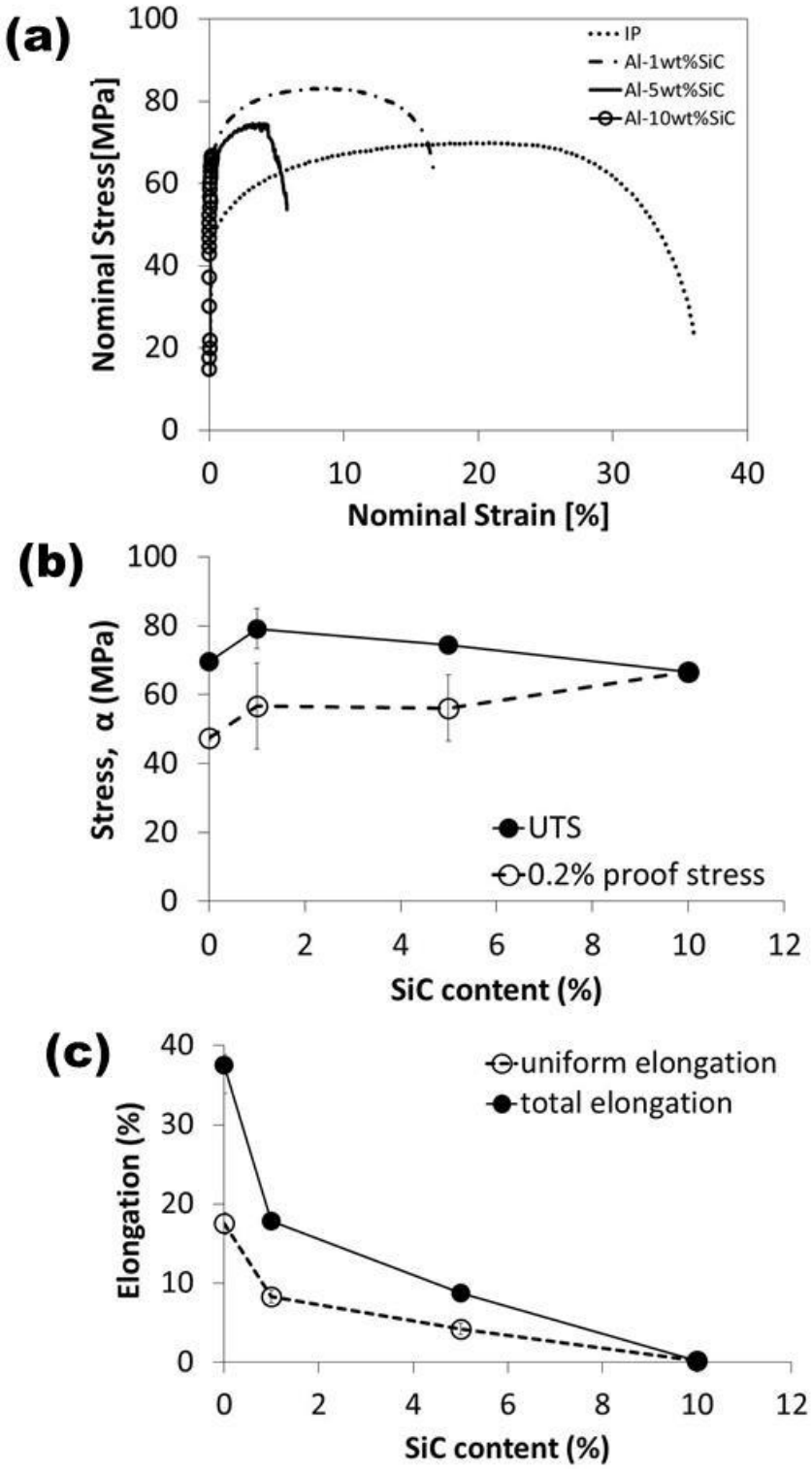


**Figure 13** Tensile properties of harmonic structured Al-SiC compact with different SiC content.

## 5.4 Conclusions

In present work, harmonic structured of Al was successfully fabricated by powder metallurgy route in which pure aluminum and silicon carbide (SiC) powder were subjected to controlled mechanical milling followed by subsequent spark plasma sintering. The mechanical performance was evaluated by tensile properties and the following conclusions can be drawn:

(1) Uniform distribution of SiC particles around Al particles can be achieved by controlled mechanical milling.

(2) Harmonic structured Al is comprised of soft core areas with pure aluminum matrix, enclosed into three-dimensional network of hard SiC dispersed region combined was successfully fabricated.

(3) Harmonic structured Al compact with 1% SiC content demonstrates the most optimum combination of strength and ductility.

(4) The effect of harmonic structure concept of Al-SiC fabricated via recent fabrication technique is not observed and it is envisaged that it is due to the poor sinterability amongst SiC particles at the shell region which leads to poor interparticle bonding.

**REFERENCES:**

**[1]** R.M. German: Powder Metallurgy & Particulate Materials Processing, (Metal Powder Industries Federation., New Jersey, 2005), pp.7-8.

**[2]** H. Fujiwara, R. Akada, Y. Yoshita and K. Ameyama: *Mater. Sci. Forum* **503-504** (2006) 227-232.

**[3]** H. Fujiwara, R. Akada, A.Noro, Y.Yoshita and K.Ameyama : *Mater. Trans*. **49**(2008) 90-96.

**[4]** H. Fujiwara, M. Nakatani, T. Yoshida, Z.Zhang and K. Ameyama: *Mater. Sci. Forum* **584-586** (2008) 55-60.

**[5]** H. Fujiwara, S. Takarae and K. Ameyama: The 2nd International Symposium on Steel Science, (ISSS,2009) pp.262-272.

**[6]** T.Sekiguchi, K. Ono, H. Fujiwara and K. Ameyama: *Mater. Trans*. **51** (2010) 39-45.

**[7]** H. Fujiwara, H. Tanaka, M. Nakatani, and K. Ameyama: *Mater. Sci. Forum* **638-642** (2010) 1790-1795.

**[8]** D. Orlov, H.Fujiwara and K. Ameyama: *Mater. Trans.* **54**(2013) 1549-1553.

**[9]** O.P. Ciuca, M.Ota, S.Deng and K.Ameyama: *Mater.Trans.* **54**(2013) 1629-1633.

**[10]** Z.Zhang, S.K.Vajpai, D.Orlov and K.Ameyama: *Mater.Sci.Eng.A* **598**(2014) 106-113.

**[11]** C.Sawangrat, O. Yamaguchi, S.K. Vajpai and K. Ameyama: *Mater.Trans.* **55** (2014) 99-105.

**[12]** C. Sawangrat, S.Kato, D.Orlov and K.Ameyama: *J.Mater.Sci*. **49**(2014) 6579-6585.

**[13]** Z.Zhang, D.Orlov, S.K.Vajpai, B.Tong and K.Ameyama: *Adv. Eng. Mater.* **17**(2015) 791-795.

**[14]** S.K. Vajpai, M.Ota, T.Watanabe, R.Maeda, T.Sekiguchi, T.Kusaka and

K.Ameyama: *Metall. Mater. Trans. A* **46** (2015) 903-914.

**[15]** A.Nouri, P.D.Hodgson and C.Wen: *Mater.Sci.Eng.C* **31**(2011) 921-928.

# Chapter 6

# Mechanical Properties of Harmonic Structured Al Based Alloy and its Deformation Behaviour

## 6.1 Introduction

In recent years, extensive investigations have been conducted in order to meet the demand of structural materials with superior mechanical properties than the conventional one with an emphasis on improving the existent material's properties. The improved mechanical properties will not only reduce the cost by providing small sized components with high strength, but also enable the generation of novel lightweight material for emerging industrial applications.

Recently, Ameyama and co-workers have proposed a microstructural design to improve mechanical properties by obtaining both high strength and ductility in metallic material, through the formation of so-called "harmonic structured material" **[1-13].** Essentially, it is an exquisite heterogeneous microstructural design, consisting of bimodal grain size distribution, in which ductile coarse grained regions (termed "core") are enclosed in a continuously connected three-dimensional networks regions with high strength ultra-fine grained structure, known as "shell". It has been reported that a variety of metals and alloys with such structure demonstrate excellent combination of strength and ductility, when compared to its homogeneous counterpart.

It is well known that there are several strengthening mechanisms in metallic material, such as grain refinement strengthening, solid solution strengthening, dispersion strengthening and dislocation strengthening. With regard to harmonic structured material,

it was revealed that the effective strengthening mechanism is the grain refinement strengthening. In conventional harmonic structured material, ultra-fine grain structure at the "shell" region is achieved through the surface severe plastic deformation (surface SPD) process of metallic powder, via controlled mechanical milling process. The severely deformed powder exhibited heterogeneous microstructure, which has fine grain structure at the "shell" region and coarse grain structure at the "core" region.

Considering the improved ductility in harmonic structured material, in earlier works, **[9, 14]** it has been experimentally demonstrated that improvement in ductility is attributed to the large uniform deformation under tensile loading. In other words, strain hardening is kept to larger strain region, and thus resulting in the improvement of ductility. Through multi scale finite element analysis (FEA), Yu et. al **[15]** have validated that the existence of the network in the harmonic structured materials results in the avoidance of deformation localization leading to homogeneous deformation behavior.

In the present work, an attempt has been made to explore the possibility to fabricate harmonic structured material through a novel approach, namely by semi-solid reaction. By utilizing the harmonic structure concept, an attempt has been made to fabricate a network structure of soft phase, which is enclosed by three dimensional interconnected network regions of hard phase. In the proposed approach, attempt has been made to design the "shell" region with a different strengthening mechanism than that of the conventional harmonic structured material, while maintaining the "core" region as the softer phase.

As described earlier, strengthening mechanism of the typical harmonic structured material relies on the grain refinement via SPD during controlled mechanical milling.

However, with regard to aluminum alloy, the formation of fine grains via mechanical

milling and/or retention of the same during subsequent sintering is rather difficult to achieve due to the low melting point of aluminum. Therefore, it is expected that by applying semi-solid reaction between Al and Si, it will provide another strengthening alternative to the "shell" region in harmonic structure of this alloy. In particular, it is anticipated that the formation of Al-Si solid solution phase combined with dispersion of Si particles will provide two strengthening mechanisms, namely, solid solution strengthening and dispersion strengthening. Hence, by applying the semi solid reaction, it is expected that alternative and multiple strengthening mechanisms on the "shell" region of the harmonic compact Al alloy can be achieved.

In particular, by applying the semi-solid reaction of Al and Si, an attempt has been made to form a "shell" region with the above mentioned strengthening mechanism, while maintaining the "core" region as the ductile pure aluminum phase (**Figure 1**). Apart from its hard nature, Si has been chosen as the secondary element candidate, because aluminum and silicon form a simple binary eutectic system and the formation of possible phases is relatively easier to characterize.

Therefore, present work has two main objectives; (1) to investigate the possibilities of formation such design in Al alloy and (2) to evaluate whether or not the harmonic structure fabricated by semi-solid reaction of Al and Si, is effective in improving mechanical properties of Al alloy in the similar manner as in the conventional harmonic structure material. In this work, the harmonic structure is fabricated through powder metallurgy route, which comprises of controlled mechanical milling of aluminum and silicon powder, followed by consolidation by spark plasma sintering (SPS) at eutectic temperature. Mechanical milling was employed to achieve uniform distribution of Si around Al particles. Finally, the deformation behavior of sintered compacts is also

presented and discussed.

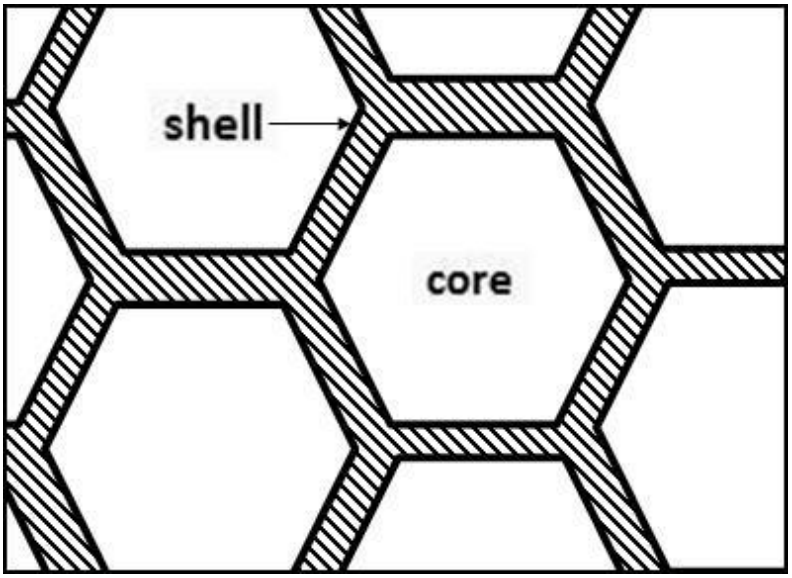


**Figure 1** Schematic of harmonic- structured design.

## 6.2 Experimental Procedures

In the present work, commercially pure Al powder prepared by plasma rotating electrode process (PREP) and pure Si powder were used as starting material. The chemical composition of the as received Al powder is shown in **Table 1**. **Figure 2** shows the morphology of as received Al and Si powders. It can be noted that, as received Al powder has smooth surface with spherical morphology as shown in Fig.2 (a). It is also noted that the Al particles have more or less uniform particle size, which is the typical characteristic of PREP powder. The average particle size is 283μm. As received Si powders demonstrate an irregular morphology with a wide range of particle size as shown in Fig.2 (b). The mean particle size is 11 μm. **Figure 3** shows the morphology and cross-sectional of as received Al powder particle. It is confirmed that the as received Al powder demonstrates a dendritic microstructure. It is also worth mentioning that the

dendritic morphology is one of typical features of atomized powders which are governed by the cooling rate during solidification of metal droplets. Dendritic structure is a result of slow cooling rate and the cooling rate can be calculated by the characterization of dendrite arm spacing **[16]**. The mixture of aluminum and silicon powder was subjected to controlled mechanical milling using Fritch P-5 planetary ball mill, under Ar atmosphere at room temperature. A constant rotation of 150 rpm and a total time of 36 ks were used to mill the powders and the ratio of the grinding ball to powder mixture was 10: 1 by mass. WC-Co vial and high carbon chromium steel balls (SUJ2) of 3 mm in diameter were used as grinding media. Stearic acid ($C_{17}H_{35}CO_2H$) in 1.0wt% of the total powder mass was used as process control agent to minimize the agglomeration/sticking amongst Al powders and to the milling media. The silicon content was varied from 0~5wt% of the total powder mass during mechanical milling. Subsequently, the milled powder was subjected to spark plasma sintering under 50MPa for 1.8 ks (0.5 h) at 850 K. Phase and microstructural characterization of sintered compacts were carried out using mirror polished specimen by the means of SEM equipped with EBSD and EDS detectors. The mechanical properties of sintered compacts were evaluated by Vickers indentation and tensile tests. The initial strain rate for tensile test was $2.7 \times 10^{-3} s^{-1}$ at room temperature. The tensile specimens were prepared with a gauge length of 3 mm, width of 1 mm and thickness of 1 mm.

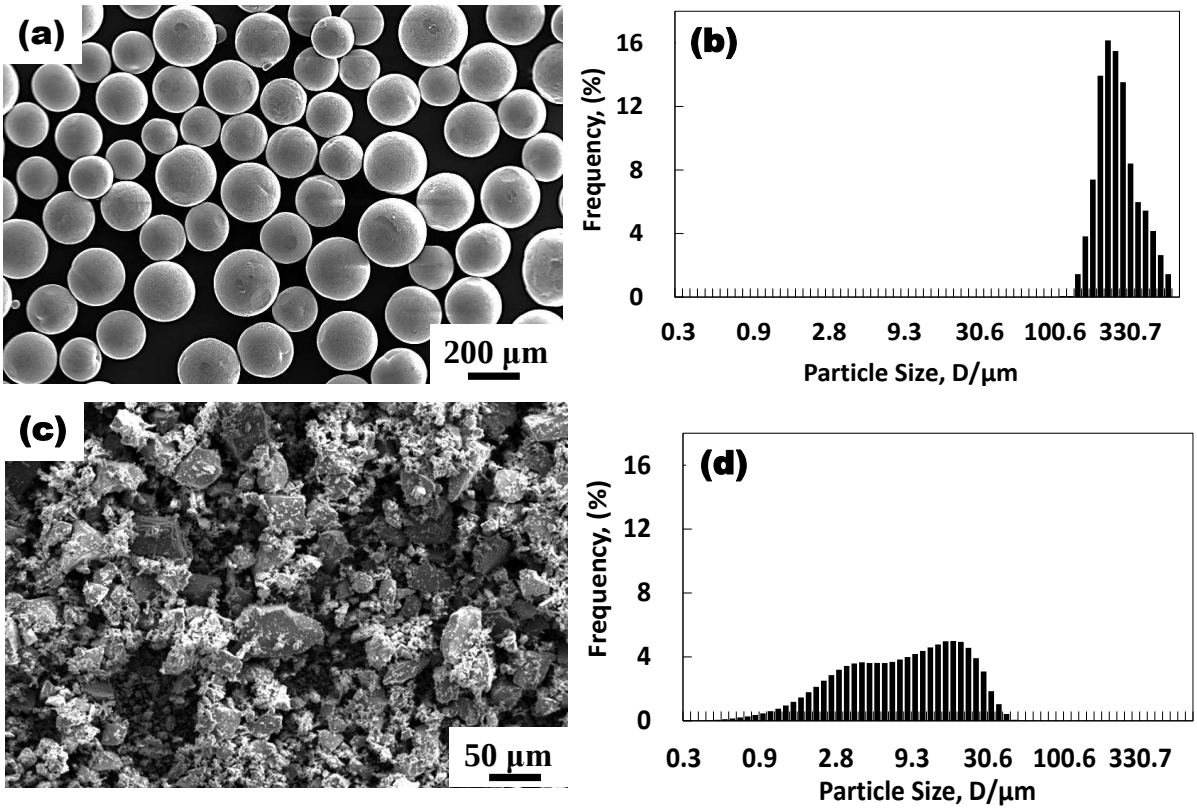


**Figure 2** Morphology and particle size distribution of as received powders (a) and (c) are morphology of as received Al and Si powders respectively (b) and (d) are particle size distribution Al and Si powder respectively.

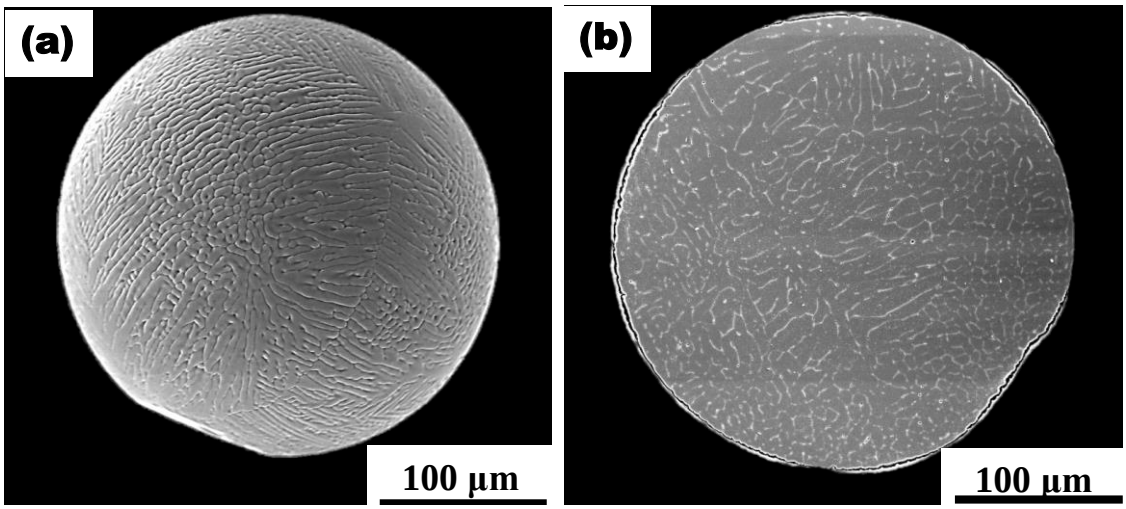


**Figure 3** SEM micrographs of initial Al powder (a) Morphology and (b) Cross section.

**Table 1** Chemical composition of as received Al powder.

| Element | Si | Fe | Cu | Ti | Al |
|---|---|---|---|---|---|
| mass (%) | 0.07 | 0.14 | 0.01 | 0.01 | Bal. |

## 6.3 Results and Discussions

6.3.1 Characterization of Mechanically Mixed Powders

**Figure 4** shows the morphology of the mechanically mixed (MM0ks) powders in both low and high magnifications. An aluminum powder was mixed with 5 weight percent silicon powder using pestle and mortar for 15 minutes (900 seconds). It can be observed that Si particles are agglomerated and are not uniformly distributed as shown in Figure 4(a). At this stage, it is crucial to justify that in the mixed powders, Si particles is agglomerated and do not demonstrate the anticipated uniform distribution around Al particle (Figure 4 (b)). These observations are the evident that mechanical mixing is inadequate for achieving uniform distribution of Si around Al particles and thus, mechanically milling is adopted to increase the uniformity of Si particles in the mixture.

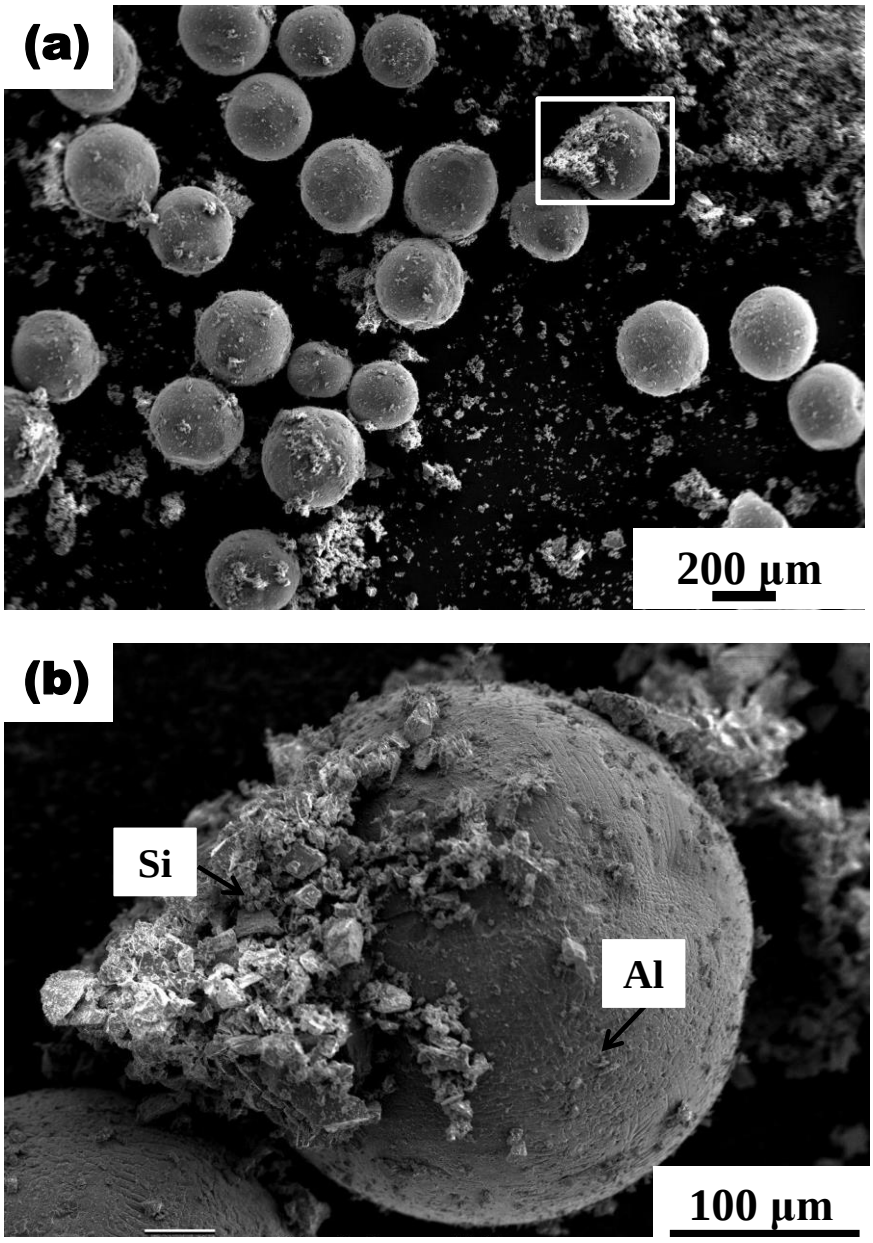


**Figure 4** Morphology of mechanically mixed (MM 0 ks) Al-Si powder (a) low magnification (b) high magnification.

6.3.2 Characterization of Mechanically Milled Powders

**Figure 5** shows the morphology of the as milled Al-5wt%Si powder with particle size distribution (PSD) for initial Al powder and MMed powder. It is also critical to emphasize that the MMed powder retains more or less of its initial shape without appreciable distortion, as shown in Fig.5 (a). This is due to the optimization made to mechanical milling parameters and condition, including the usage of stearic acid, so that it will not lead to any agglomeration and/or sticking and fractures to the Al particles. It can also be observed that after mechanical milling was conducted, PSD for MMed powder shifts to smaller particle size when compared to its initial state Fig.5 (b). Moreover, it can also be noticed that the MMed powders' PSD also demonstrates somewhat a unimodal distribution when compared to initial powder. At this stage, the mean particle size for MMed powder is reduced to 210 μm from 283 μm in the initial powder. This might be attributed to the higher number fraction of the Si particles as compared to number fraction of Al particles when Si is added , leading to the smaller mean particle size of the overall powder mass.

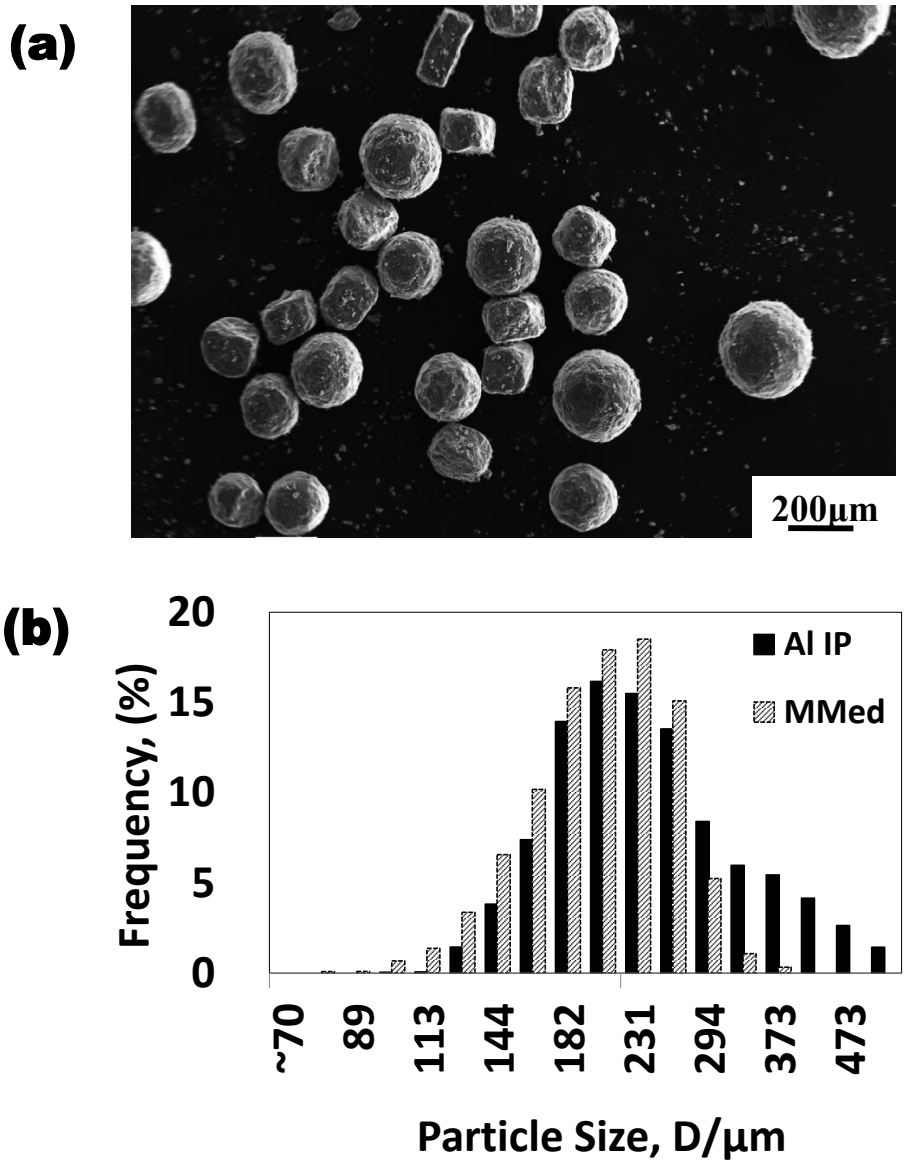


**Figure 5** (a) Morphology of as MMed Al-5wt% Si powder (b) Particle size distribution of Al initial and MMed powder.

**Figure 6** illustrates the XRD profile of the mechanically mixed and milled Al-5wt%Si powders. It is observed that there was no tertiary Phase present after mechanical milling was conducted, which suggest that mechanical alloying does not take place in present milling condition.

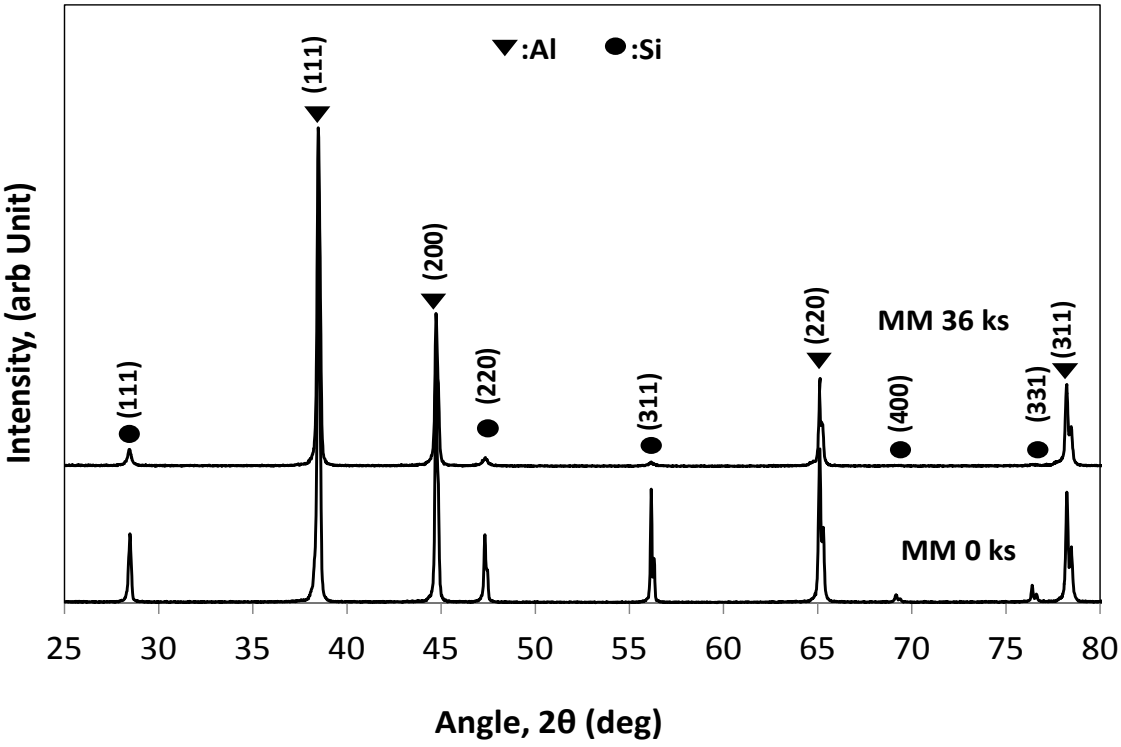


**Figure 6** X-ray diffraction patterns of mechanically mixed and milled powders.

**Figure 7** demonstrates the morphology of the MMed Al powder. After mechanical milling is conducted, the MMed powder retains more or less its initial shape without any appreciable deformation, as shown in Fig.7 (a). It is worth emphasizing that, this is due to the optimization made to mechanical milling parameters and condition, so that it will not lead to any agglomeration and/or sticking and fractures to the Al particles. Moreover, it can also be observed that the Al powders surface demonstrates the formation of a deformed rough surface. This suggests that plastic deformation is induced while

mechanical milling was conducted. It appears that the plastic deformation is only limited to the surface of powder. Similar morphological observations have been reported also in literature **[9, 12-13]**. Moreover, it is also noticed that the Si particles have fragmented to significantly smaller particle size after mechanical milling was conducted. As shown in Figs.7 (b)-(d), in the MMed powder, Si particles are uniformly distributed around Al particles. It is worth noting that at this stage, the anticipated uniform distribution of Si particles around Al particles has been achieved. Similarly, **Figure 8** demonstrates the enlargement of the cross-sectional area of the MM powder and its EDS mapping result. It can be observed that some of the Si particles with relatively smaller size have also embedded in the vicinity of the powder surface forming a layer of Si particles around Al particle.

**Table 2** Vickers hardness of initial and MMed powder.

| Powder | Hardness (HV) | |
|---|---|---|
| | Surface | Centre |
| IP | 27.3 ± 3 | |
| MM 36 ks | 39.9 ± 5 | 34.6 ± 3 |

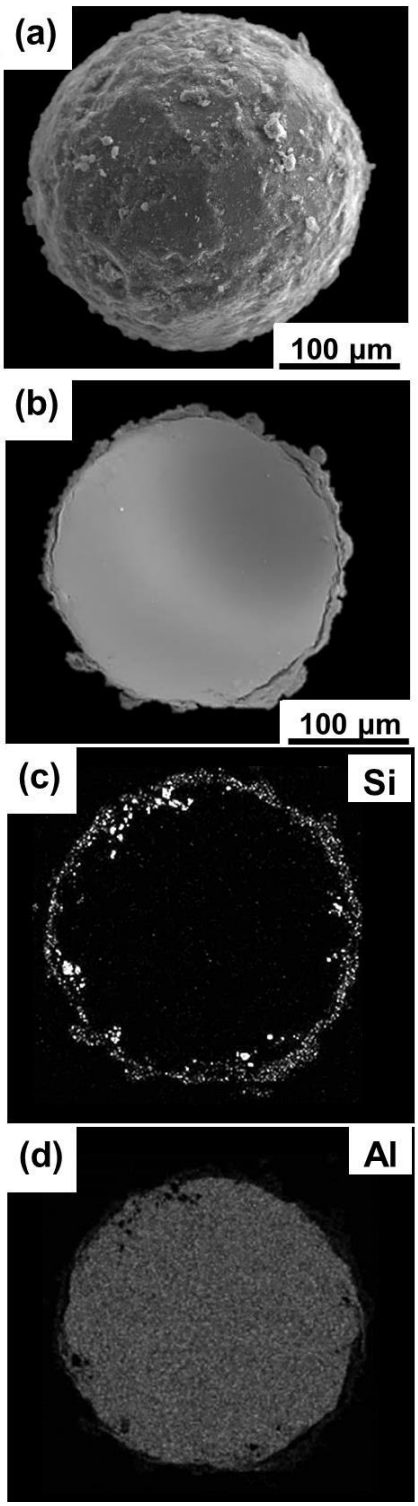


**Figure 7** Morphology and cross sectional image of MM Al-5wt%Si (a) Morphology (b) cross-sectional image (c) and (d) are EDS results illustrating distribution of Si and Al element, respectively.

**Table 2** shows powders hardness result of initial and MMed powder with its standard deviation. The indentation was made at 98.07 mN for 5 seconds of holding time. The measurements were taken in two separate regions namely, surface and center region. For surface region, the measurements were conducted approximately 25μm from the surface of Al particles. Meanwhile, for center region, the measurements were taken at the center of the respective particles. The measurement was made at different powder particles for each region to avoid any possible work hardening effect due to indentation. Apparently, the average hardness of both center and surface region of MMed powder was significantly higher than that of the initial powder. The increment of hardness in the MMed powder particle can be attributed to the work hardening effect, which is caused by plastic deformation, while mechanical milling was conducted. As a result, the hardness in the MMed powder is increased. Considering the increment in hardness value in the center region of the MMed powder as compared to the initial powder, it is apparent that the work hardening effect is not only limited to the surface area of the MMed powder, but also extends to some extent to the center region as well. Furthermore, in the MMed powder, it can also be observed that the hardness of surface region is higher than that of the center region. It is worth emphasizing that, the higher average hardness value of the surface region, as compared to that of the center region in the MMed powder reflects that, the work hardening is relatively higher at the powder surface as compared to the center region. Similar observations have been reported in the other work also **[11].** Moreover, the existence of Si particles on the surface region also contributes to hardness increment in surface region by acting as obstacles to dislocation movement.

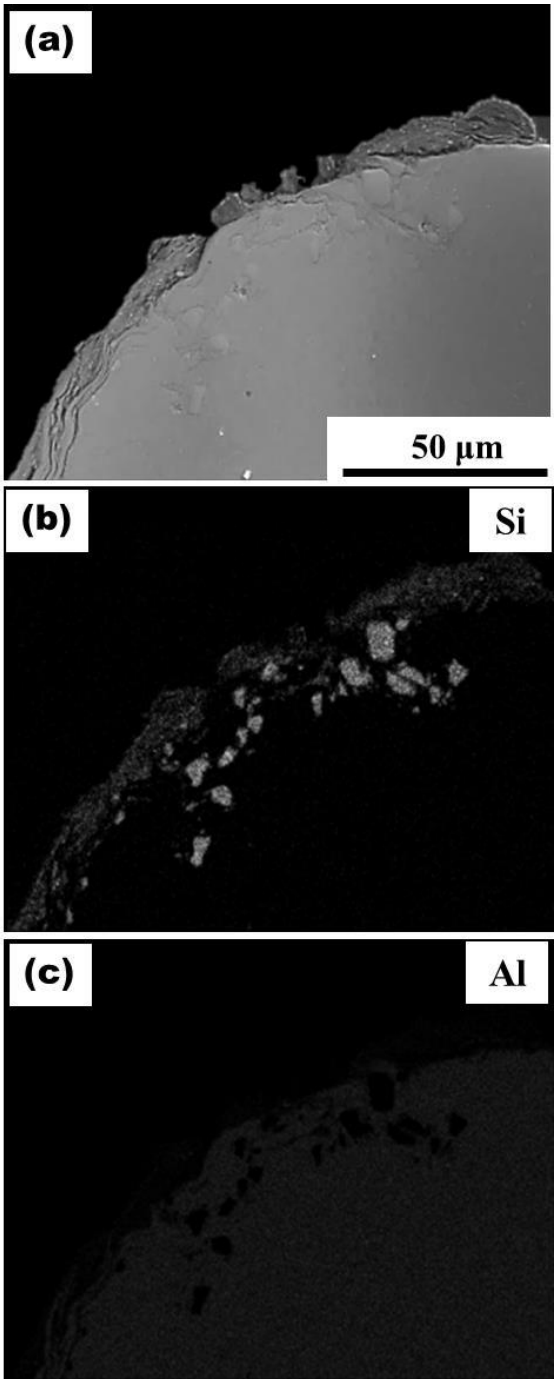


**Figure 8** (a) Enlargement of the cross-sectional area of the MM Al-5wt%Si powder with EDS mapping (b) and (c) are EDS results illustrating distribution of Si and Al element, respectively.

6.3.3Thermal Behavior of Mechanically Milled Powder

**Figure 9** illustrates the differential scanning calorimetry (DSC) profile of the MM Al-5wt%Si powder. It can be seen that during heating, the DSC curve demonstrates two distinct endothermic peaks at ①and ②. It can be observed that at ①, the endothermic peak falls at approximately 580°Cwhile the second endothermic peak ②,the temperature falls at approximately 660°C. It is envisaged that the first endothermic peak, ① is a result of eutectic reaction between Al and Si which occur a theoretical temperature of 577°C. Meanwhile, for the second endothermic peak ② is a result of the melting of pure aluminum at 660°C. Accordingly, with regard to cooling curve, it is envisaged that the first exothermic peak ③ is a result of the solidification of Al phase while the second exothermic peak ④correspond to the solidification of Al-Si phase at the powder surface region. A preliminary investigation has been conducted to observe the behavior of Al-5wt%Si powder compact at point A where the complete melting of Al-Si on the powder surface takes place. For this purpose, a cold compacted MM Al-5wt%Si powder was heat treated at 600° C for 1.8 ks.

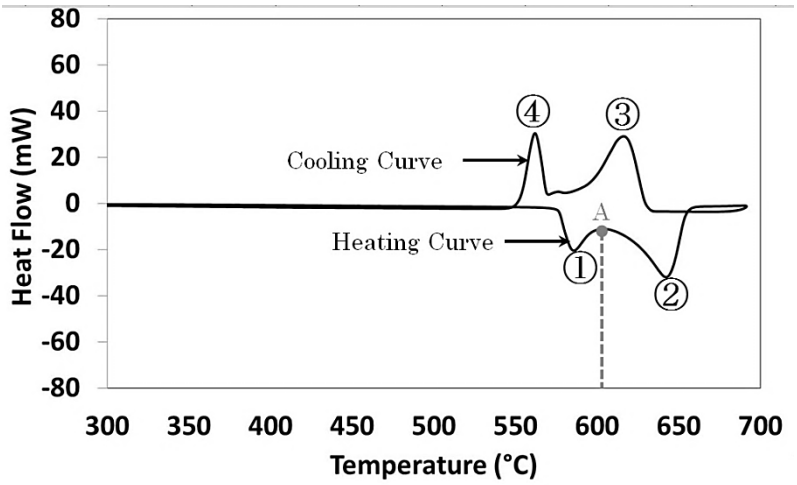


**Figure 9** DSC profile of the MM Al-5wt%Si powder.

6.3.4 Microstructure of Cold Compacted Powder

**Figure 10** shows the microstructure of the cold compacted Al-5wt%Si followed by heat treatment at 600° C. **Figure 11** illustrates the corresponding EDS analysis result. From these results, it can be seen that in this compact, that here are the presence of elongated silicon precipitates at the particle boundary which imply that there are the existence of eutectic morphology the particle boundary as illustrated in Figures 10(c) - (d). This observations imply that at 600° C, the powder surface region containing Al and Si at eutectic composition underwent melting and during cooling consolidate to from the eutectic microstructure.

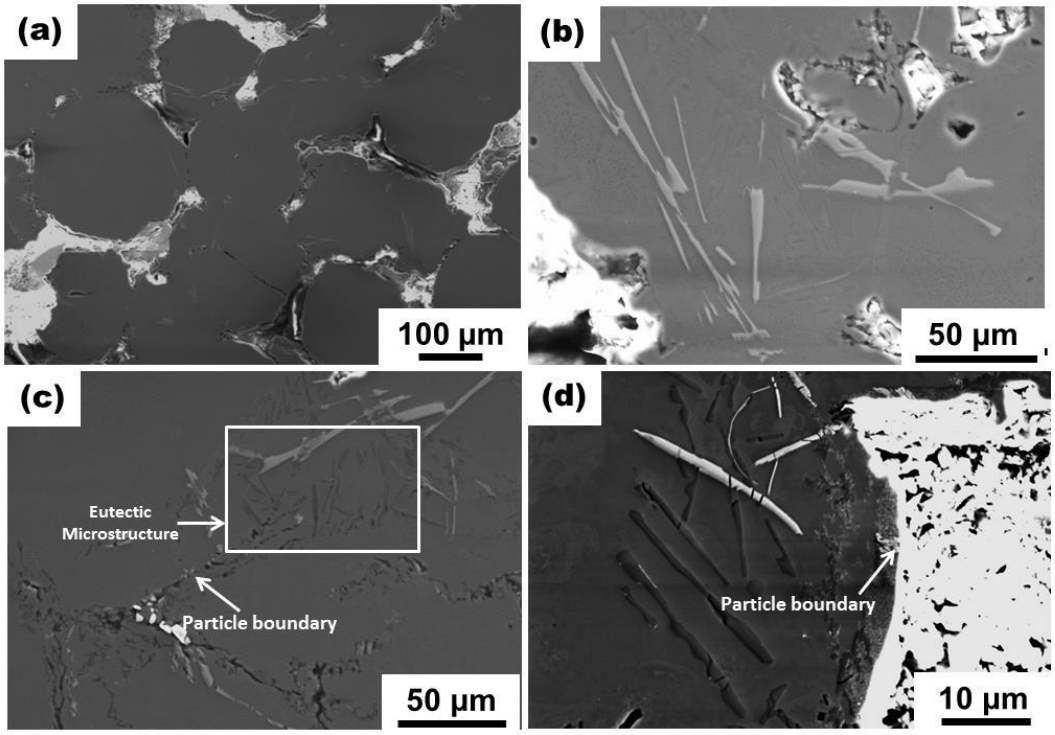


**Figure 10** Microstructure of the cold compacted compact followed by heat treatment at 600° C at (a) low magnification (b) precipitation of Si (c) and (d) Eutectic microstructure at particle boundary.

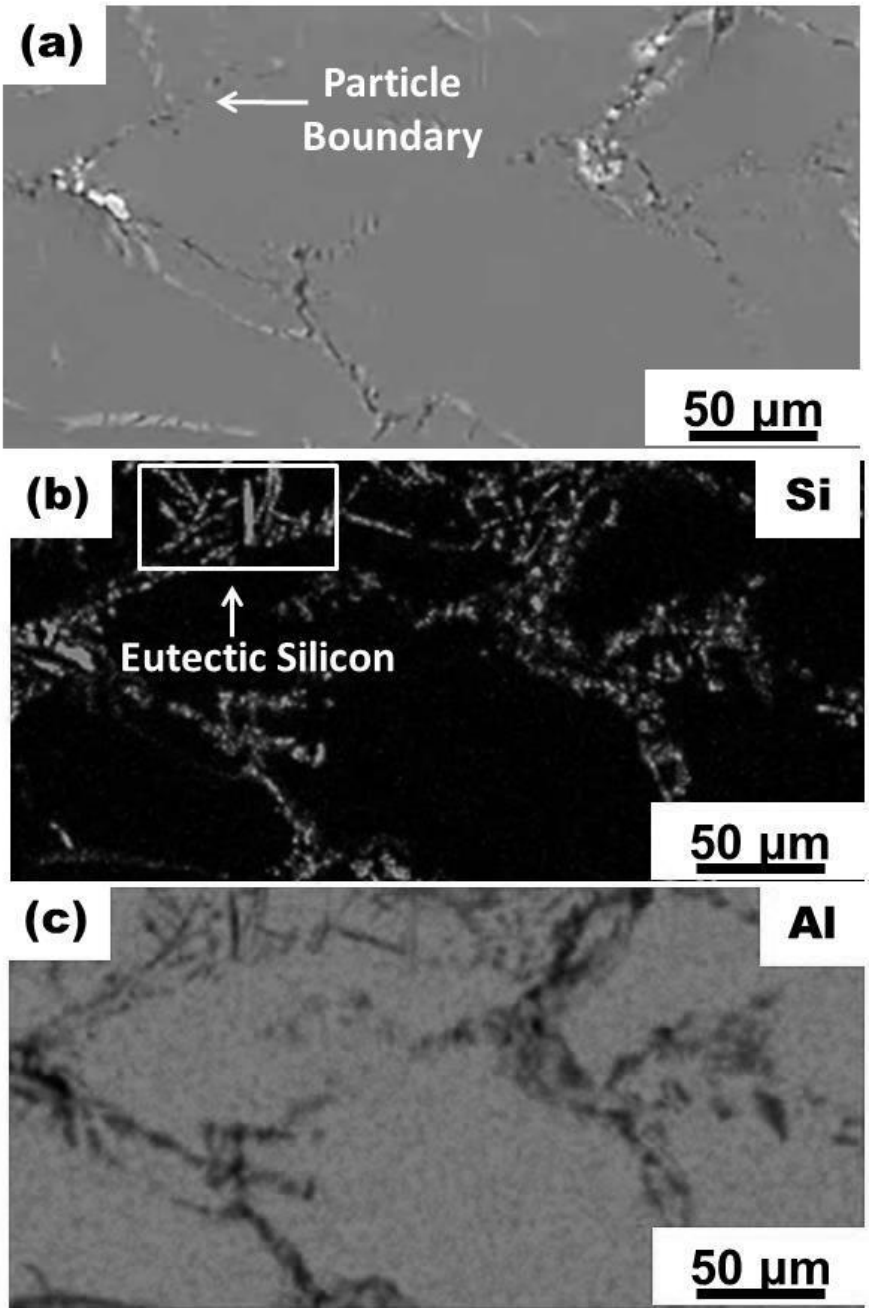


**Figure 11** Microstructure and the corresponding EDS analysis result on the particle boundary of cold compacted MM Al-5wt%Si followed by HT at 600° C (a) SE image (b) and (c) illustrate the distribution of Si and Al elements respectively.

From these observations, it appears that at a sintering temperature of 600° C, the particle boundary underwent melting which results in the exaggerate Si precipitates. This is undesirable for harmonic structure at the shell region because it is envisaged that under tensile loading, the crack will initiate at the boundary of those precipitates resulting in a poorer ductility of sintered compact. Therefore, in order to achieve the solid solution strengthening effect as mentioned at the introduction of present chapter while avoiding exaggerate Si precipitations, the sintering of MM powder has been conducted at relatively lower sintering temperature at around 577°C (point A) in **Figure 12** which partial melting of the Al-Si region takes place.

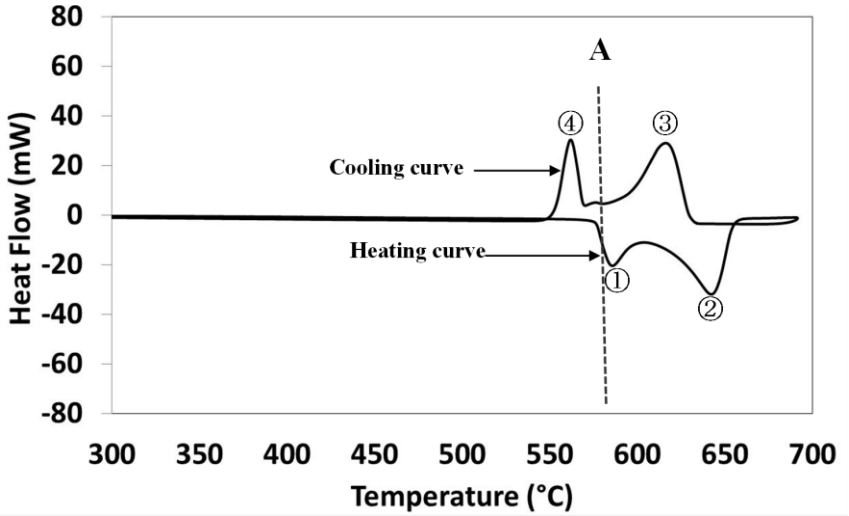


**Figure 12** DSC profile of the MM Al-5wt%Si powder.

6.3.5 Microstructural Characteristics of the Sintered Harmonic Al Compact.

**Figure 13** shows the BSE image of the sintered harmonic compact and EDS mapping images at the same magnification. Apparently, the BSE image reveals that the sintered compact demonstrates a formation of continuous network structure of two phases; dark phase in the "shell" region and grey phase in the "core" region, as shown in Fig.13 (a). The EDS analysis result demonstrates that the "shell" region corresponds to Si-rich region (Fig.13 (b)) while the "core" region corresponds to Al rich region (Fig.13(c)). At

this stage, it is worth emphasizing that the formation of desired harmonic structure consisting three- dimensional network of interconnected silicon dispersed region surrounding isolated aluminum matrix region has been achieved. **Figure 14** depicts an enlargement of the "shell" region in the harmonic compact. From BSE image, it is observed that mainly three phases exist in the "shell" region. They are present as dark phase (area "I"), grey phase (area "II") and white phase (area "III"). These areas are marked as "I", "II" and "III" respectively in Fig. 14(a). From Figs. 14(b)- (c), it is revealed that area "I" corresponds to the Al-Si solid solution phase (α), area "II" corresponds to pure Al while area "III" corresponds to pure silicon particles. Moreover, it is worth emphasizing that in area "III", Si particles exhibit two distinct morphologies, namely blocky particles and acicular particles, which is not presence in the initial Si powder. It has been reported elsewhere **[17]** that the co-existence of blocky faceted primary Si and acicular eutectic Si is a product of a hypereutectic composition during solidification. Hence, it appears that in present work the consolidation process by SPS occurs in the presence of liquid phase of hypereutectic composition in some parts of the "shell" regions. As a result, during solidification process, the liquid phase solidifies to form pure Si precipitates of different morphology, as illustrated in Fig. 14(a). From these observations, it can be concluded that, the formation of the desired harmonic structure consisting of three- dimensional network of interconnected silicon dispersed region combined with α phase (i.e: shell), surrounding isolated aluminum matrix region (i.e: core) has been achieved. In this work, the estimated "shell" fraction in harmonic structured Al compact is 15.3%.

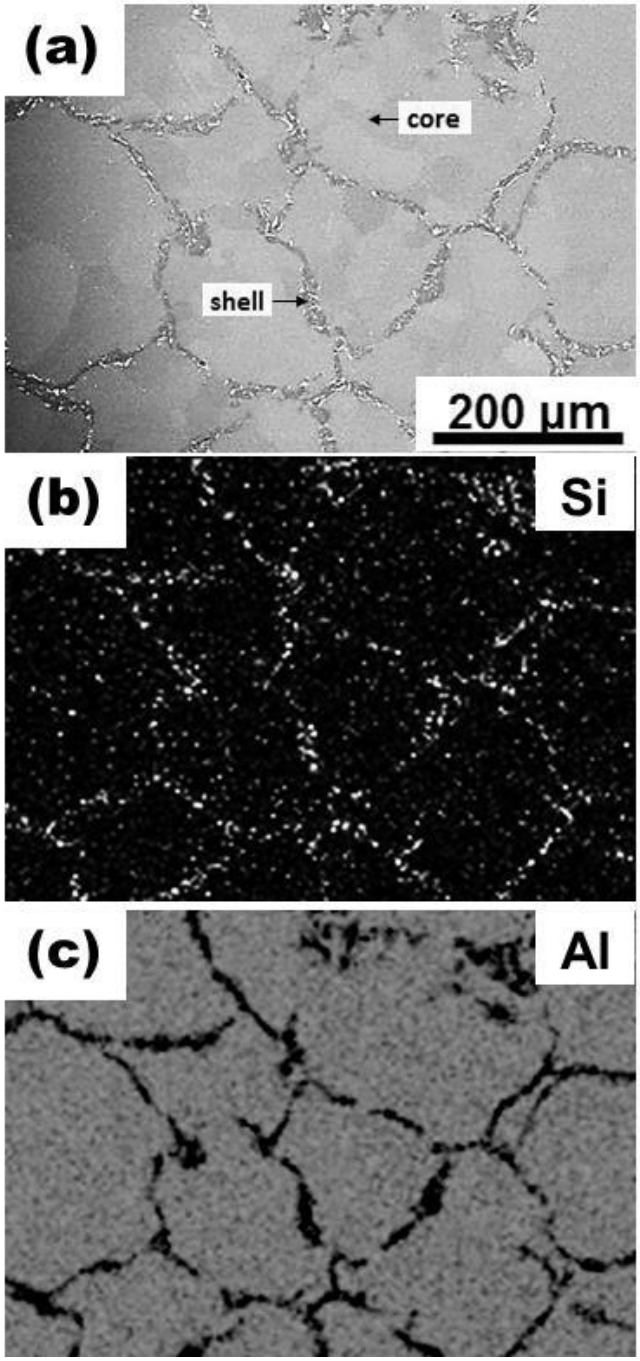


**Figure 13** Phase distribution in the sintered harmonic structured compact with "shell" fraction= 15.3% (a) BSE image of the sintered compacts showing different contrast in the "shell" and "core" region (b) and(c) are EDS analysis results showing the distribution of Si and Al elements respectively.

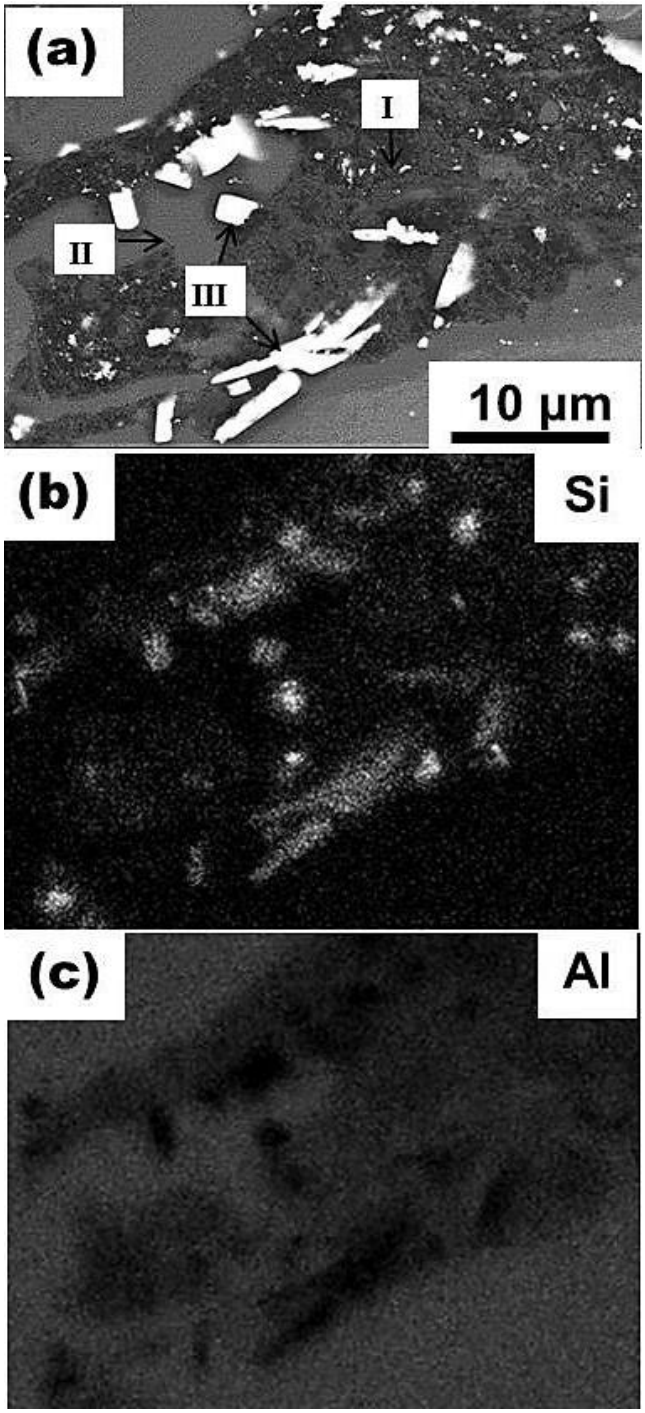


**Figure 14** Enlargement of the "shell" area for harmonic structured compact (a) BSE image of the shell region showing the presence of three main phases (b) and (c) are EDS analysis results illustrating the distribution of Si and Al elements respectively.

**Figure 15** shows the EBSD image quality map overlaid with grain boundaries in both low and high magnifications together with the inverse pole figure (IPF) of the enlargement of the "shell" region of the harmonic structure Al compact. It can be observed that, the shell region is composed of relatively fine size grains. These fine grains are the combination of α phase grains and silicon particles.

In the harmonic structured Al compact, hardness indentations were conducted separately in the shell and the core regions, and the average hardness of the respective region was Hv: 111.9±39.8 and Hv: 40.7± 3.1. The higher average hardness in the shell region compared to core region can be attributed to the formation of fine grain structure, α phase and the existence of Si particles.

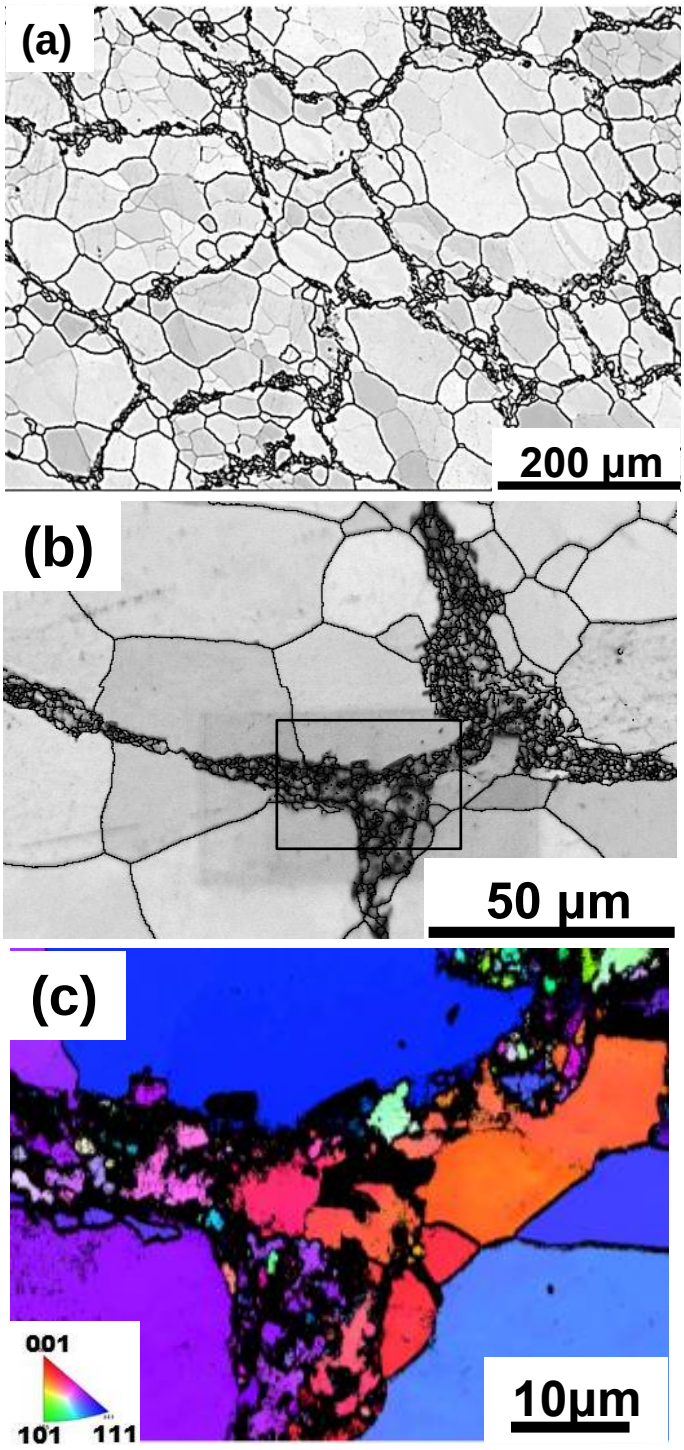


**Figure 15** Microstructure on the "shell" region for harmonic structured compact by EBSD band contrast map overlaid with grain boundary map in (a) low magnification and (b) high magnification (c) inverse pole figure of the enlargement in (b).

6.3.6 Properties of Sintered Compacts and its Deformation Behavior

In present work, the variation of Si content during mechanical milling implies the completeness of network structure formation in the final sintered compact, in such that the increasing Si content results in a completer network structure. In this work, the variation of silicon content results in three hard phase fraction $h_f$., namely, 0%, 2.5% and 15.3%. It is to clarify that in this work, the term "hard phase" is used to define the combination of Si dispersed region and α phase, while the term "shell" is used to describe the continuous network structure of the hard phase in the harmonic structured Al compact as discussed in 6.3.5.

**Figure 16**(a) shows the microstructure of the compacts with zero percent hard phase fractions, $h_f$. This compact refers to initial Al powder compact with no hard phase (Henceforth referred as homogeneous compact.) Figs.16 (b)-(c) illustrate the compact with $h_f$ = 2.5% at low and high magnifications. It is observed that this compact exhibit the heterogeneous bimodal structure, without the unique network structure specific to harmonic structured compact. (Henceforth, referred as heterogeneous bimodal compact).

**Figure 17** illustrates the EBSD image quality map overlaid with grain boundaries with its inverse pole figure (IPF) for homogeneous compact. It is confirmed that in the homogenous compact it is consisted of coarse grained microstructure. The average grain size is 132.5μm. Similarly, **Figure 18** illustrates the EBSD image quality map overlaid with grain boundaries in both low and high magnifications together with its inverse pole figure (IPF) of the enlargement of the hard phase region in the heterogeneous bimodal compact. It is also observed that in this compact, hard phase region demonstrates the existence of fine grained structure as observed in the harmonic compact. The estimated

average grain size of aluminum phase is estimated as 107.2μm.

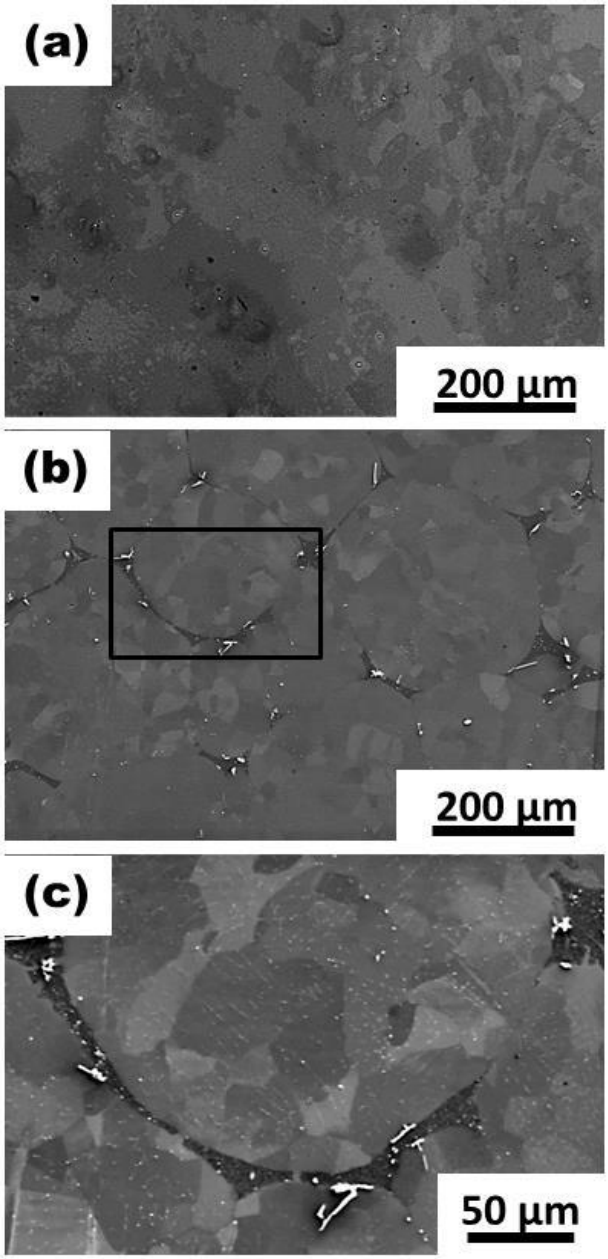


**Figure 16** Microstructure of sintered compacts at different $h_f$ fraction (a) homogeneous compact, $h_f$ =0%, (b) microstructure of heterogeneous bimodal compact, $h_f$ =2.5% (c) enlargement of the black rectangle shown in (b).

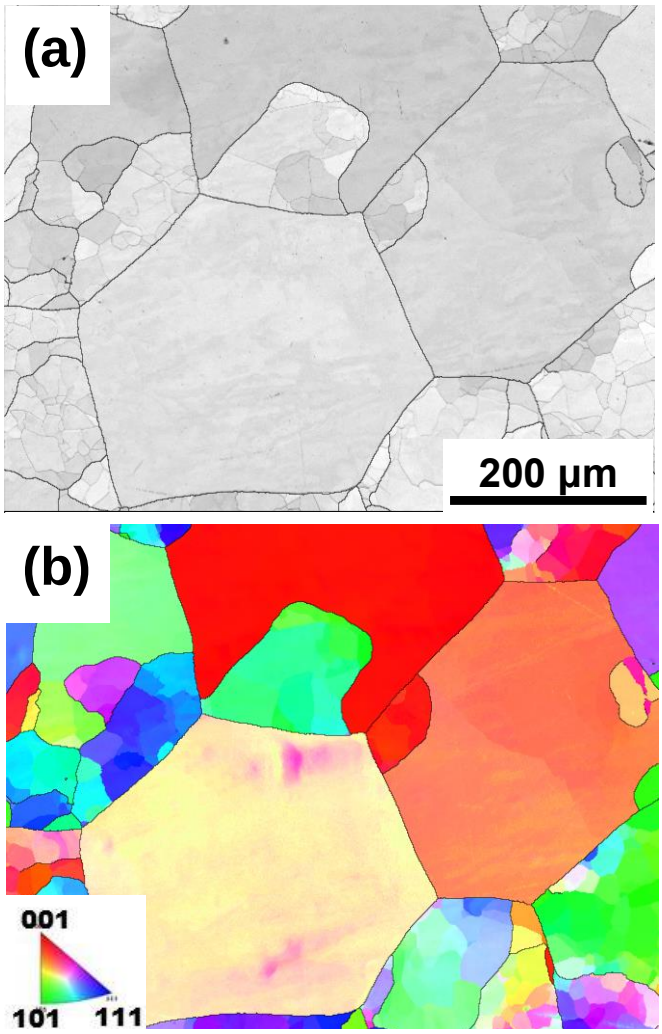


**Figure 17** Microstructure of the homogeneous compact $h_f$ =0% (a) EBSD band contrast map overlaid with grain boundary map and (b) inverse pole figure.

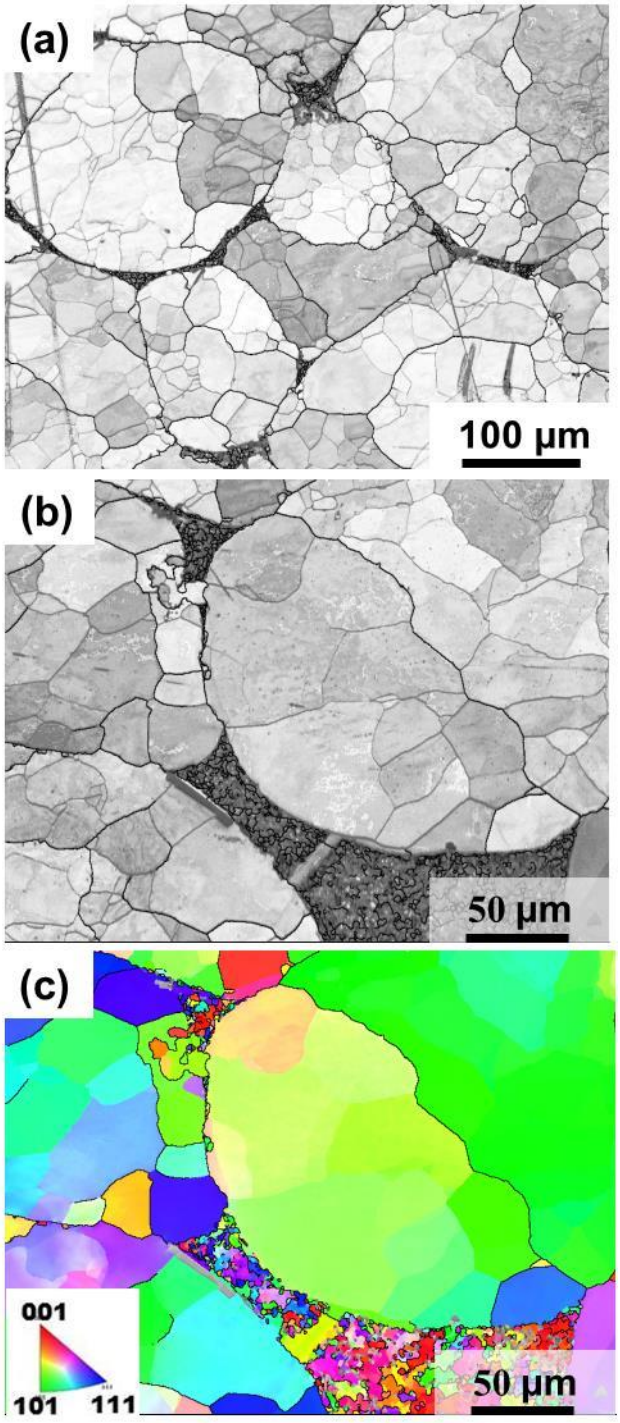


**Figure 18** Microstructure on the hard phase region for heterogeneous bimodal compact $h_f$ =2.5% (a) EBSD band contrast map overlaid with grain boundary map (b) enlargement of the hard phase region (c) inverse pole figure of the enlargement in (b).

**Figure 19**(a) illustrates the representative nominal stress-nominal strain curves of the sintered Al compacts having different hard phase fraction, $h_f$. Figs.19 (b) - (c) summarize the relation between stress and elongation a function of $h_f$. It is observed that, as compared to homogeneous compact, heterogeneous bimodal and harmonic compacts demonstrate significant increment in both 0.2% proof stress and UTS. It must be emphasized that the stresses increment in these compacts is expected, due to the larger strengthening with increasing $h_f$, combined with the existence of fine grain structure. In general, the tensile properties trend of homogeneous materials includes the decrease in ductility with increasing strength, which is related to the early plastic instability. With respect to present work, the harmonic compact is expected to have lower ductility as compared to that of the heterogeneous bimodal compact, due to the higher strength in the harmonic compact. Nevertheless, harmonic compact demonstrates retention in both total and uniform elongation, when compared to heterogeneous bimodal compact. It is to mention that the retention/improvement in ductility is the typical behavior in general for harmonic structured material, and this is associated with the existence of unique network structure which suppresses the deformation localization specific to harmonic compact as already mentioned in the introduction of present paper.

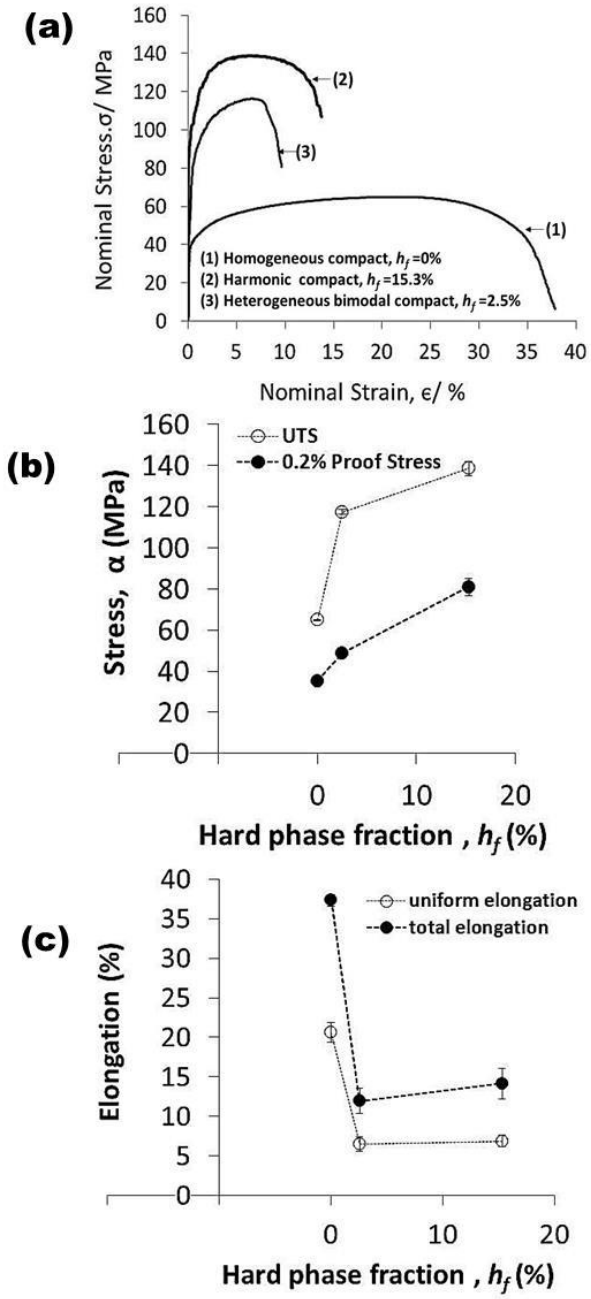


**Figure 19** Tensile properties of Al alloy samples with different hard phase fraction, $h_f$ (a) representative nominal stress-strain curve, (b) and (c) illustrate the correlation between hard phase fraction, $h_f$ with stress and elongation respectively.

To understand the deformation behavior of the harmonic structured Al compact, the true stress and true strain along with its corresponding strain hardening rate curve (SHR= dσ/dε),was presented in **Figure 20**. Essentially, in the early stage of deformation, dσ/dε comprise of relatively rapid decrease with increasing true strain, followed by relatively small decreasing rate, until the dσ/dε crosses the true stress-true strain curve at the point of plastic instability (i.e dσ/dε=σ),in which the necking of the specimen starts thereafter. With regards to homogenous compact, dσ/dε demonstrates a relatively sluggish strain hardening rate at the early stages of deformation when compared to that of the harmonic and heterogeneous bimodal counterpart. It is worth noting that this is the typical trend in coarse grained structure. On the other hand, it is observed that the harmonic structured compact undergoes higher strain hardening at the early stage of deformation, when compared to that of its homogeneous and heterogeneous bimodal structure counterpart. It is to mention that the higher strain hardening at earlier stage of deformation is a general trend for fine grained structure. When compared to the heterogeneous bimodal compact, harmonic compact demonstrated a shift of dσ/dε=σ towards a higher strain values which indicates, in harmonic structured compact, the plastic instability is delayed towards higher strain value. This implies that the plastic deformation localization is delayed, leading to the delayed necking of the specimen which results in the higher uniform elongation in the harmonic compact. Therefore, from these observations, there are two main conclusions that can be drawn for the present harmonic structured Al compact: 1) in the early stage of deformation, harmonic Al compact exhibits somewhat similar strain hardening behavior to the fine grained structure and 2) when compared to the heterogeneous bimodal structure, the point of plastic instability dσ/dε=σ in harmonic

compact is delayed to a higher strain rate, leading to improved uniform elongation in harmonic Al compact. To summarize, as compared to the homogeneous pure Al material, harmonic structured Al exhibits significant improvement in strength while retaining sufficient ductility.

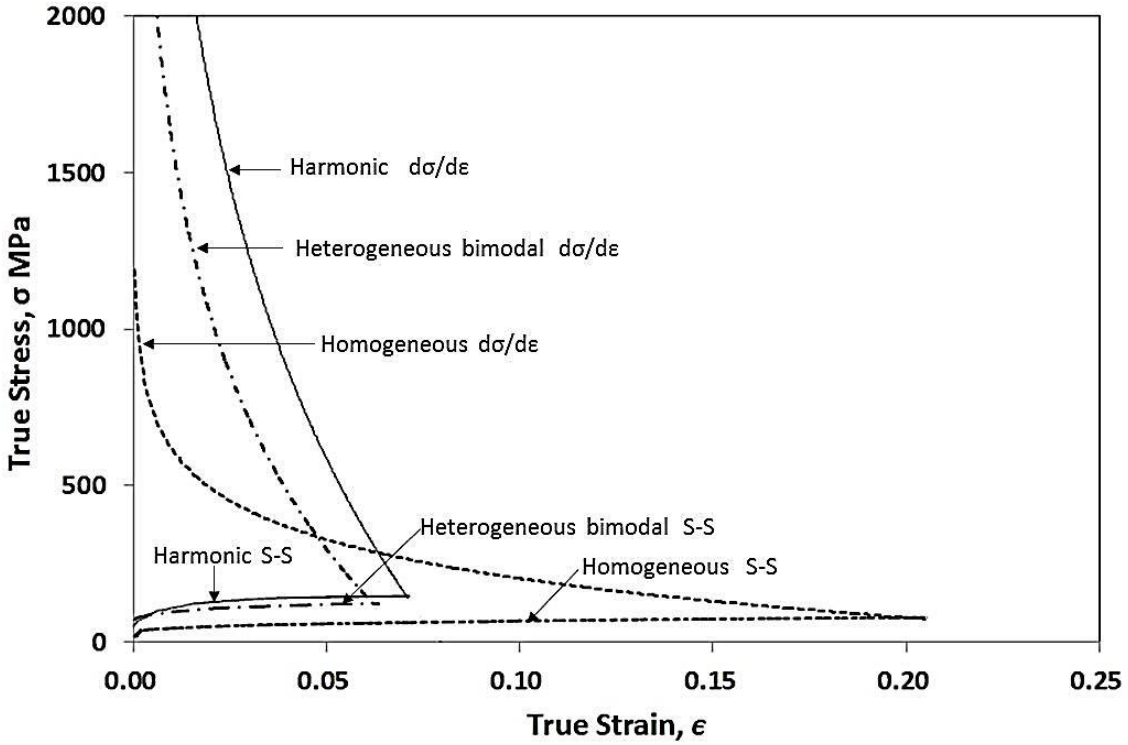


**Figure 20** True stress–true strain curves, along with their corresponding strain hardening rate (SHR) curves.

### 6.3.4 The Control of Hardness Properties during Fabrication of Harmonic Structured Al Alloy

To evaluate the effect of hardness properties on the mechanical properties of harmonic structured Al-Si alloy, the silicon content was varied from 0 to 12.6 weight percent during powder preparation. From **Figure 21** (a), it can be observed that as silicon content is increased, hardness of the core region do not demonstrate any significant change. On the contrary, for "shell" region, it is noted that the hardness is increased substantially as silicon content increases. This observation implies that the increment in silicon content only results in the increase of the "shell" hardness. Figures 21 (b)-(c) depict the relationship between tensile properties of harmonic structured Al-Si alloy as a function of shell to core hardness ratio. It can be observed that as the hardness ratio is increased, the 0.2% proof stress is also increasing substantially. Meanwhile, the increment in UTS is observed to be only limited up until the hardness ratio is approximately 2.7. Further increment in the hardness ratio demonstrates no significant increase in UTS. On the other hand, uniform elongation $\epsilon_u$ shows a decreasing trend as the hardness ratio is increased. These observations indicate that, the important balance between "shell" and "core" hardness to achieve the optimum combination of properties in harmonic structured Al-Si alloy. In present work, harmonic structured with approximately shell to core hardness ratio of 2.7 demonstrated the most optimum combination for achieving mechanical properties improvement.

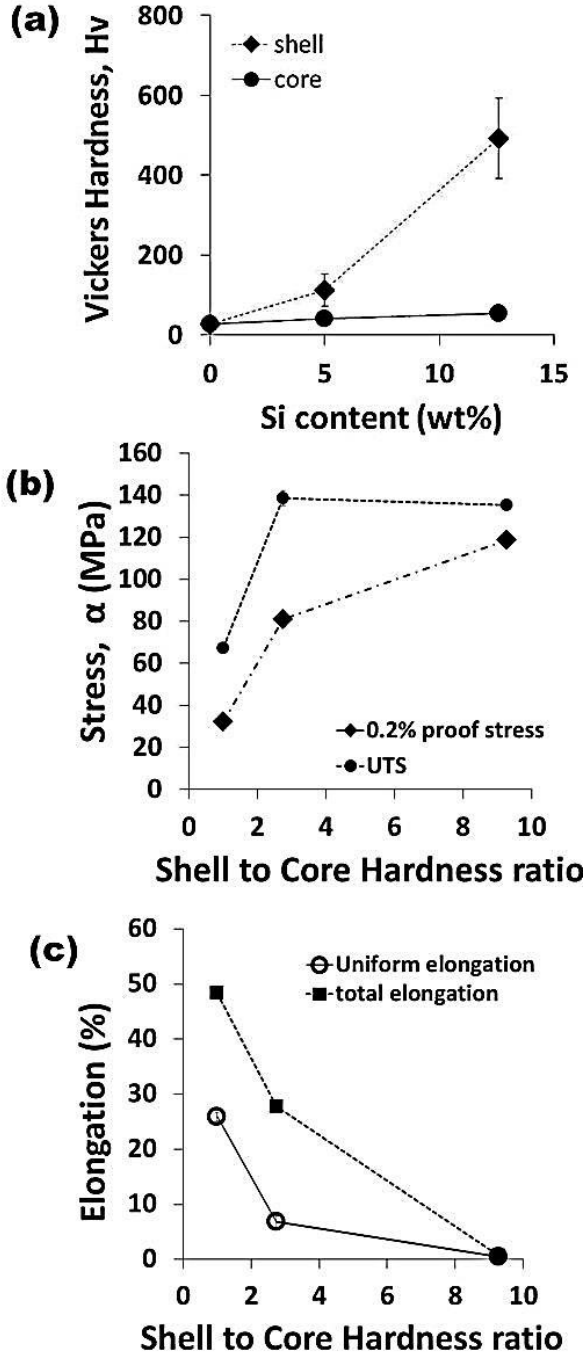


**Figure 21** Dependence of tensile properties on hardness properties in harmonic structured Al alloy (a) illustrates the variation of average hardness of the "shell" and "core" regions with silicon content (b) and (c) depicts the correlation between tensile properties with hardness ratio in harmonic structured Al compacts.

## 6.4 Conclusions

In present work, harmonic structured of Al was successfully fabricated by powder metallurgy route in which pure aluminum and silicon powder were subjected to controlled mechanical milling followed by subsequent spark plasma sintering. The mechanical performance was evaluated by tensile properties and the following conclusions can be drawn:

(1) Uniform distribution of silicon particles around Al particles can be achieved by controlled mechanical milling.

(2) Harmonic structured Al is comprised of soft core areas with pure aluminum matrix, enclosed into three-dimensional network of hard Si dispersed region combined with α phase structure was successfully fabricated. The shell region of harmonic structured Al demonstrates the existence of fine grains structure. Harmonic structured Al compact demonstrates improvement in both strength and ductility when compared to its homogeneous structure counterpart.

(3) When compared to its heterogeneous bimodal counterpart, harmonic structured Al compact demonstrates delayed plastic instability, which results in the improvement of uniform and total elongations.

(4) Network structure of three dimensional interconnected network regions of hard phase, enclosing soft phase is effective in improving mechanical properties of Al based alloy.

(5) The control of shell to core hardness ratio hardness is very important to achieve the optimum combination of mechanical properties in harmonic structured Al-Si alloy.

**REFERENCES:**

**[1]** H. Fujiwara, R. Akada, Y. Yoshita and K. Ameyama: *Mater. Sci. Forum* **503-504** (2006) 227-232.

**[2]** H. Fujiwara, R. Akada, A.Noro, Y.Yoshita and K.Ameyama : *Mater. Trans.* **49**(2008) 90-96.

**[3]** H. Fujiwara, M. Nakatani, T. Yoshida, Z.Zhang and K. Ameyama: *Mater. Sci. Forum* **584-586** (2008) 55-60.

**[4]** H. Fujiwara, S. Takarae and K. Ameyama: The 2nd International Symposium on Steel Science, (ISSS, 2009) pp.262-272.

**[5]** T.Sekiguchi, K. Ono, H. Fujiwara and K. Ameyama: *Mater. Trans*. **51** (2010) 39-45.

**[6]** H. Fujiwara, H. Tanaka, M. Nakatani, and K. Ameyama: *Mater. Sci. Forum* **638-642** (2010) 1790-1795.

**[7]** D. Orlov, H.Fujiwara and K. Ameyama: *Mater. Trans.* **54**(2013) 1549-1553.

**[8]** O.P. Ciuca, M.Ota, S.Deng and K.Ameyama: *Mater.Trans.* **54**(2013) 1629-1633.

**[9]** Z.Zhang, S.K.Vajpai, D.Orlov and K.Ameyama: *Mater.Sci.Eng.A* **598**(2014) 106-113.

**[10]** C.Sawangrat, O. Yamaguchi, S.K. Vajpai and K. Ameyama: *Mater.Trans.* **55** (2014) 99-105.

**[11]** C. Sawangrat, S.Kato, D.Orlov and K.Ameyama: *J.Mater.Sci*. **49**(2014) 6579-6585.

**[12]** Z.Zhang, D.Orlov, S.K.Vajpai, B.Tong and K.Ameyama: *Adv. Eng. Mater.* **17**(2015) 791-795.

**[13]** S.K. Vajpai, M.Ota, T.Watanabe, R.Maeda, T.Sekiguchi, T.Kusaka and K.Ameyama: *Metall. Mater. Trans. A* **46** (2015) 903-914.

**[14]** S.K.Vajpai, C.Sawangrat, O.Yamaguchi, O.P. Ciuca and K.Ameyama: *Mater.Sci.Eng.C* **58**(2016) 1008-1015.

**[15]** H.Yu, I.Watanabe and K.Ameyama: *Adv. Mater. Res*. **1088** (2015) 853-85.

**[16]** R.M. German: *Powder Metallurgy & Particulate Materials Processing*, (Metal Powder Industries Federation., New Jersey, 2005), pp.96-97.

**[17]** R. Asthana, A. Kumar and N. B. Dahotre: *Materials Processing and Manufacturing Science*, (Elsevier, Butterworth-Heinemann, 2006) pp. 149.

# Chapter 7

# Conclusions

This thesis has described the work conducted in order improve mechanical properties in structural materials via particle size control. Specific approach has been designed for two different classes of materials. Silicon Carbide as a representative ceramic material and Aluminum based alloy as metallic material representative has been chosen to achieve the aforementioned objective. The summery of each works including the specific objective, methodology and findings are concluded in the following:

1) In chapter 4, a work describing the improvement of sinterability in SiC ceramic via particle size control has been discussed. The specific objective of this chapter includes the clarification of the effect of dispersion in particle size distribution to the sinterability and mechanical properties of SiC ceramic. In this chapter, two types of SiC powders of different sizes were subjected to mechanical milling in order to produce various patterns of particle size distributions followed by spark plasma sintering. The sinterability and mechanical properties of sintered bodies were evaluated by relative density and flexural strength. This work has also suggested the usage of coefficient of variation Cv in obtaining relatively accurate dispersion level in distributions with different variables. It is also found that the sinterability and mechanical properties of sintered SiC compacts increases with the increase of dispersion level in initial powder which is best described by Cv.

2) In chapter 5, the specific objective is to assess the feasibility to fabricate harmonic structured Al based alloy via a novel approach. The proposed harmonic structured design includes fabrication of a network structure of soft phase, which is enclosed by three dimensional interconnected network regions of hard phase. An attempt has been made to design the "shell" region with a different strengthening mechanism than that of the conventional harmonic structured material, while maintaining the "core" region as the softer phase. Specifically, the shell region has been made to be dispersion strengthened region and SiC particles has been chosen as the secondary elemental phase for that purpose. The harmonic structure of Al-SiC was fabricated by powder metallurgy route in which pure aluminum and silicon carbide (SiC) powder were subjected to controlled mechanical milling followed by subsequent spark plasma sintering. Harmonic structured Al is comprised of soft core areas with pure aluminum matrix, enclosed into three-dimensional network of hard SiC dispersed region was successfully fabricated. The effect of variation in SiC content to mechanical properties of harmonic structure Al-SiC has also been analysed. It is found that the effect of harmonic structure design in Al-SiC is not observed and it is envisaged that it is due to the poor sinterability amongst SiC particles at the shell region. In the SiC range investigated, it is found that Al-1wt%SiC demonstrates the most optimum balance of strength and ductility.
3) In chapter 6, fabrication of harmonic structure of Al alloy via a novel approach through the semi-solid reaction between Al and Si has been discussed. The harmonic structured Al was prepared by subjecting Al and Si powder to

controlled mechanical milling followed by subsequent spark plasma sintering to make a compact. The sintered compact resulted in a network structure of hard interconnected silicon dispersed region combined with Al-Si solid solution phase, known as "shell", enclosing the soft phase of pure aluminum matrix known as "core". The harmonic structured Al compact demonstrated retention of both uniform and total elongation as compared to its heterogeneous bimodal structure counterpart, which is the typical feature of the harmonic structured material. Network structure of three dimensional interconnected network regions of hard phase, enclosing soft phase is effective in improving mechanical properties of Al based alloy. In this chapter, discussions on the deformation behavior of the sintered compacts, with respect to its strain hardening behavior has also been made.

# Acknowledgement

First of all, all praises and thank to Allah, Lord of the entire world for giving me the courage and momentum to undergo this journey for which I couldn’t have completed if it is not because of Him.

Secondly, I would like to express my deepest gratitude to Prof. Kei AMEYAMA for giving me such a wonderful and humbling experiences to be part of Ameyama lab members and to first introduce me to materials science field. All the advises and encouragements from him through the hard times during this journey are mostly appreciated. Not to mention his wide experiences and knowledges in this field has helped me a lot in improving and building basic and fundamentals in materials science field. I would also like to express my appreciation on the motivations he initiates in me to be a researcher with a critical thinking.

I also wish to express my deepest appreciation to Dr. Sanjay Kumar Vajypai, a senior researcher in Ameyama lab for his critical comments and suggestions on my scientific work through the completion of this thesis. I am also indebted to him for his time to give me a very honest and insightful comments/ suggestions/ debates through my works in which I found to be very important to help me build the way of thinking a researcher should have.

Special thanks also to Dr. Mie OTA for her guidance, assistant and a very helping suggestion through the completion of this thesis. I would also want to convey my appreciation for all the times she spends to assist me in using many experimental instruments in which I couldn’t have done it without. I would also like to thank her a lot

for her warm company throughout this journey in which has made my journey in Ritsumeikan University a lot more enjoyable.

To all Ameyama lab past and present members especially Mrs. Nurul Nadiah binti Mahmud and Mr. Sahara Takayuki, I would like to thank them a lot for their very kind assistant and company which has helped me tremendously during my stay in Ameyama lab.

Last but not least, I would like to thank my family for their understanding and motivation they have provide me with. For all the trusts and supports they have given me, I am indebted to them.

*Nur Zalikha Binti Khalil*

*Kusatsu, September 2016*